uOttawa

L'Université canadienne
Canada's university

FACULTÉ DES ÉTUDES SUPÉRIEURES ET POSTOCTORALES

uOttawa

L'Université canadienne
Canada's university

FACULTY OF GRADUATE AND POSDOCTORAL STUDIES

Raymond Wang
AUTEUR DE LA THÈSE / AUTHOR OF THESIS

M.A.Sc. (Mechanical Engineering)
GRADE / DEGREE

Department of Mechanical Engineering
FACULTÉ, ÉCOLE, DÉPARTEMENT / FACULTY, SCHOOL, DEPARTMENT

Bearing Fault Detection and Oil Debris Monitoring by Adaptive Noise Cancellation

TITRE DE LA THÈSE / TITLE OF THESIS

Ming Liang
DIRECTEUR (DIRECTRICE) DE LA THÈSE / THESIS SUPERVISOR

CO-DIRECTEUR (CO-DIRECTRICE) DE LA THÈSE / THESIS CO-SUPERVISOR

EXAMINATEURS (EXAMINATRICES) DE LA THÈSE / THESIS EXAMINERS

Mojtaba Ahmadi

Dan Necsulescu

Gary W. Slater
Le Doyen de la Faculté des études supérieures et postdoctorales / Dean of the Faculty of Graduate and Postdoctoral Studies

Bearing Fault Detection and Oil Debris Monitoring by Adaptive Noise Cancellation

by

Raymond Yi-Wen Wang

A thesis submitted to the School of Graduate Studies and Research in partial fulfillment of the requirements for the degree of

Master of Applied Science
in Mechanical Engineering

Ottawa-Carleton Institute for Mechanical and Aerospace Engineering

University of Ottawa
Ottawa, Ontario, Canada

Your file Votre référence
ISBN: 978-0-494-41685-3
Our file Notre référence
ISBN: 978-0-494-41685-3

To my wife Maria and our daughter Emma

Abstract

Bearing fault detection is critical in preventing machine failure and ensuring machine is operating in optimal condition. However, the monitored bearing vibration signal is often corrupted by interference signals from other sources in the machine. Adaptive noise canceller can be used to extract the bearing signal from the corrupting interference signals, thus enable bearing fault detection. Adaptive noise canceller utilizing least mean square algorithm is also suitable for on-line monitoring because of its computational efficiency.

The effectiveness of the adaptive noise canceller is controlled by its operating parameters: the transversal filter length and the step-size parameter. This thesis establishes the criteria in determining the proper operating parameters. The Akaike information criterion is used to obtain the transversal filter length because of the adaptive noise canceller's autoregressive structure. The adaptive filter weight fluctuations affect the performance of the adaptive noise canceller. The misadjustment positively correlates to the filter weight fluctuations. A small misadjustment value can be used to obtain the required step-size parameter to ensure the satisfactory performance of the adaptive noise canceller. A procedure to achieve zero settling time in on-line monitoring under the stationary environment is also illustrated in this thesis. Simulation and experiments are performed to demonstrate the effectiveness of the adaptive noise canceller in bearing signal extraction.

Inductive oil debris monitoring sensor is used to detect metal particles in the lubricating oil. However, the sensor is affected by the interfering vibration signal and the metal particle signatures can no longer be correctly detected from the resulting mixed signal. In order to obtain reliable metal particle counts and sizes, it is critical that the interfering vibration signal is removed.

The metal particle signal in the oil debris monitoring signal is non-periodic and can be considered a broadband signal. Thus a special form of the adaptive noise canceller which does not require a separate reference input source can be used. A delay is incorporated to the collected signal to derive the reference input. A delay value longer than the length of the characteristic output signal sampling units is needed to achieve the

decorrelation between the metal particle signal in the primary input and the metal particle signal in the reference input. The criteria to determine the operating parameters established in bearing fault detection application can also be implemented in oil debris monitoring application. Simulation and experiments are performed to verify that the adaptive noise canceller can effectively remove the interfering periodic signals and reveal the metal particle signal from the corrupted signal.

Acknowledgement

I would like to thank my supervisor, Dr. M. Liang for providing me financial support and guidance in my research to complete this thesis. I am deeply in debt to his help throughout my graduate study.

I would like to express my gratitude toward my colleagues: Dr. Hoonbin Hong and Mr. Iman Soltani. Through the stimulating discussions I had with them, I have learned so much more to my study. In addition, I have gained two good friends in my life.

I like to thank Mr. Leo Denner and Mr. John Perrins from the machine shop. They have been most wonderful whenever I need their help. I also like to thank Dr. Fan for collecting and providing the metal particle signals used in this thesis.

I am blessed that I have the unconditional support of my family. Without my parents and my sister's encouragement, I cannot accomplish this thesis. I owe so much to my wonderful wife, Maria. In the darkest time of my study, she makes me believe there is light at the end of the tunnel. She is the light at the end of the tunnel for me.

Table of Contents

List of Figures

Nomenclature

$A[x(n)]$	Analytic signal of $x(n)$
$a(n)$	Magnitude of the analytic signal $A[x(n)]$
$b(n)$	Modelled bearing vibration signal
$c(n)$	Exponential decay of vibration of the machine response
D_b	Diameter of bearing rolling element
D_c	Pitch diameter of bearing rolling element
$d(n)$	Primary input signal in the ANC, desired signal in the LMS algorithm and Wiener filter theory
$E\left[\left\|\mathbf{u}(n)\right\|^2\right]$	Ensemble average of the total input power $\left\|\mathbf{u}(n)\right\|^2$
$e(n)$	Error signal in the ANC, the LMS algorithm, and Wiener filter theory
$\left\|e(n)\right\|^2$	Squared estimation error
F	Sampling frequency
f_b	Bearing rolling element frequency
f_c	Bearing cage frequency
f_d	Bearing characteristic frequency
f_i	Bearing inner race frequency
f_o	Bearing outer race frequency
f_r	Resonance frequency of the machine
f_s	Shaft rotation frequency
G	Numbers of gear meshing harmonics
$g(n)$	Modelled gear vibration signal and interference source
$H[x(n)]$	Hilbert transform of signal $x(n)$
$H(z)$	Transfer function from the interference source to the reference input
H^∞	Minimax performance criterion
$i(n)$	Modelled bearing vibration impulse series

i_0	Amplitude of the modelled bearing impulse
$J(n)$	Ensemble average mean square error of the LMS filter
$J(\infty)$	Steady state ensemble average mean square error of the LMS filter
$J_{ex}(\infty)$	Steady state ensemble average excess mean square error of the LMS filter
$J_{\min}$	Minimum mean square error of the Wiener filter
L	Number of gear teeth
$L(z)$	Transfer function from the bearing signal to the reference input
Lf_s	Gear meshing frequency
l	Autoregressive model order
M	Length of the transversal filter weight vector
N	Number of data samples
N_B	Number of bearing rolling element
n	Index of discrete time and the number of iterations
$\mathbf{R}$	Correlation matrix of the input vector $\mathbf{u}(n)$
$S_{bb}(z)$	Power spectrum of the bearing signal
$S_{bb,out}(z)$	ANC output bearing signal power spectrum
$S_{bb,ref}(z)$	ANC reference input bearing signal power spectrum
$S_{gg}(z)$	Power spectrum of the interference signal
$S_{gg,out}(z)$	ANC output interference signal power spectrum
$S_{gg,ref}(z)$	ANC reference input interference signal power spectrum
$S_{ud}(z)$	Cross power spectrum between the input and desired signal
$S_{uu}(z)$	Power spectrum of the input signal
T_e	Time constant of the modelled exponential decay
T_o	Time period between two consecutive impulses of bearing outer race fault (the reciprocal of the bearing outer race frequency f_o)
$tr[\mathbf{R}]$	Trace of the input correlation matrix $\mathbf{R}$

$\mathbf{u}(n)$	Input signal vector
$\|\mathbf{u}(n)\|^2$	Total input signal power
$u(n)$	Reference input signal in the ANC, input signal in the LMS algorithm and Wiener filter theory
$W^O(z)$	Optimal unconstrained Wiener transfer function
$\mathbf{w}(n)$	Transversal filter weight vector
$w_k(n)$	Tap weight of the k th transversal filter
X_m	Amplitude of the m th gear meshing harmonic
$\bar{x}$	Average of the vibration signal $x(n)$
$x(n)$	Vibration signal
$y(n)$	Adaptive filter output signal in the ANC, the LMS algorithm, and Wiener filter theory
β	Misadjustment, the ratio of the steady state excess mean square error $J_{ex}(\infty)$ to the minimum mean square error $J_{\min}$
$\delta(n)$	Unit impulse function
ε_l	Error power associated with the model order l
ϕ_m	Phase of the m th gear meshing harmonic
$\varphi(n)$	Phase of the analytic signal $A[x(n)]$
λ_{av}	Average eigenvalue of the correlation matrix $\mathbf{R}$
λ_l	l th eigenvalue of the input correlation matrix $\mathbf{R}$
$\lambda_{\max}$	Largest eigenvalue of the correlation matrix $\mathbf{R}$
μ	Step-size parameter, a positive constant, also refers to as learning rate in the ANC and the LMS algorithm
θ	Contact angle between the bearing rolling element and the race
$\rho_{out}(z)$	Signal to interference ratio at the ANC output
$\rho_{ref}(z)$	Signal to interference ratio at the ANC reference input
σ^2	Noise power

τ_{av}	Average time constant of the exponential decay learning curve
τ_l	Time constant of the l th exponential natural mode
Δ	De-correlation delay
$\nabla(n)$	Instantaneous gradient vector of the squared error signal

Acronym

AIC	Akaike information criterion
AR	autoregressive
ANC	adaptive noise canceller
LMS	least mean square
ODM	oil debris monitoring
RLS	recursive least squares
SANC	self adaptive noise canceller

1 Introduction

1.1 Overview

Time-based preventive maintenance is the standard maintenance technique that is used in the industry. Preventive maintenance sets a periodic interval to perform maintenance regardless of the health status of the machine. However, as components of the machine are made with higher quality while the machine becomes more complex, the preventive maintenance approach is becoming less effective and more costly. More efficient maintenance methods such as condition-based maintenance are being implemented in a variety of applications. Condition-based maintenance approach monitors the machine health while it is operating and detects machine fault when component failure first occurs. Condition-based maintenance can therefore detect incipient fault better than preventive maintenance while reduces maintenance cost by eliminating the number of unnecessary maintenance operations.

Bearing fault detection is one of the applications in condition-based maintenance. The need to detect incipient bearing faults in critical machine operation such as aircraft engines and helicopter gearboxes was stressed by Simon et al (2004). Early detection of bearing fault can prevent defects of other components and machine breakdown. Many researchers have developed a variety of methods in the analysis, prediction and detection of bearing fault. However, when the available measured bearing signal is corrupted by interfering signals originating from other sources, many of these available methods do not work well. Adaptive noise canceller (ANC) utilizing the least mean square (LMS) algorithm offers a viable solution to remove the interfering signals and extracts the desired signal when the statistics of the operating environment is unknown. However, one main problem concerning the adaptive noise canceller is the difficulty in determining the operating parameters of the LMS algorithm, which greatly affects the adaptive noise canceller's performance. In order to effectively apply the ANC for bearing fault detection applications, methods and guidelines to determine the operating parameters need to be established and verified.

Another area of the condition-based maintenance is the oil-debris monitoring (ODM). Inductive ODM sensor detects the small metal particles which are discharged from the defective machine components in the lubricating oil line. Inductive ODM sensor identifies metal particles signature by detecting changes in the inductance coil when metal particles pass through the sensor. However, inductive ODM sensor installed in engine oil line during operation is subject to heavy vibration which corrupts the metal particles signal. ANC can be applied to remove the interfering vibration signal and extract the metal particle signal provided the operating parameters can be properly determined.

1.2 Motivation and objectives

Adaptive filter provides a solution to process signals resulting from operations in an environment with unknown statistics, e.g., in the cases of bearing fault detection and oil debris monitoring. ANC utilizing the LMS algorithm is computationally efficient and suitable for on-line monitoring. However, when applying the ANC to extract desired signal from interferences, three main issues should be addressed:

- The selection of the transversal filter length. The transversal filter length affects the adaptive noise canceller's frequency selectivity to separate the desired signal from the interfering signal.
- The choice of the step-size parameter used in the LMS algorithm. The step-size parameter affects the stability and rate of convergence of the LMS algorithm and the performance of the ANC.
- The specification of the settling time needed for the ANC.

The main objective of this thesis is to establish appropriate selecting methods and guidelines for determining the operating parameters of the LMS based ANC. The ANC with the properly selected operating parameter is used to remove other interfering periodic signal from the corrupted bearing signal. The ANC is expected to deliver:

- efficient and fast computation so that it can be applied for on-line monitoring,

- enough frequency selectivity to separate interference signal (i.e. gear signal) that has frequency spectrum close to the bearing characteristic frequencies or the resonance frequency region of the system,
- easy-to-apply and robust criteria to determine the operating parameters of the LMS based ANC, and
- the adaptive process settling time

In order to verify that the ANC can successfully extract bearing signal from the corrupting interference signal, time domain and frequency domain fault identification methods will be introduced to compare and analyze the corrupted bearing signal and the extracted bearing signal in the simulation and experiment section.

One of the issues in an on-going industrial project is to cancel the vibration signal experienced by the inductive ODM sensor. ANC can be applied to remove the vibration signal and reveal the metal particles signal in the ODM application. As demonstrated later, these criteria to determine the operating parameters established in bearing fault detection can also be implemented in the ODM applications.

With the newly established selecting criterion of the ANC operating parameters detailed in this thesis, the effectiveness of the ANC in two different applications: 1) extracting the bearing signal from the interfering gear vibration signal in bearing fault detection and 2) removing the periodic interference vibration signal in the ODM application will be demonstrated and validated through simulations and experiments in this thesis.

1.3 Organization

The remainder of this thesis is organized as follows: Chapter 2 provides literature review of adaptive filtering with emphasis on least mean square adaptive noise canceller. Literature review on bearing fault detection and oil debris monitoring are also included. Chapter 3 reports the selecting criterion and design details of the operating parameters used in the adaptive noise canceller for extracting bearing vibration signal from the corrupted interference gear vibration signal. In Chapter 4, adaptive noise canceller is applied to extract non-periodic metal particle signal from interfering vibration signal in

the oil debris monitoring application. Conclusion and possible future research are given in Chapter 5.

2 Literature Review

This review focuses on: least mean square adaptive noise canceller, bearing fault detection, and oil debris monitoring. In the end of the chapter, a conclusion is given to summarize the review.

2.1 Least mean square adaptive noise canceller

There are two distinct approaches to time updating of the adaptive filter weights on a sample by sample basis (Haykin 2002). These two approaches are the stochastic gradient approach that utilizes the LMS algorithm and the least squares estimation method that applies the recursive least squares (RLS) algorithm. One major difference between these two algorithms is the computational complexity. The RLS algorithm has a computational complexity in the order of M^2, where M is the number of the adjustable filter weights. On the other hand, the computational complexity of the LMS algorithm is in the order of M. When the length of the adaptive filter weights M is large, the computational complexity of the RLS algorithm may become too excessive to apply for on-line application. Another difference between these two approaches is that the LMS algorithm is model independent while the RLS algorithm is model dependent. Therefore, the LMS algorithm in general exhibits a more robust tracking capability in a nonstationary environment than the RLS algorithm (Haykin 2002).

ANC was first implemented for echo cancellation of the speech signal (Haykin 2002). Acoustic echo cancellation used in the telecommunication industry is a form of the ANC. Mader et al. (2000) illustrated using acoustic echo canceller to cancel the acoustic echo in a hands-free telephone environment. ANC requires two input signals: the primary input signal and the reference input signal. The primary input signal contains the desired signal and the interfering signal that is not correlated with the desired signal. The ideal reference input signal contains only the interfering signal that is correlated to the interfering signal in the primary input. ANC operates on the reference input signal to provide an estimated interfering signal in the primary input signal. The error, which is the subtraction of the estimated interfering signal from the primary input signal, is fed back

to adjust the adaptive filter weights. The output of the ANC provides an estimate of the desired signal in the minimum mean square error sense.

Another form of the ANC which does not require a separate reference signal source was shown by Widrow et al (1975a). In this case, the primary input signal contains the desired signal and the interfering signal, and the two are not correlated. The reference input signal is a delayed version of the primary input signal. The assumption is that the delay causes the desired signals in the primary input and the reference input to become de-correlated. Obviously, in order to use this special form of the ANC, the desired signal has to become de-correlated with itself after delay.

The LMS algorithm used in the ANC originates with Widrow and Hoff (Widrow and Stearns 1985). In a stationary environment, the LMS algorithm converges to the optimum Wiener solution after an iteration process. In a nonstationary environment, the LMS algorithm is able to tract time variations in the statistics of the input data, provided that the variations are sufficiently slow (Haykin 2002). The LMS algorithm built around a transversal (i.e. tapped-delayed-line) structure can be described as
(updated tap-weight vector) = (one step before tap-weight vector) + (step-size parameter)(tap-input vector)(error signal)

Widrow et al (1975a) indicated that the desired adaptive noise canceller's frequency resolution is related to the transversal filter length. Ziedler et al (1978) further demonstrated that the adaptive transversal filter length affects the selectivity of the adaptive noise canceller's frequency response. However, their studies do not provide a practical guideline to select the transversal filter length in applications with unknown system statistics.

The step-size parameter determines the stability and the rate of convergence of the LMS algorithm. The step-size parameter also controls the LMS filter weight fluctuations (Widrow and Stearns 1985 and Haykin 2002). Fluctuations of the LMS filter weights influence individual LMS applications and therefore affect the ANC performance. There are many studies on the stability of the LMS algorithm and the step-size parameter boundary (Guo et al. 1997, Solo 1997, and Butterweck 2001). However, the stability boundary of the step-size parameter does not translate to the satisfactory performance of the ANC. When the step-size is just below the stability boundary, individual LMS

applications experience large filter weight fluctuations and therefore the ANC does not achieve satisfactory performance.

Hassibi and Sayed (1996) and Hassibi et al (1993) discussed the H^∞ optimality of the LMS algorithm. They derived the boundary condition of the LMS algorithm step-size parameter which results the LMS algorithm to be H^∞ optimal. However, we can not use the derived H^∞ optimal step-size parameter boundary condition of the LMS algorithm to measure the LMS filter weight fluctuations. Therefore, no direct association can be drawn between the performance of the ANC and the H^∞ optimality of the LMS algorithm.

2.2 Bearing fault detection

Rolling element bearings can be found in many domestic and industrial applications. The proper functioning of these appliances and machines depends on the effective operation of these bearings. A defect in a rolling element bearing can lead to machine malfunctions, and if not detected and fixed in time it may cause failures of other components and catastrophic failure of the machine. In industrial applications such as helicopter gearbox or jet engine monitoring, bearing fault detection is critical and necessary. There are numerous bearing fault detection and diagnosis methods which include vibration analysis, acoustic measurements, temperature measurement, oil debris monitoring and others. More detailed reviews of various bearing fault detection and diagnosis methods can be found in Tandon and Nakra (1992), Tandon and Choudhury (1999), and Randall (2001).

Among these methods, vibration analysis is the most widely used (Tandon and Choudhury 1999). Vibration analysis is often done based on the bearing vibration signal measured by an accelerometer, usually a piezoelectric sensor, to convert the vibration signal to electrical signal. Many types of defects or damage on the rolling surfaces affect the machinery vibration. These defects include the cracks, pits and spalls of the races or the rolling elements. When a defect on an element makes contact with its mating element, the impact generates a pulse of very short duration. It is these series of impulses that provides the faulty bearing signature in the vibration signal.

Many different techniques have been applied to analyze the vibration response of the rolling element bearings. The time domain techniques include the use of crest factor, kurtosis value, and others. However, the reliability of these methods depends largely on the ability to obtain clean bearing signal. When the monitored bearing signal is corrupted by other interference signals, these methods may not provide reliable results.

The most widely used bearing fault detection techniques are based on the spectral analysis of the vibration signal. Each bearing element has a characteristic rotational frequency. When a defect occurs on a particular bearing element, an increase in the contact stress at this element's rotational frequency occurs. These bearing characteristic frequencies are given below (Raymond and Guyer 1996, Lipovszky et al 1990, and Li et al 2000):

$$\text{Outer race frequency, } f_o = \frac{N_B}{2} f_S \left(1 - \frac{D_b \cos\theta}{D_c}\right), \tag{2-1}$$

$$\text{Inner race frequency, } f_i = \frac{N_B}{2} f_S \left(1 + \frac{D_b \cos\theta}{D_c}\right), \tag{2-2}$$

$$\text{Rolling element frequency } f_b = \frac{D_c}{2D_b} f_S \left(1 - \frac{D_b^2 \cos^2\theta}{D_c^2}\right), \text{ and} \tag{2-3}$$

$$\text{Cage frequency } f_c = \frac{1}{2} f_S \left(1 - \frac{D_b \cos\theta}{D_c}\right), \tag{2-4}$$

where f_s is the shaft rotation frequency, N_B is the number of the rolling element, D_b is the diameter of the rolling element, D_c is the pitch diameter of the rolling element, and θ is the contact angle. The bearing characteristic defect frequencies are usually provided by the bearing manufacturers.

These bearing characteristic frequencies can be used to detect the bearing defects in the frequency spectrum. Each specific bearing characteristic frequency also indicates the location or source of the defect in a rolling bearing. However, a significant peak at these bearing characteristic frequencies in the direct spectrum can be hard to obtain from a faulty bearing and further signal processing is usually needed.

The contact between a defect on an element and its mating element produces pulse of very short duration. These pulses excite the natural frequencies of bearing elements and housing structures and result an increase in the vibration energy at these

resonance frequencies (Harris 1984 and Tandon and Choudhury 1999). Many signal processing techniques utilize this phenomenon to design band-pass filter around the resonance regions in order to obtain stronger bearing vibration signal. The shock pulse method and the demodulated resonance analysis (envelope spectrum analysis) are techniques based on this principle (Butler 1973, Morando 1988, McFadden and Smith 1984b, and Hockmann and Bechhoefer 2005). However, resonance frequencies of the system can be difficult to locate and can vary widely from one system to another. Since the resonance frequencies of a system can not be obtained accurately, there are no reliable methods to design the band-pass filters and this would undermine the effectiveness of these techniques.

2.3 Oil debris monitoring

The purpose of oil debris monitoring is to provide non-destructive examination of oil-wetted parts of a machine by monitoring the content of the lubricating oil. Particles contained in the lubricating oil carry important information about the condition of the machine. Some researchers have compared the debris monitoring in the oil line to the blood monitoring of a human (Whittington et al 1992).

One widely used oil debris monitoring method is the magnetic sump plug. A magnetic sump plug or the so-called magnetic chip detector uses a magnet to capture metallic debris from the lubricating oil flow path. The amount of the metallic debris captured indicates the wear state of the machine. However, this method requires shutting down the machine to retrieve the sump plug and is prone to false alarms due to the build up of fine ferromagnetic debris (Howe and Muir 1997). Another oil debris monitoring method, the ferrographic technique, uses magnets of increasing strength to separate wear particles from the lubricating oil and grades particles by size and magnetic susceptibility on a glass slide (Westcott and Seifert 1975). However, the interpretation of the results is rather subjective and the ferrographic method cannot be applied for on-line application (Whittington et al 1992 and Roylance 2005).

An on-line oil debris monitoring system is needed to eliminate the need for regular human intervention and improve operating efficiency. The inductive ODM

system can be implemented for on-line operation (Flanagan et al 1990 and Yin et al 2003). Inductive ODM sensor is used to detect metal particles in the lubricating oil. When a metal particle in the lubricating oil flows through a transducer coil, it causes small changes in the inductance of the coil. The amplitude of the output signal can be used to identify the particle size. Ferromagnetic particles increase coil inductance and non-ferromagnetic particles reduce coil inductance (Whittington et al 1992). Hence, these two different types of particles create opposite phases in their respective output signals. Therefore, inductive sensors can also distinguish between ferrous and non-ferrous metal particles.

Miller and Kitaljevich (2000) applied on-line ODM to detect bearing failure in an aircraft engine and concluded that the ODM sensor is capable of detecting early bearing damage and monitoring the progression of damage toward failure. Dempsey (2001) and Dempsey et al (2004) used on-line ODM to detect gear failure in the helicopter transmission gearbox and showed that particle counts and oil debris mass increase in correlation with the damage magnitude. As the same ferrous or non-ferrous material is commonly used to construct both bearings and gears, Dempsey et al (2004) concluded that ODM sensor alone cannot discriminate between bearing and gear fatigue damage when both share a common lubrication system. Dempsey (2000) and Dempsey and Afjeh (2002) further integrated on-line ODM and vibration analysis into a health monitoring system using fuzzy logic and the result indicated improved detection and decision-making capabilities.

Aircraft engines and helicopter transmission gearboxes experience strong vibration during operation. Vibration affects the capability of using the inductive ODM sensor to detect metal particles. Howe and Muir (1997) indicated that the minimum detectable particle sizes of the inductive sensor are determined primarily by the inner diameter of the coil assembly and the operating environment such as vibration and temperature. The vibration signal experienced by the sensor corrupts the metal particle signal and the metal particle signatures can no longer be correctly detected from the resulting signal mixture. In order to obtain reliable metal particle counts and sizes, it is critical that the interfering vibration signal is removed.

2.4 Summary

1. Least mean square adaptive noise canceller:
    - LMS algorithm is computationally efficient and is model independent (Haykin 2002).
    - The LMS based ANC requires two input signal: the primary input signal and the reference input signal.
    - A special form of the ANC requires only one input signal provided that the desired signal in the input signal is de-correlated from the desired signal in the delayed input signal.
    - The adaptive noise canceller's frequency selectivity is controlled by the transversal filter length (Ziedler et al 1978 and Widorw et al 1975b).
    - The step-size parameter determines the least square algorithm's stability and converging rate. A large step-size achieves faster convergence but an excessive large step-size results divergence of the LMS algorithm (Gu et al 2003).
    - The step-size parameter also controls the LMS transversal filter weight fluctuations and affects the adaptive noise canceller performance (Haykin 2002).
2. Bearing fault detection
    - Time domain bearing fault detection techniques such as the crest factor and the kurtosis value are not reliable when the monitored bearing signal is corrupted by other interfering signals.
    - Bearing characteristic frequencies are used to indicate the locations of the faults in the signal spectrum.
    - The shock pulse method and the demodulated resonance analysis rely on the band-pass filtering of the system resonance frequencies. However, there are no reliable methods for the design of the band-pass filter due to the difficulty of locating the system resonance regions.
    - When the collected bearing signal is corrupted by strong interfering signals, many of the existing bearing fault detection techniques do not perform well.
3. Oil debris monitoring

- The inductive ODM system is suitable for on-line monitoring (Flanagan et al 1990 and Yin et al 2003).
- The amplitude of the ODM sensor output signal is used to estimate the wear particle size. The phase of the sensor output signal can be used to distinguish ferromagnetic particles from non-ferromagnetic particles (Whittington et al 1992).
- Vibration affects the capability of the ODM inductive sensor to detect metal particles.
- Strong vibration signal experienced by the ODM sensor corrupts the metal particle signal and the metal particles signature can no longer be correctly detected from the resulting mixed signal.

3 Bearing Signal Extraction and Fault Detection using Adaptive Noise Cancellation

In rotational machinery, bearings are crucial components and are prone to failure. Bearings are usually enclosed inside the machine and require a great deal of effort to inspect physically. Vibration analysis based on vibration signal collecting from accelerometers is an effective tool for detecting incipient bearing faults for on-line machine health monitoring. In vibration analysis, accelerometers are placed close to the component that needs to be monitored in order to collect the best available vibration signal from that component. However, there are usually many components inside rotating machinery and it is inevitable that the collected vibration signal also contains signals from other components.

This condition is evident in monitoring the bearing vibration signal in an enclosed environment like a gearbox. An accelerometer is placed in the vicinity of the monitored bearing outside the gearbox. The collected vibration signal contains the monitored bearing signal corrupted by interfering signals from other components such as gears. Often times the monitored bearing signal is weaker than the interfering gear meshing signals and as a result, the characteristic of the monitored bearing signal can no longer be recognized and detected from the acquired vibration signal.

Adaptive noise cancellation is a method to estimate signal corrupted by additive interference. For machine health monitor vibration analysis, ANC can be applied to separate the periodic faulty impulsive bearing signal from the interference gear signal. The performance and the stability of the ANC depend on its operating parameters: the length of the adaptive filter and the step-size parameter. In this chapter, a brief introduction to the ANC is provided. Methods and guidelines for selecting the adaptive filter length and the step-size parameter for applying the ANC in bearing fault detection are given. The settling time issue of the ANC in on-line monitoring is also addressed. Simulations and experiments using these operating parameters will verify the effectiveness of the ANC in extracting the faulty bearing signal from the corrupting signal.

3.1 Introduction

In machines fault detection, the acquired monitored bearing signal is often corrupted by the stronger gear signals. Gear signal constitutes mainly gear meshing vibration and the spectrum is dominated by the harmonic gear meshing frequency. If the interfering gear meshing frequency is known, we can design a fixed notch filter tuned to the frequencies of interference. However, in order to design such a filter, the precise interference sinusoidal frequencies need to be known beforehand. In situations where no prior knowledge of the interference signal is available or the interference sinusoidal frequencies vary slowly, fixed notch filter cannot be used to remove the interference signal.

Widrow et al (1975a) has shown that ANC is able to track the interference signal without prior knowledge of the interference frequency. ANC is capable of handling both stationary and non-stationary signals and can track the interference signal if it drifts slowly (Widrow et al 1976). These characteristics make the ANC a suitable tool to deal with machine vibration signals because: a) the rotating machine operates at various speeds and the interference gear meshing frequency varies with the operating speed of the machine, and b) due to the motor speed variation and the load condition, the interference gear signal can drift slowly from time to time.

3.2 Adaptive noise cancellation

This section will illustrate the basic concept of the adaptive noise cancellation method. Least mean square algorithm, the basic element of the adaptive noise cancelling system, is examined in order to get a good understanding of the adaptive nature of the adaptive noise canceller. Methods and guidelines to select the proper operating parameters when applying the ANC in bearing fault detection will be given and explained. A procedure to reach the steady state ANC without any settling time in on-line application is shown. In the end, the steps to apply the adaptive noise cancellation method in bearing fault detection will be summarized.

3.2.1 Least mean square algorithm

The least mean square algorithm is a linear adaptive filtering algorithm. Haykin (2002) described the LMS algorithm as two basic processes: filtering process and adaptive process. In the filter process, the output of the filter is calculated by multiplying the transversal filter weights with the tap inputs. An estimation error is then generated by subtracting this output from a desired response. In the adaptive process, the filter weights are automatically adjusted according to the estimation error using the recursive optimization method known as the method of steepest descent, a gradient search method. The combination of the filter process and the adaptive process includes a feedback loop, as illustrated in Figure 3-1.

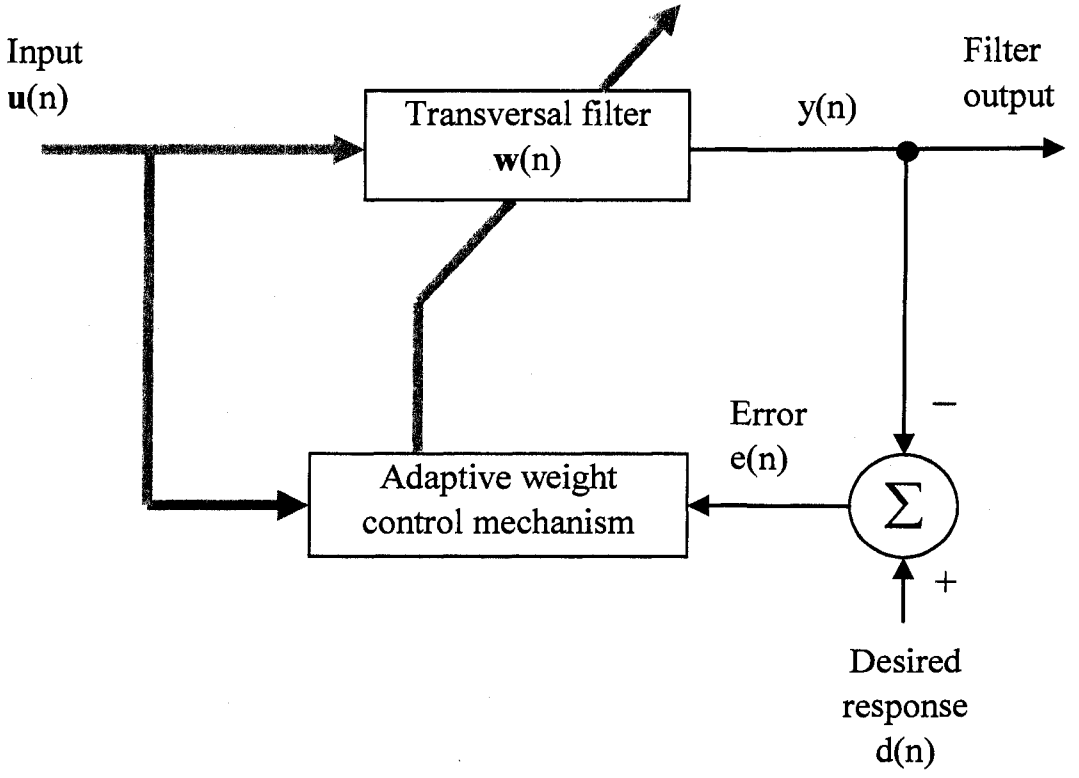

Figure 3-1. Block diagram of adaptive transversal filter

The input signal vector $\mathbf{u}(n)$ is defined as

$$\mathbf{u}(n) = \begin{bmatrix} u(n) \\ u(n-1) \\ \vdots \\ u(n-M+1) \end{bmatrix} \tag{3-1}$$

and the transversal filter weight vector $\mathbf{w}(n)$ is

$$\mathbf{w}(n) = \begin{bmatrix} w_0(n) \\ w_1(n) \\ \vdots \\ w_{M-1}(n) \end{bmatrix} \tag{3-2}$$

where n is the index of the discrete time and M is the length of the transversal filter weights. Notice that $n >= M$ since the length of the filter weights cannot exceed the signal length. The output of the transversal filter $y(n)$ is the result of the matrix multiplication of $\mathbf{u}$(n) and $\mathbf{w}(n)$ which can be represented as

$$y(n) = \mathbf{u}(n)^T \mathbf{w}(n) = \mathbf{w}(n)^T \mathbf{u}(n) \tag{3-3}$$

where the symbol ^{T} means the matrix transpose. The estimation error $e(n)$ is obtained by subtracting the output of the filter $y(n)$ from the desired response $d(n)$, i.e.,

$$e(n) = d(n) - y(n) = d(n) - \mathbf{w}(n)^T \mathbf{u}(n) \tag{3-4}$$

As the name "least mean square algorithm" suggests, the algorithm adjusts the weights of the filter to minimize mean square error. A general expression for mean square error as a function of the weight values can be derived by squaring both sides of Eq. 3-4. Then we obtain the instantaneous squared error as follows

$$e^2(n) = d^2(n) - 2d(n)\mathbf{w}(n)^T \mathbf{u}(n) + \mathbf{w}(n)^T \mathbf{u}(n)\mathbf{u}(n)^T \mathbf{w}(n) \tag{3-5}$$

The instantaneous gradient vector $\nabla(n)$ of the squared error function is obtained by partial differentiation of Eq. 3-5 with respect to the weight component and is expressed as (Widrow et al 1975b and Monzingo and Miller 1980)

$$\nabla(n) = \begin{bmatrix} \dfrac{\partial e^2(n)}{\partial w_0(n)} \\ \dfrac{\partial e^2(n)}{\partial w_1(n)} \\ \vdots \\ \dfrac{\partial e^2(n)}{\partial w_{M-1}(n)} \end{bmatrix} = -2d(n)\mathbf{u}(n) + 2\mathbf{u}(n)\mathbf{u}(n)^T\mathbf{w}(n) = -2\mathbf{u}(n)[d(n) - \mathbf{u}(n)^T\mathbf{w}(n)] \quad (3\text{-}6)$$

Substituting Eq. 3-4 into Eq. 3-6, we obtain

$$\nabla(n) = -2\mathbf{u}(n)e(n) \quad (3\text{-}7)$$

The LMS algorithm is an implementation of the method of steepest descent. Steepest descent is a form of iterative adjustments applied to the weight vector $\mathbf{w}(n)$ in the direction opposite to the gradient vector. According to this method, the next discrete time weight vector $\mathbf{w}(n+1)$ is equal to the present weight vector $\mathbf{w}(n)$ plus a change proportional to the negative gradient (Widorw et al 1975b and Haykin 2002):

$$\mathbf{w}(n+1) = \mathbf{w}(n) - \mu\nabla(n) = \mathbf{w}(n) + 2\mu\mathbf{u}(n)e(n) \quad (3\text{-}8)$$

where μ is a positive real number, called the step-size parameter, and controls the stability and rate of convergence of the LMS algorithm.

The detailed signal-flow-graph representation of the LMS algorithm is depicted in Figure 3-2 where the recursive scheme to update the filter transversal weights can be seen. The LMS algorithm can be summarized as the following three steps:

Step 1. Output filtering by

$$y(n) = \sum_{k=0}^{M-1} w_k(n)u(n-k), \ k = 0,1,2,...,M-1 \quad (3\text{-}9)$$

Step 2. Error estimation, i.e.,

$$e(n) = d(n) - y(n) \quad (3\text{-}10)$$

Step 3. Filter weights adaptation using

$$w_k(n+1) = w_k(n) + \mu u(n-k)e(n), \ k = 0,1,2,...,M-1 \quad (3\text{-}11)$$

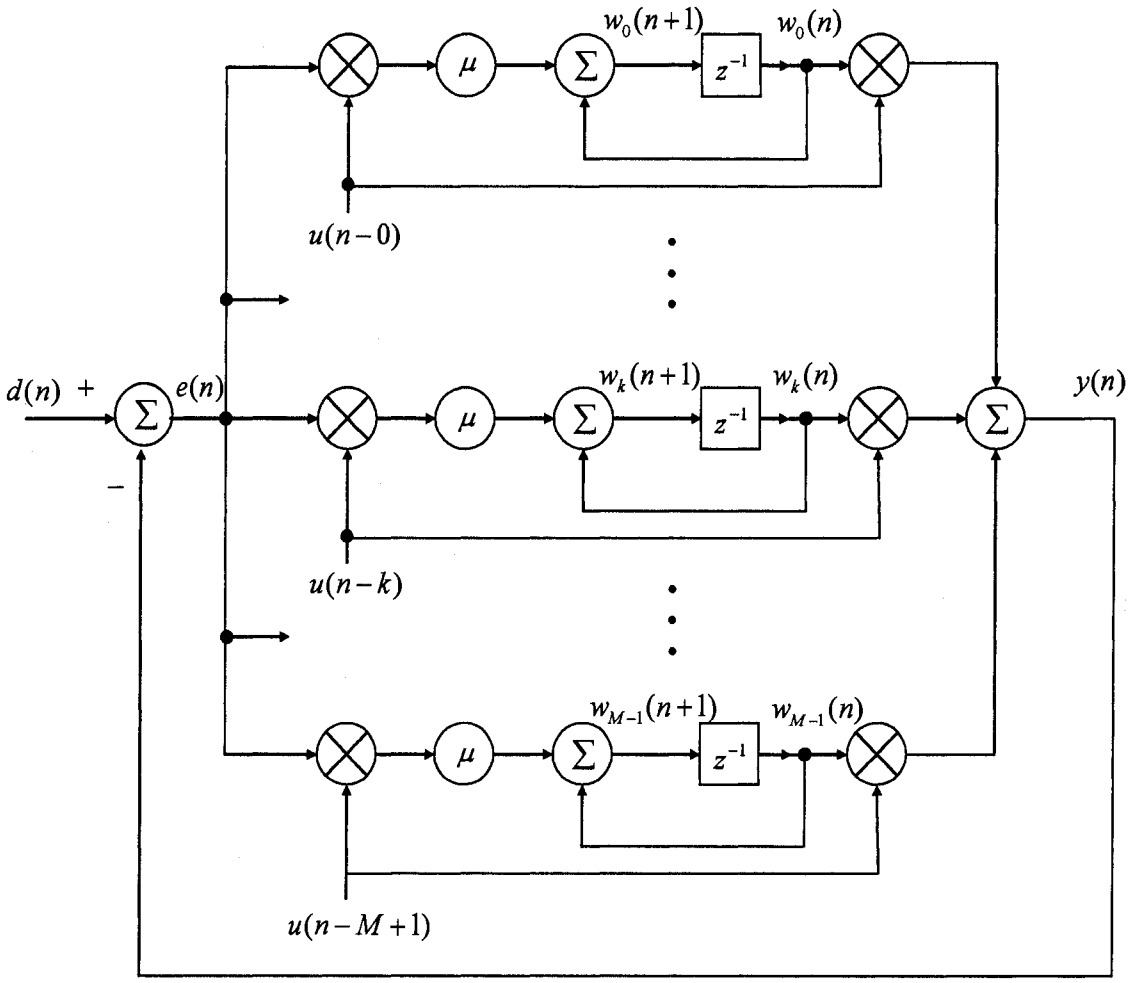

Figure 3-2. Signal-flow-graph representation of an adaptive noise canceller

Widrow et al (1975a) indicated that the filter weights using LMS algorithm converges to the Wiener filter weights in the statistic sense if the step-size parameter μ is sufficiently small. The Wiener filter is a linear optimum discrete time filter (see appendix A for the Wiener filter theory). The LMS algorithm is a practical method for finding a close approximate solution to the Wiener filter in actual practice. However, unlike the Wiener filter, the LMS algorithm does not require measurements of the correlation matrix and matrix inversion. However, the performance of the LMS algorithm is limited by statistical sample size since the weight values found are based on real-time measurements of the input signal (Widorw et al 1975b). The simplicity and computation

efficiency of the LMS algorithm makes it the most extensively used adaptive filtering algorithm (Zeidler 1990).

3.2.2 Adaptive noise canceller in machine fault detection

The general concept of the ANC was discussed in detail by Widrow et al (1975a). Figure 3-3 shows the block diagram of an ANC. The primary input signal $d(n)$ (the desired signal in the LMS algorithm) contains the monitored component signal and periodic interference signal from other components in the machine that are uncorrelated with each other. In the ideal situation, the reference input signal $u(n)$ (the input signal in the LMS algorithm) supplies only the periodic interference signal which is a correlated version of the periodic interference in the primary input signal. The transversal filter weights are adapted through the response of the error signal $e(n)$ using the LMS algorithm. The adaptive filter output $y(n)$ provides an estimate of the periodic interference signal contained in the primary input. By subtracting the adaptive filter output $y(n)$ from the primary input, the effect of the periodic interference is diminished.

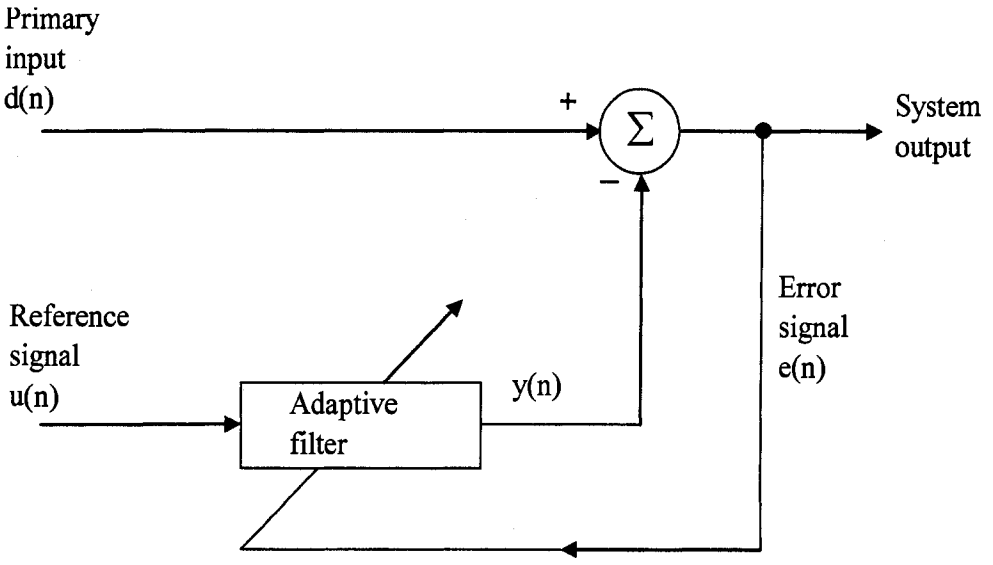

Figure 3-3. Block diagram of an adaptive noise canceller

ANC using the LMS algorithm behaves like an adaptive notch filter whose null point is determined by the periodic interference frequency. ANC is tuneable and the

tuning frequency moves with the periodic interference frequency. Widrow et al (1975a) showed that the notch in the frequency response of the ANC can be made very sharp at precisely the frequency of the periodic interference by choosing a small enough value of the step-size parameter μ.

When applying the ANC to monitor bearing health condition in rotating machinery, the sensor is mounted near the monitored bearing and the collected primary input signal contains a mixture of the bearing signal and the interference gear signal. Another sensor is mounted close to the gears and farther away from the monitored bearing. The collected reference input signal contains mostly interference gear signal but can also contains some bearing signal component. The effect of the reference input signal containing some monitored signal has been discussed by Widrow et al (1975a) and Chaturvedi and Thomas (1981). To see the statistical analysis of the ANC in bearing health monitoring subject to interference gear signal and the effect of the bearing signal present in the reference input, please refer to appendix B and C.

3.2.3 The length of the adaptive filter M

Ziedler et al (1978) demonstrated that the adaptive transversal filter length M determines the selectivity of the filter's frequency response. If the filter length is too small, the filter will not have enough spectral resolution and results a highly smoothed spectrum. If the filter length is too large, the filter introduces spurious detail into the spectrum (Kay and Marple 1981). Widrow et al (1975a) suggested setting the transversal filter length equal to twice the ratio of the total signal bandwidth to the desired frequency resolution of the filter. However, this guideline is not useful in applications such as machine fault detection. The main reason is that, in bearing health monitoring, the total signal bandwidth of the reference input signal which contains mainly the interference gear meshing frequencies and their respective harmonics is difficult to estimate. The desired frequency resolution of the filter requires enough frequency selectivity to separate the gear meshing frequencies and their harmonics from the faulty bearing characteristic frequencies and the system resonance frequency regions. For many real applications, the system resonance frequency regions are not known. In addition, as the operating speed of the machines changes, the desired frequency resolution changes as well. Therefore, no

practical estimation of the filter length can be obtained from this guideline for bearing fault detection.

The LMS algorithm uses an autoregressive (AR) model to construct the adaptive transversal filter. The output signal $y(n)$ (Eq. 3-9) is obtained from the AR model of the reference input signal $\mathbf{u}(n)$. A common approach to estimate the AR model order (filter length M) is to construct AR models of increasing order until the computed prediction error power reaches a minimum (Kay and Marple 1981 and Kay 1988). However, for real signals with noise, the error power obtained from the least squares estimation procedure decreases monotonically with increasing model order. Akaike (1974) used a maximum likelihood approach to determine the model order by minimizing an information theoretic function. The Akaike information criterion (AIC) is

$$AIC(l) = N \ln(\varepsilon_l) + 2l \tag{3-12}$$

where l is the model order, N is the total data length, and ε_l is the error power associated with the model order l which can be obtained by the well-established Levinson-Durbin recursion. The first term in Eq. 3-12 decreases as the model order increases since the error power decreases monotonically. The second term in Eq. 3-12 represents the penalty for increasing spectral variance due to increasing model order. The model order l which minimizes the AIC is the optimal model order. The AIC method is frequently used in AR model order selection and has shown to provide high frequency resolution (Kay and Marple 1981, Wang and Wong 2002).

In both simulations and experiences, filter lengths determined by Eq. 3-12 have shown to be able to provide enough frequency resolution for bearing fault detection. The AIC method can be used under different sampling rates and different signal data length, and does not require any prior signal content information. In practice, the adaptive filter length M does not need to be recalculated every time for on-line monitoring. When the machine operating speed is constant, the filter length does not change or changes very little from each sampled data block. Therefore, the filter length only needs to be recalculated and updated when the operating condition changes. Thus, the computation time and power required to perform Levinson Durbin recursion for the AIC will not impede the on-line application.

3.2.4 The step-size parameter μ

The LMS algorithm used in the ANC involves feedback and therefore, the algorithm is subject to the possibility of becoming unstable. An excessively large value of the step-size μ can result in instability of the LMS algorithm. A large value of μ, even if it does not cause instability of the LMS algorithm, can result in large adaptive filter weight fluctuations. From Eq. 3-11, we can see that a large value μ produces large changes of the updated weights throughout iterations of the LMS algorithm. Large filter weight fluctuations affect the performance of the ANC and are undesirable in individual applications of the LMS algorithm. A small value μ ensures small adaptive filter weight fluctuations but comes at the expense of the converging rate. For short data length, a slow convergence rate can mean that the steady state is not reached before the adaptive process reaches the end of the signal samples. However, excessively long data length means long delay and will make on-line application impractical.

The small-step-size statistical theory (Haykin 2002) shows that the stability of the LMS algorithm for stationary, stochastic signals is determined by two factors: the step-size parameter μ and the correlation matrix $\mathbf{R}$ of the input vector $\mathbf{u}(n)$. The small-step-size statistical theory is based on the assumption that the step-size parameter μ is small and therefore only zero-order solution of the LMS filter needs to be considered. The weights of the adaptive filter according to small-step-size statistical theory will converge and remain stable as long as the step-size parameter satisfies the following condition (Haykin 2002)

$$0 < \mu < \frac{2}{\lambda_{max}} \tag{3-13}$$

where λ_{max} is the largest eigenvalue of the input correlation matrix $\mathbf{R}$. In practice, the input correlation matrix $\mathbf{R}$ of real signal is not available and therefore, Eq. 3-13 cannot be used to determine the step-size parameter μ.

For the above reason, the step-size parameter μ can be determined based on the mean square error. The mean square error $J(n)$ is the ensemble averaging of the squared estimation error $|e(n)|^2$ of the LMS filter and can be expressed as (Haykin 2002)

$$J(n) = E\left[|e(n)|^2\right] \tag{3-14}$$

If we denote $J(\infty)$ as the steady state value of the mean square error of the LMS filter and $J_{\min}$ as the minimum mean square error of the Wiener filter, the steady state value of the excess mean square error $J_{ex}(\infty)$ can be expressed as (Haykin 2002)

$$J_{ex}(\infty) = J(\infty) - J_{\min} \tag{3-15}$$

The ratio of the steady state value of the excess mean square error $J_{ex}(\infty)$ of the LMS filter to the minimum mean-square error $J_{\min}$ of the Wiener filter is defined as the misadjustment. The misadjustment, β, is related to the step-size parameter μ and the sum of the eigenvalues of the input correlation matrix $\mathbf{R}$ by (Haykin 2002)

$$\beta = \frac{J_{ex}(\infty)}{J_{\min}} = \frac{\mu}{2}\sum_{l=1}^{M}\lambda_l \tag{3-16}$$

where λ_l is the lth eigenvalue of the input correlation matrix $\mathbf{R}$. From the result of the eigendecomposition, the trace of the input correlation matrix $\mathbf{R}$ is equal to the sum of its eigenvalues. Furthermore, for a stationary process, the trace of the input correlation matrix $\mathbf{R}$ is equal to the mean square value of the input at each of the M taps in the transversal filter. Thus, Eq. 3-16 becomes (Haykin 2002)

$$\beta = \frac{\mu}{2}tr[\mathbf{R}] = \frac{\mu}{2}E\left[\|\mathbf{u}(n)\|^2\right] \tag{3-17}$$

where $tr[\mathbf{R}]$ is the trace of the input correlation matrix $\mathbf{R}$ and $E\left[\|\mathbf{u}(n)\|^2\right]$ is the ensemble average of the total tap-input power $\|\mathbf{u}(n)\|^2$. The misadjustment is positively correlated to the filter weight fluctuations of individual LMS applications. The smaller the misadjustment, the smaller the individual LMS filter weight fluctuations. We can also see from Eq. 3-17 that a small misadjustment translates to a small step-size parameter μ which means a slower convergence rate of the LMS filter.

In order to achieve satisfactory performance of the ANC, small individual adaptive filter weight fluctuations are required. Therefore, we can estimate the required misadjustment which ensures a small enough weight fluctuation of the ANC and obtained the proper step-size parameter μ using Eq. 3-17.

In simulations and experiments, satisfactory performance of the ANC is achieved with a misadjustment of 0.025. This misadjustment value means that the LMS algorithm produces a mean square error that is 2.5 percent greater than the minimum mean square error $J_{\min}$ of the Wiener filter. Depending on the application, a larger misadjustment can be used to ensure faster convergence when the ANC is applied in a non-stationary environment.

3.2.5 Steady state adaptive noise canceller

This section provides a procedure that results in no settling time to reach the steady state ANC output signal in a stationary environment (constant machine operating speed). The convergence speed of the LMS algorithm depends on two factors: the eigenvalue distribution of the input autocorrelation matrix $\mathbf{R}$ and the chosen initial adaptive filter weights (Flores and Widrow 2004). Since the input autocorrelation matrix $\mathbf{R}$ is not attainable in actual practice, we can only estimate the convergence speed of the LMS algorithm in actual practice.

The curve obtained by plotting the ensemble average of the squared estimation error $|e(n)|^2$ verses the number of iterations, n, is called the learning curve. The learning curve of the LMS filter consists of a sum of exponential natural modes, each of which corresponds to an eigenvalue of the input correlation matrix $\mathbf{R}$. The time constant of the lth exponential natural mode is related to the lth eigenvalue λ_l of the input correlation matrix $\mathbf{R}$ and the step-size parameter μ by (Haykin 2002)

$$\tau_l = \frac{1}{2\mu\lambda_l} \tag{3-18}$$

The average eigenvalue λ_{av} for the input correlation matrix $\mathbf{R}$ can be defined as (Haykin 2002)

$$\lambda_{av} = \frac{1}{M}\sum_{l=0}^{M}\lambda_l \tag{3-19}$$

The ensemble average learning curve of the LMS algorithm can be approximated by a single exponential with average time constant τ_{av} which can be defined as (Haykin 2002)

$$\tau_{av} = \frac{1}{2\mu\lambda_{av}} \tag{3-20}$$

For a stationary process, using Eq. 3-16 and 3-17, Eq. 3-20 becomes

$$\tau_{av} = \frac{M}{4\beta} \tag{3-21}$$

From Eq. 3-21 and Eq. 3-17, we can see that a large average time constant τ_{av} corresponds to a small misadjustment and a small step-size parameter μ. The settling time of the LMS algorithm is proportional to the average time constant τ_{av} of the ensemble average learning curve. Depending on the values of the initial adaptive filter, the settling time of the LMS algorithm to reach steady state ANC can take from $0\tau_{av}$ to $3\tau_{av}$ (less than 5 percent of the initial ensemble average squared error value) iterations.

In practice, when applying the ANC for on-line bearing signal monitoring at constant machine operating speed (stationary environment), the first sampled data block which has more than $3\tau_{av}$ sampled data can be used to obtain the steady state adaptive filter weights. The last updated filter weights of the first sampled data block is saved and used as the initial filter weights to process the second sampled data block. The last updated filter weights of the second sampled data block is again used as the initial filter weights for the next sampled data block. Through this procedure, the steady state filter weights are used as the initial filter weights for all the sampled data blocks. The steady state ANC output signal is thus obtained without any settling time when monitoring bearing signal at constant machine operating speed.

3.2.6 Summary steps to apply ANC in bearing signal extraction

The following steps summarize procedures utilizing ANC for on-line bearing signal extraction when the monitored bearing signal is corrupted by other periodic interfering sources.

Step 1. Find a location to mount the accelerometer that is closest to the monitored component. Use the acquired signal as the primary input signal.

Step 2. Find a location to mount another accelerometer that is close to the interference source and farther away from the monitored component such that it will acquire

mainly the interfering signal components. The signal collected by this sensor is used as the reference input signal.

Step 3. Set the transversal filter length. Minimize $AIC(l) = N\ln(\varepsilon_l) + 2l$ where l is the model order, N is the total data length, and ε_l is the error power associated with the model order l which can be obtained by Levinson-Durbin recursion. The model order l which minimizes the AIC is equal to the transversal filter length M.

Step 4. Set the step-size parameter. The step-size parameter μ is obtained by setting the misadjustment $\beta = \frac{\mu}{2} E\left[\|u(n)\|^2\right] \approx 0.025$ where $E\left[\|\mathbf{u}(n)\|^2\right]$ is the average total reference input power.

Step 5. The last adaptive filter weights are saved from each sampled data block and used as the initial filter weights of the next sampled data block. In a stationary environment, the ANC has no settling time.

Step 6. Apply the ANC. The ANC output signal removes the corrupting interference gear signals and reveals the bearing signal.

3.3 Simulation

In this section, bearing and gear vibration signal models will be established. The mixed bearing and gear simulated vibration signals will be used to create the primary input and reference input signal. Time domain and frequency domain fault indicators will be introduced to analyze the performance of the ANC. The simulation result shows that the ANC with the above established operating parameters selecting methods can be used to extract the faulty bearing signal from the corrupted primary input signal and the resulting ANC output signal can be used to detect bearing fault.

3.3.1 Gear vibration signal model

In the following, a signal model of the normal gear vibration signal is presented. In general, vibration signals for healthy gears are dominated by gear meshing vibration accompanied by some modulation effects caused by geometric and assembly errors,

speed and load fluctuations (Wang and Wong 2002, Fan and Zuo 2006). The signal model $g(n)$ of a pair of normal gears meshing under constant load and speed with identical and equally spaced tooth can be represented by (McFadden 1986)

$$g(n) = \sum_{m=1}^{G} X_m \cos(2\pi m L f_s n + \phi_m), \tag{3-22}$$

where $m(1,2,...,G)$ is the meshing harmonic number, X_m and ϕ_m are the amplitude and the phase of the m th meshing harmonic respectively, L is the number of gear teeth, f_s is the shaft rotation frequency, n is the index of the discrete times and Lf_s is the meshing frequency. Eq. 3-22 is a summation of a series of sinusoidal functions and indicates that the vibration signal acquired from a normal gear exhibits general predominant frequency components at the meshing frequency and its harmonics.

Figure 3-4 shows the simulation of the gear meshing vibration signal of a pair of gears based on Eq. 3-22 mixed with white Gaussian noise. The gear meshing frequency (Lf_s) is 52 Hz and the simulated gear signal contains five meshing harmonics (G=5). The amplitudes (X_m) and phases (ϕ_m) of the corresponding gear meshing harmonic are assigned arbitrarily with the second and third harmonic dominating the frequency spectrum at 104 Hz and 156 Hz respectively. The white Gaussian noise is generated with random numbers whose elements are normally distributed with a mean of 0 and variance of 1. The ratio of the amplitude of the largest gear meshing harmonic X_2 vs. the noise power σ^2 is 1.33. The sampling rate is 4000Hz.

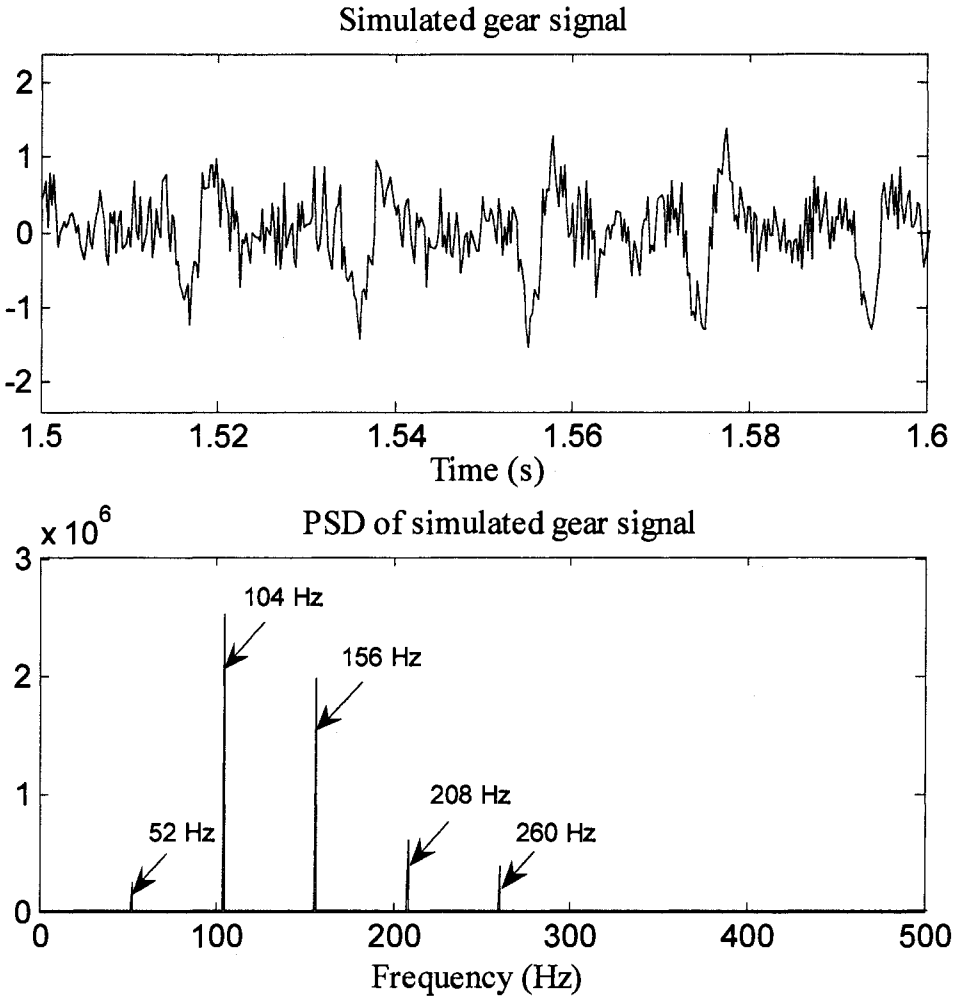

Figure 3-4. Simulated normal gear vibration signal

3.3.2 Faulty bearing vibration signal model

McFadden and Smith (1984a) introduced an inner race fault bearing vibration signal model by taking into account of the impulse series, the modulation of the periodic signal caused by non-uniform load distribution, the vibration transmission of rolling element bearings and the exponential decay of vibration. An outer race fault bearing vibration signal model can also be developed following McFadden and Smith's analysis. When developing an outer race fault bearing model, the modulation of the periodic signal caused by non-uniform load distribution and the vibration transmission of rolling element bearings do not need to be taken into consideration because the outer race fault is fixed

and do not rotate with the shaft like the inner race fault bearing. Therefore, only the impulse series $i(n)$ and the exponential decay of vibration $c(n)$ need to be included in the outer race fault bearing model. The impulse series $i(n)$ produced by the defect can be modelled as an infinite series of impulses of equal amplitude i_0. The period between the impulses is equal to T_o which is the reciprocal of the outer race characteristic frequency f_o. The function $i(n)$ is accordingly given by (McFadden and Smith 1984a)

$$i(n) = \sum_{p=-\infty}^{\infty} i_0 \delta(n - pT_o), \tag{3-23}$$

where $\delta(n)$ is the unit impulse function defined as $\delta(n) = \begin{cases} 1, n = 0 \\ 0, else \end{cases}$ and p is an integer ranging from negative infinite to positive infinite with increment of one.

The exponential decay of vibration $c(n)$ of the response of the machine can be modelled by (McFadden and Smith 1984a)

$$c(n) = e^{-n/T_e} \sin(2\pi f_r n), \tag{3-24}$$

where T_e is the time constant of the exponential decay and f_r is the resonance frequency of the system. The vibration signal of a faulty outer race bearing $b(n)$ is then obtained by the convolution of the series of impulses $i(n)$ with the response of the system $c(n)$ and can be represented as

$$b(n) = i(n) * c(n), \tag{3-25}$$

Eq. 3-25 indicates the resonance frequency f_r and the additional frequency components $f_r \pm f_o$ of the vibration signal $b(n)$ will appear in the frequency spectrum. Figure 3-5 shows the simulation of an outer race fault bearing vibration signal with outer race characteristic frequency (f_o) 50 Hz, resonance frequency (f_r) 500 Hz and added white Gaussian noise. The sampling rate is 4000Hz and the time constant of the exponential decay (T_e) is 8 data samples. The white Gaussian noise is generated with normally distributed random numbers with mean 0 and variance of 1. The ratio of the impulse amplitude (i_0) vs. the noise power σ^2 is 6.7.

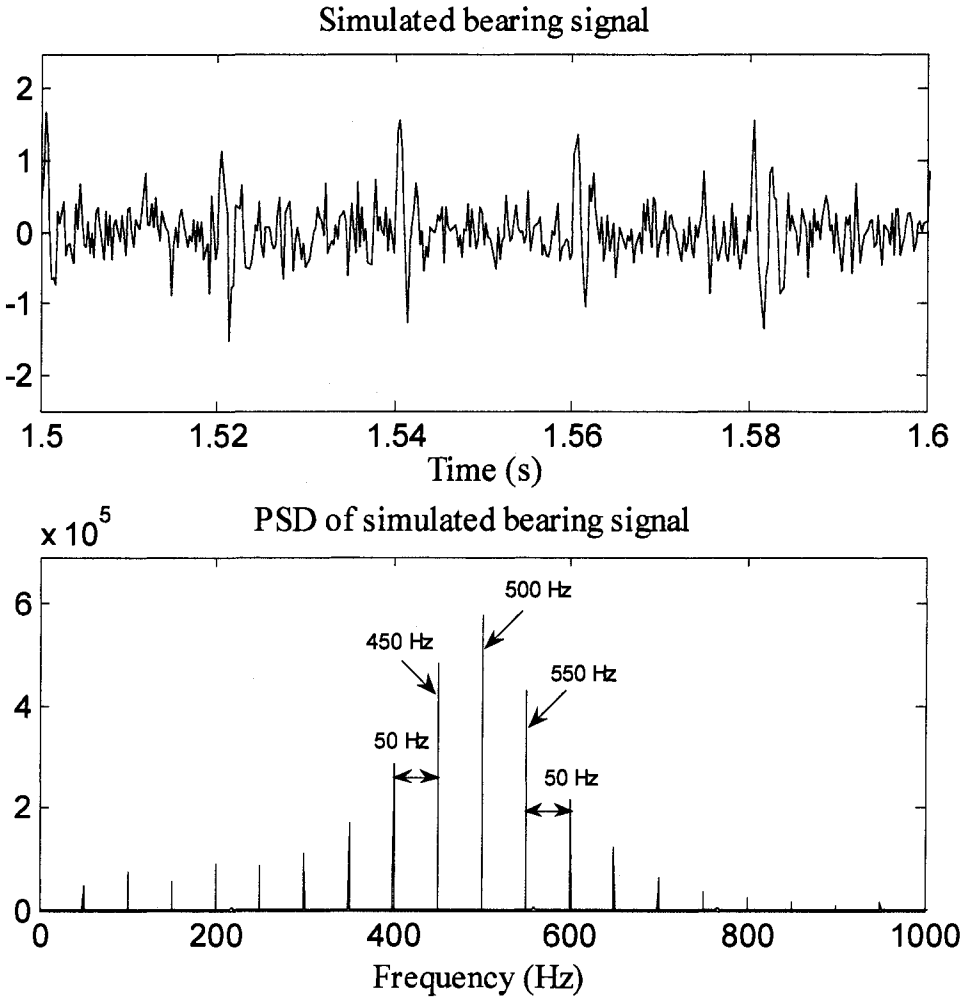

Figure 3-5. Simulated outer race fault bearing vibration signal

3.3.3 Fault identification in time and frequency domains

This section will introduce two commonly used fault identification techniques in bearing fault detection: kurtosis and envelope analysis techniques. Kurtosis is the fourth statistical moment and measures the peakedness of the probability density function. It is often used to indicate the level of impulsiveness in the signal and can be used as a condition indicator of a rolling element bearing in the time domain (Samanta et al 2004 and Dyer and Stewart 1978). Envelope analysis is a powerful tool in the frequency domain to remove the bearing resonance frequency and consequently reveal the bearing fault characteristic frequency. Envelope analysis has been widely used in numerous

applications and has shown successful results in the early detection of bearing faults (Harting 1978 and McFadden and Smith 1984b). It can reveal the type of bearing failure such as outer race, inner race, or cage faults by inspecting the actual bearing defect characteristic frequencies.

3.3.3.1 Kurtosis method

As mentioned above, kurtosis is a statistical parameter used to measure the relative peakedness or flatness of a distribution as compared to the normal distribution. It provides a measure of the size of the tails of distribution and is used as an indicator of major peaks in a set of data. Kurtosis can be written as

$$Kurtosis = \frac{(1/N)\sum_{n=1}^{N}\left(x(n)-\bar{x}\right)^4}{\left[(1/N)\sum_{n=1}^{N}\left(x(n)-\bar{x}\right)^2\right]^2} \tag{3-26}$$

where N is the number of data samples in the time domain, $x(n)$ is the vibration signal, and $\bar{x}$ is the average of the vibration signal $x(n)$. When a bearing is healthy, the vibration signal in the time domain displays Gaussian distribution with the kurtosis value close to three (Tandon and Choudhury 1999). When a faulty bearing presents impulse series in the vibration signal, the kurtosis value becomes larger. The magnitude of the kurtosis value can also indicate the extent of the impulse magnitude which corresponds to the severity of the bearing fault in the early stage (Pachaud et al 1997). In this thesis, kurtosis value is used to measure the impulse characteristic of the faulty bearing vibration signal in the time domain.

3.3.3.2 Hilbert transform and envelope spectrum analysis

Envelope spectrum analysis which is also known as demodulated resonance analysis is widely used in detecting bearing characteristic frequency from other machine elements (Tse et al 2001, Ocak and Loparo 2001, and Yu et al 2005). An impulse is produced each time when a loaded rolling element makes contact with a defect on another surface in the bearing. This impulse has an very short duration, which is modelled by the exponential decay in the faulty bearing model in section 3.3.2, compared to interval between the pulses. The energy from the impulse is distributed at a very low

level over a wide range of frequencies. It is this wide distribution of energy that makes bearing defects so difficult to detect by conventional spectrum analysis in the presence of vibrations from gears and other machine components. Many studies (e.g., McFadden and Smith 1984b, and Lebold et al 2000) have shown that the impact usually excites a resonance in the system at a frequency higher than the vibration generated by other components. This structural energy is usually concentrated into a narrow band that is easier to detect than the widely distributed energy of the bearing fault characteristic frequencies.

The envelope spectrum analysis focuses on the structure resonance to detect the bearing fault characteristic frequencies. To improve the bearing fault detectability, a band-pass filter is used to filter the vibration signal around the structure resonance and this filtered signal is then processed by Hilbert transform to detect envelope. However, the resonance frequency band can be difficult to detect and locate, and the structure resonance varies from one machine to another. Therefore, there is no practical way to design a band-pass filter around the structure resonance frequency band.

In this thesis, ANC is used to remove the interfering gear signals and it behaves like a high pass filter when the resonance band is in the high frequency range. Therefore, it can provide an effective solution to mitigate the difficulty in designing a band-pass filter around the structure resonance frequency band before the Hilbert transform can be applied.

Hilbert transform is a time domain convolution that maps one real-valued time history into another (Bennett and Sharpley 1988 and Carcaterra and Sestieri 1997). It is defined by

$$H[x(n)] = \frac{1}{\pi}\int_{-\infty}^{\infty}\frac{x(\tau)}{n-\tau}d\tau, \tag{3-27}$$

where $x(n)$ is the discrete time domain signal (vibration signal), and $H[x(n)]$ is the Hilbert transform of $x(n)$. Demodulation is accomplished by forming a complex value time domain signal called the analytic signal $A[x(n)]$ which is defined as

$$A[x(n)] = x(n) + iH[x(n)] = a(n)e^{i\varphi(n)},\ i = \sqrt{-1}, \tag{3-28}$$

where

$$a(n) = \sqrt{x^2(n) + H^2[x(n)]}, \tag{3-29}$$

and

$$\varphi(n) = \arctan \frac{H[x(n)]}{x(n)}, \tag{3-30}$$

$a(n)$ and $\varphi(n)$ are the magnitude and phase of the complex value time signal $A[x(n)]$ respectively. The envelope is the magnitude $a(n)$ and represents an estimate of the modulation presented in the signal $x(n)$. When a Hilbert transform is used to process the faulty bearing vibration signal, it removes the carrier signal which is the resonance frequency f_r and reveals the modulating signal f_d which is the bearing fault characteristic frequency.

3.3.4 Simulation results

The simulation tries to imitate a practical situation. It is assumed that an accelerometer (sensor P) is mounted near a faulty bearing. The simulated faulty bearing vibration signal uses the faulty bearing vibration signal from section 3.3.2 with an outer race characteristic frequency of 50 Hz and a resonance frequency of 500 Hz. Two simulated interference gear vibration signals are included in this simulation. The first simulated gear vibration signal is the gear vibration signal from section 3.3.1 with gear meshing frequency 52 Hz and its five meshing harmonics. The second simulated gear vibration is also modelled by Eq. 3-22. The gear meshing frequency is 170 Hz and there are 5 harmonics. The amplitudes of the second gear meshing harmonics are comparable to the first gear signal and the frequency spectrum is dominated at the second harmonic (340 Hz) and third harmonic (510 Hz). White Gaussian noise is added to the mixed bearing and gear vibration signal. The ratio of the bearing signal impulse amplitude (i_0) vs. the noise power σ^2 of the white Gaussian noise is 6.7, the same ratio used in section 3.3.2 of the simulated faulty bearing vibration model. The simulated sampling rate is 4000 Hz and data blocks of 2 seconds are used.

Figure 3-6 shows the time domain signal, the frequency spectrum, and the envelope spectrum of the simulated primary input signal from the accelerometer mounted

near the outer race fault bearing. In the time domain (Figure 3-6a), it is difficult to detect the impulsive characteristic of bearing faulty signal and its kurtosis value equals 3.4.

The frequency spectrum (Figure 3-6b) displays the gear harmonic meshing frequencies, dominated by second harmonic (104 Hz) and third harmonic (156 Hz) of the first gear signal as well as the second harmonic (340 Hz) and third harmonic (510 Hz) of the second gear signal. Frequencies separated with the outer race characteristic frequency (50Hz) from the resonance frequency and the resonance frequency (500 Hz) can also be observed in the frequency spectrum.

The envelope spectrum shown in Figure 3-6c is obtained by applying the Hilbert transform directly to the signal mixture. The Hilbert transform has removed the resonance frequency (500 Hz). The gear meshing frequencies 52 Hz and 170 Hz dominate the envelope spectrum and it is hard to detect the outer race characteristic frequency (50 Hz). Figure 3-7 provides a close up look of Figure 3-6c in the frequency range from 0 Hz to 160 Hz. We can see that the outer race characteristic frequency (50 Hz) and its harmonics are revealed in Figure 3-7. However, in real circumstances a sharp peak on the outer race characteristic frequency is not obtainable because the faulty bearing signal is not deterministic. Therefore, it will be difficult to identify the bearing characteristic frequency in the presence of interference gear meshing frequency when both frequencies are very close.

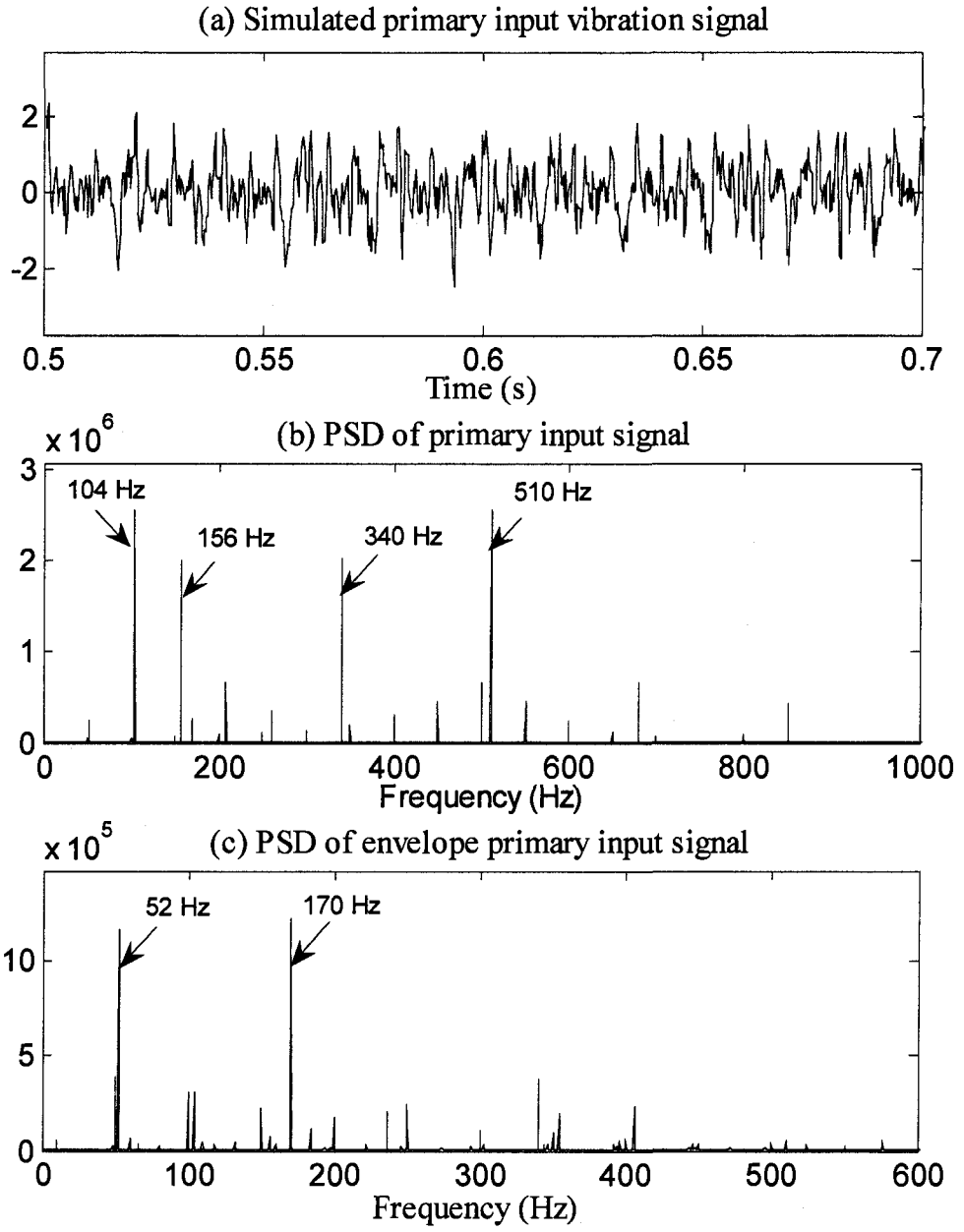

Figure 3-6. Primary input signal (a), its frequency spectrum (b), and envelope spectrum (c) of the simulated mixture of bearing and gear vibration signals

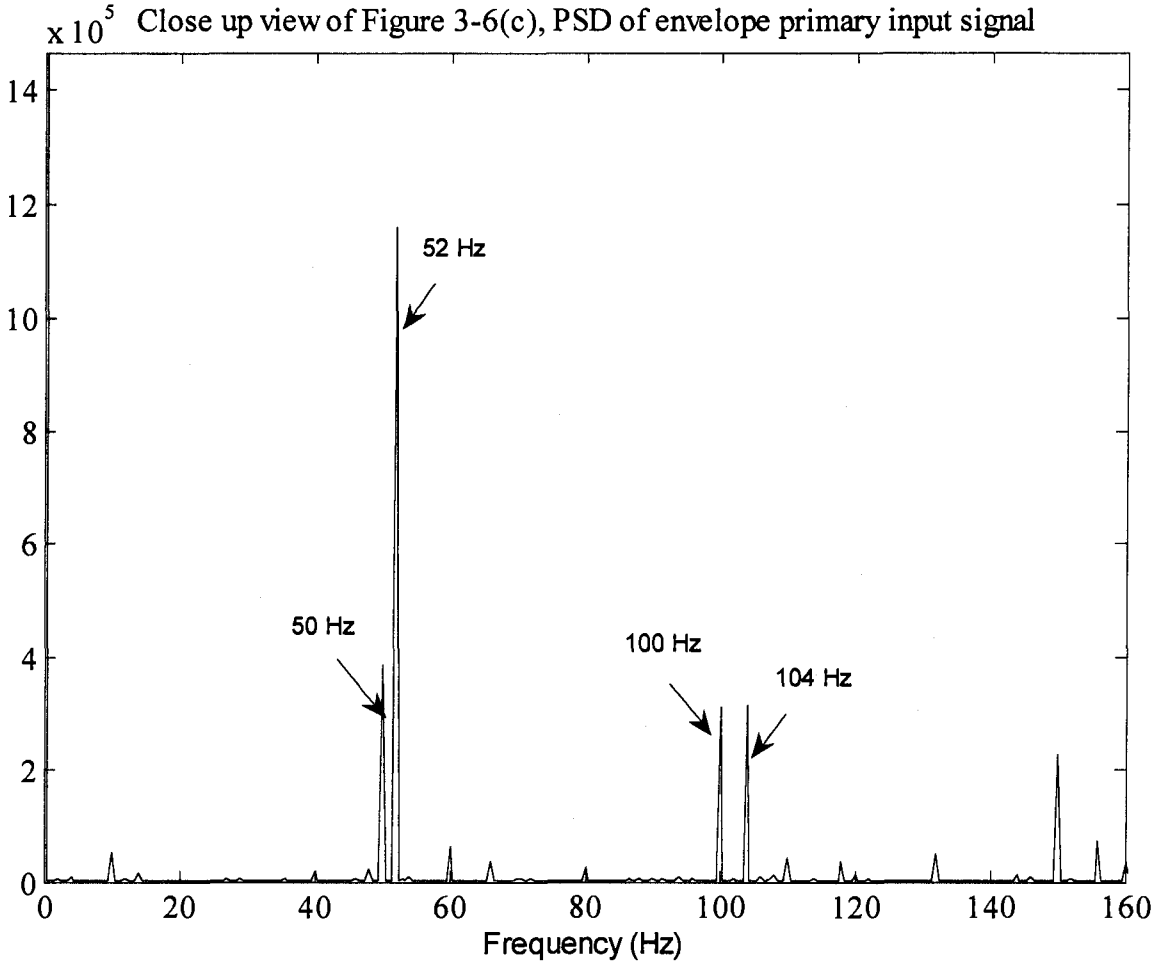

Figure 3-7. Envelope spectrum of the simulated mixture of bearing and gear vibration signals (close up view of Figure 3-6c)

Assuming another accelerometer (Sensor R) mounted close to the interference gears source is used to collect the reference input signal. Since the Sensor R is mounted farther away from the faulty bearing, it is reasonable to assume the reference input signal contains only 20% of the magnitude of the primary input faulty bearing signal. Since the collected reference input signal will not be in phase with the primary input signal, a phase shift of the primary input faulty bearing signal is incorporated into the reference input faulty bearing signal. It is also assumed that the gear signal in the reference input signal has similar gear signal content in the primary input signal with a phase shift. Figure 3-8 displays the time domain signal, the frequency spectrum, and the envelope spectrum of the simulated reference input signal from the accelerometer mounted near the

interference gears source. The frequency spectrum (Figure 3-8b) shows the interference gears meshing harmonic frequencies with high peaks at 104 Hz, 156 Hz, 340 Hz and 510 Hz which are the dominating harmonics of the first and the second gear meshing frequencies. In the envelope spectrum (Figure 3-8c), the first gear meshing frequency (52 Hz) and the second gear meshing frequency (170 Hz) are shown clearly.

The ANC operating parameters is calculated using the reference input signal. The transversal filter length $M = 262$ is calculated according to the AIC method introduced in section 3.2.3. The step-size parameter μ is obtained from Eq. 3-17 in section 3.2.4 by setting the misadjustment value equal to 0.025. The calculated step-size parameter $\mu = 0.000384$.

The ANC output signal is shown in Figure 3-9. The impulse signature of the bearing signal can now be recognized from the time domain (Figure 3-9a) with an increased kurtosis value of 4.9 comparing to the primary input kurtosis value of 3.4. The frequency spectrum (Figure 3-9b) displays only the resonance frequency (500 Hz) and frequencies resulting from the faulty bearing signal. The gear meshing harmonic frequencies dominating the primary input frequency spectrum (Figure 3-6b) are removed. The filter's high frequency selection and resolution is demonstrated as the dominating gear meshing frequency (510 Hz) is completely removed from the resonance frequency (500 Hz). In the envelope spectrum (Figure 3-9c), the bearing outer race characteristic frequency 50 Hz and its harmonics can be clearly identified while all gear meshing frequencies are removed. This result clearly shows that the interference gear signals have been removed from the primary input mixed signal. The bearing faults can thus be easily detected from the ANC output signal.

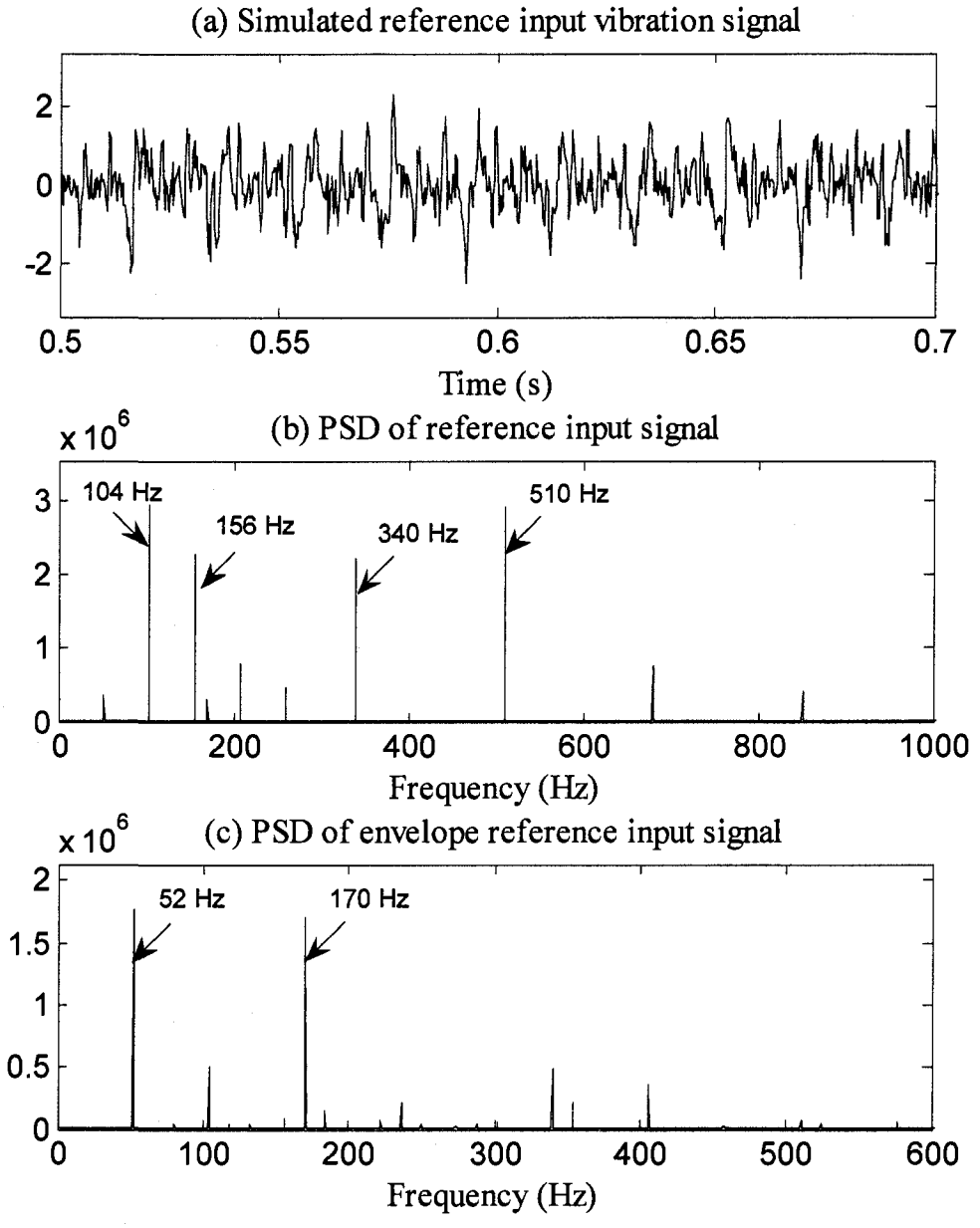

Figure 3-8. Reference input signal (a), its frequency spectrum (b), and envelope spectrum (c) of the simulated mixture of bearing and gear vibration signals

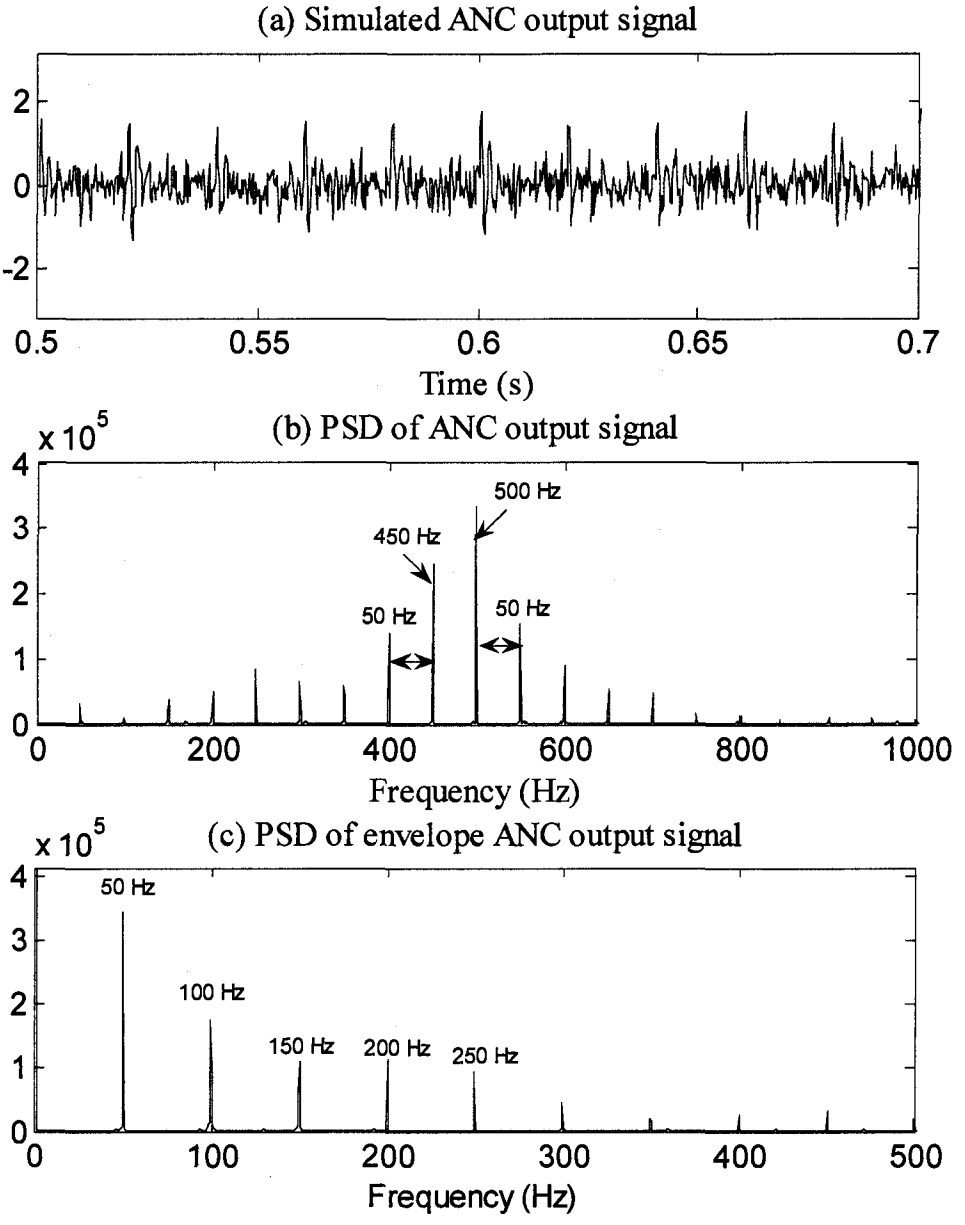

Figure 3-9. ANC output signal (a), its frequency spectrum (b), and envelope spectrum (c) of the simulated mixture of bearing and gear vibration signals

3.4 Experiments

This section reports the experiments performed to validate the proposed adaptive noise cancellation method. Three different experiment settings are considered to examine the adaptive noise canceller's performance in removing interference gear signal and enabling bearing fault detection. In the first experiment setting, the ANC is used to analyze the healthy bearing signal. In the second and third experiment settings, faulty bearing signals under different shaft speeds are collected from different sensor locations to evaluate the ANC approach. The time domain signal, frequency spectrum and envelope spectrum of the primary input, reference input and the ANC output signal of each experiment setting will be plotted for analysis and comparison.

The experiments were performed on a Spectra Quest machine fault simulator (MFK-PK5M) as shown in Figure 3-10. Two bearings (type ER10K) placed inside the bearing holders are used to support the drive shaft (5/8" in diameter) which is driven by a 3-hp AC motor through a coupling with a Hitachi controller (SJ200-022NFU). The right end of the drive shaft is connected to a smaller sheave and the gearbox shaft is connected to a larger sheave. The belts which rest on the two sheaves connect the drive shaft to drive the gearbox shaft. The diameter ratio of the smaller sheave to the larger one is roughly 1: 2.6 and the pinion of the gearbox has 18 teeth. This leads to a gear meshing frequency approximately 6.923 f_s (i.e., shaft frequency * 18 / 2.6). A Montronix model VS100-100 accelerometer with 100 Mv/g sensitivity and up to 12k Hz frequency range is used to measure the vibration signal. The accelerometer can be mounted either on each of the two bearing holders, on the gearbox, or on the base plate of the simulator. An NI AT-MIO-16DE-10 DAQ card and LabView are used to collected the vibration signal. The collected signal is then processed using MATLAB on a Pentium® 4 / 3.4GHz PC.

Ideally, the primary input and reference input signals should be collected simultaneously and fed into the ANC to produce the ANC output signal. However, since there is only one accelerometer of the same type available, the primary input signal and reference input signal are collected sequentially by a single accelerometer under the same operating condition. The primary input signal is collected first with the sensor mounted at the primary input location. The primary input locations are different for the three experiments detailed below. Then the sensor is re-mounted at the reference input location

(on top of the gearbox) to collect the reference input signal while keeping the simulator running at the same speed. As the same operating condition is maintained, the sequentially acquired primary input and reference input signals can be used to verify the adaptive noise cancellation method just as good as the simultaneously collected data.

3.4.1 Experiment 1

In this experiment (Figure 3-10), healthy bearings are used to test the adaptive noise cancellation method. Healthy bearings are installed in both the left and the right bearing holders. The sampling rate is set at 12000 Hz and the sampled data length is one second.

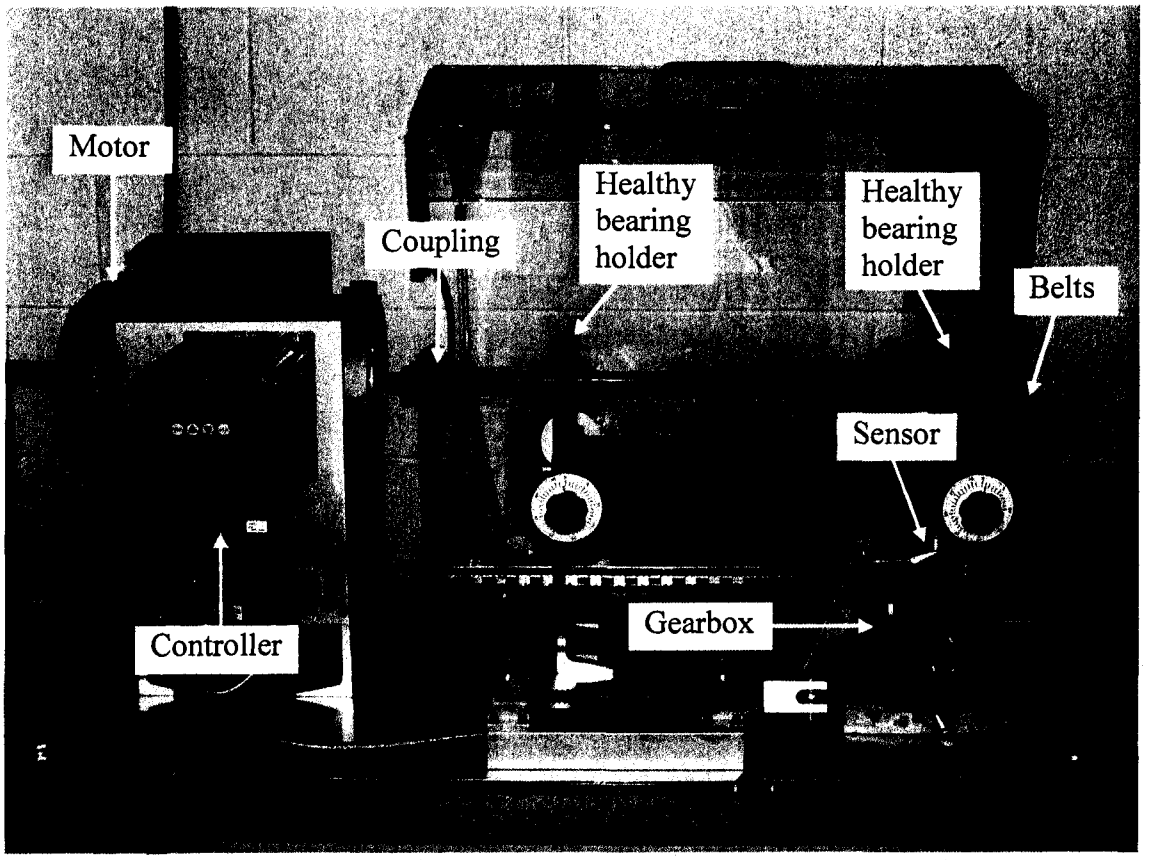

Figure 3-10. Setup of experiment 1

The accelerometer is first placed on top of the left bearing holder to collect the primary input signal. Figure 3-11 shows the time domain signal, frequency spectrum and envelope spectrum of the primary input signal. The shaft is running at 1000 rpm (16.7 Hz) and the calculated gear meshing frequency is equal to 116 Hz (=16.7×18/2.6). No

impulsive characteristic is detected in the time domain signal (Figure 3-11a) and its kurtosis value equals 3.0.

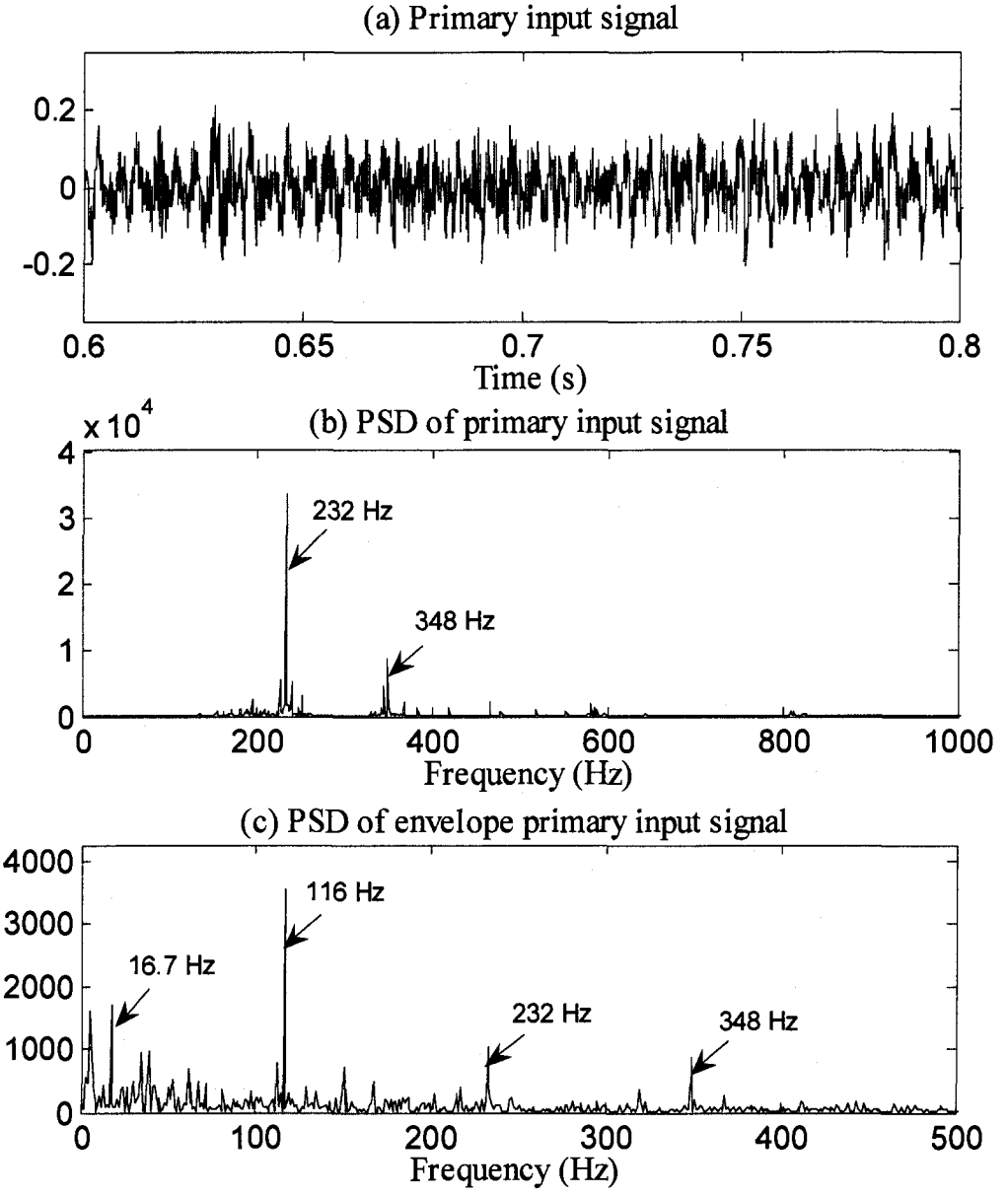

Figure 3-11. Primary input of experiment 1: (a) raw signal, (b) frequency domain representation of the primary input, and (c) envelope spectrum of the signal

In the frequency spectrum (Figure 3-11b), we see two dominating peaks at 232 Hz and 348 Hz which corresponds to the second and third harmonics of the gear meshing frequency. The envelope spectrum (Figure 3-11c) reveals the shafting frequency (16.7 Hz), the gear meshing frequency (116 Hz), the second harmonic (232 Hz) and the third harmonic (348 Hz) of the gear meshing frequencies.

Next, the reference input signal is acquired. The ideal reference sensor location should be close to the interference source and farther away from the monitored component. Thus, the accelerometer is placed on top of the gearbox (which is the source of the main interference) to collect the reference input signal. The time and frequency domain data of the signal as well as its envelope spectrum are presented in Figure 3-12. The two peaks at 232 Hz and 348 Hz, respectively corresponding to the second and third gear meshing harmonics, dominate the frequency spectrum (Figure 3-12b). In the envelope spectrum (Figure 3-12c), the gear meshing frequency (116 Hz), its second harmonic (232 Hz) and third harmonic (348 Hz) are revealed. Notice that we can see impulses in the reference input time domain signal (Figure 3-12a) and the reference input signal has a high kurtosis value (8.1). These impulses are not from the healthy bearing signal (there are no impulses shown in the primary input signal). It is observed that these impulses are generated by the gearbox. This result indicates that kurtosis value alone cannot be used for bearing fault detection when the data is a mixture of signals from different sources.

The ANC operating parameters are then calculated. The transversal filter length $M = 342$ is obtained by the AIC using Eq. 3-12. The error power in the Eq. 3-12 associated with the model order is calculated using the Levinson-Durbin recursion (the function 'lpc' in the MATLAB can be used to easily obtain the error power). The model order associated with the minimum AIC is the optimal filter length. The step-size parameter $\mu = 0.015$ is calculated using Eq. 3-17. The desired step-size parameter is obtained with the misadjustment value of 0.025 multiplied by 2 times the average tap-input power of the reference input signal. The ANC output signal, its frequency spectrum, and envelope spectrum based on this (M, μ) combination are displayed in Figure 3-13. No impulses can be detected in the ANC output time domain signal (Figure 3-13a) and the kurtosis value is 3.0, a clear indication of Gaussianality and thus the lack of

impulsiveness. Therefore, the ANC output time domain signal correctly reflects characteristic of a healthy bearing. In the frequency spectrum (Figure 3-13b), the dominating gear meshing harmonic frequencies (232 Hz and 348 Hz) in the primary input frequency spectrum (Figure 3-11b) have been removed and a distinct peak at 238 Hz is shown. As it will become clear in the next two experiments, this frequency is within the resonance region of the machine fault simulator system. In the envelope spectrum (Figure 3-13c), we no longer see the gear meshing frequency (116 Hz) and its harmonics. One peak at 16.7 Hz is clearly revealed, which corresponds to the shaft rotating frequency. After comparing the ANC output signal with the primary input signal (Figure 3-11), we can conclude that the adaptive noise cancellation method has successfully removed the interference gear signal. The extracted bearing signal reveals healthy bearing characteristics.

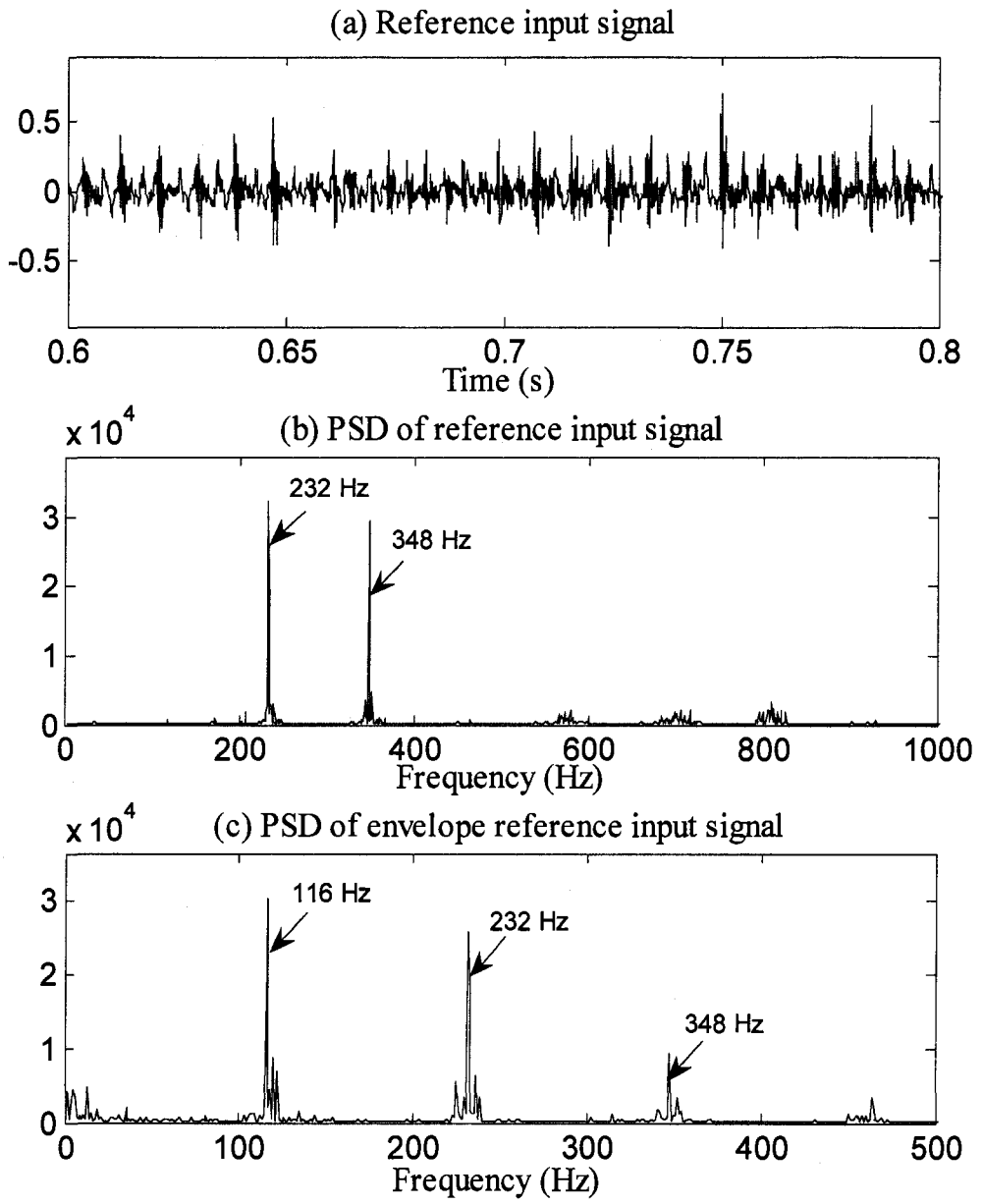

Figure 3-12. Reference input of experiment 1: (a) raw signal, (b) frequency domain representation of the reference input signal, and (c) envelope spectrum of the signal

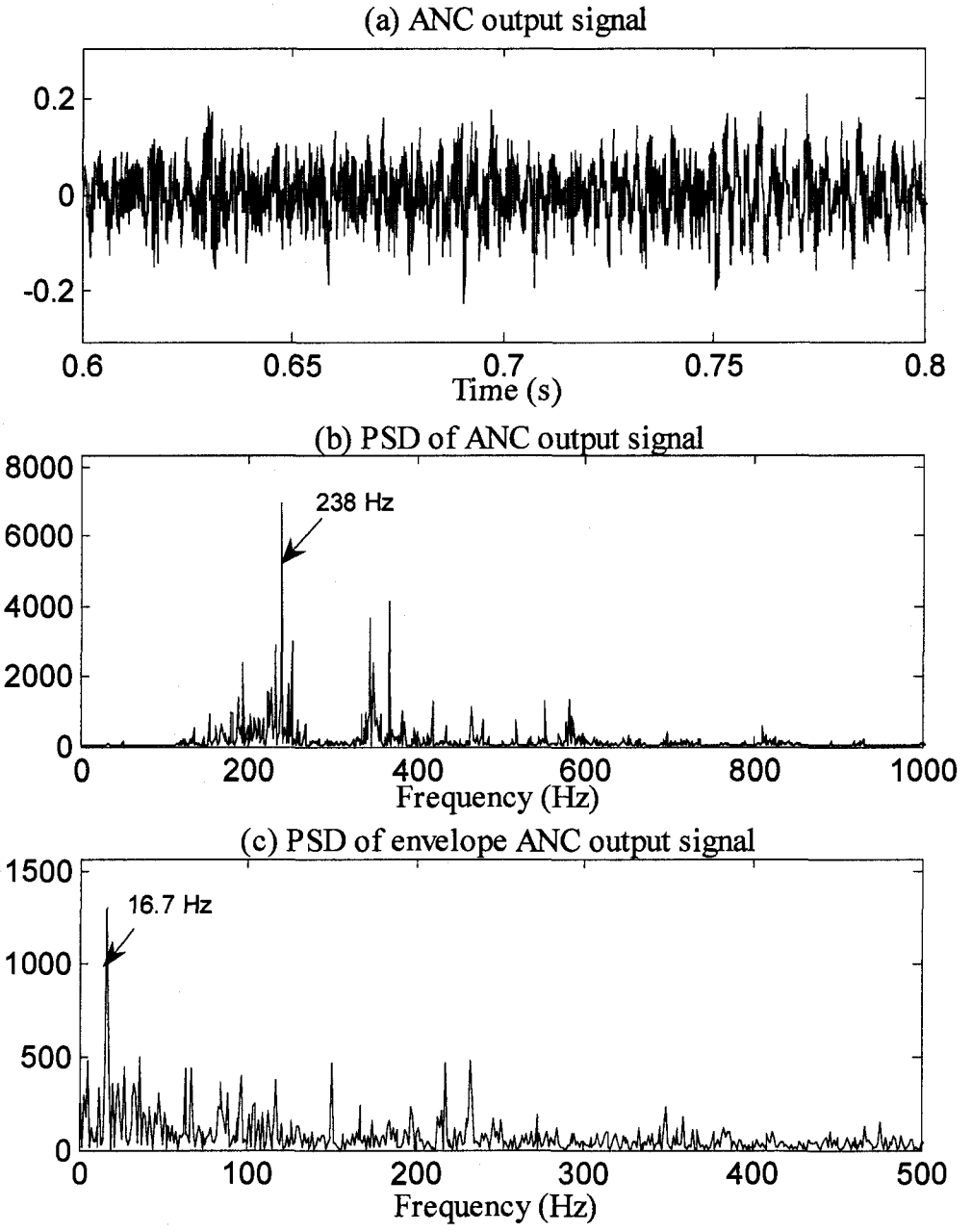

Figure 3-13. ANC result of experiment 1: (a) output signal, (b) frequency domain representation of the signal, and (c) envelope spectrum of the signal

3.4.2 Experiment 2

The setup of this test is shown in Figure 3-14. Two balanced mass rotors (2" thick, 4" in diameter and 11.1 lbs each) are used to provide radial loads to the drive shaft. A bearing with an outer race fault (provided by the supplier of the machine fault simulator) is used for both experiments 2 and 3. According to the manufacturer, the faulty bearing has an outer race fault characteristic frequency that is three times that of the drive shaft frequency. The faulty bearing is installed in the right bearing bracket, a normal bearing is installed in the left bearing bracket, and the two load rotors are installed close to the faulty bearing holder. The sampling rate is 8000 Hz and the sampled data length is 0.5 seconds.

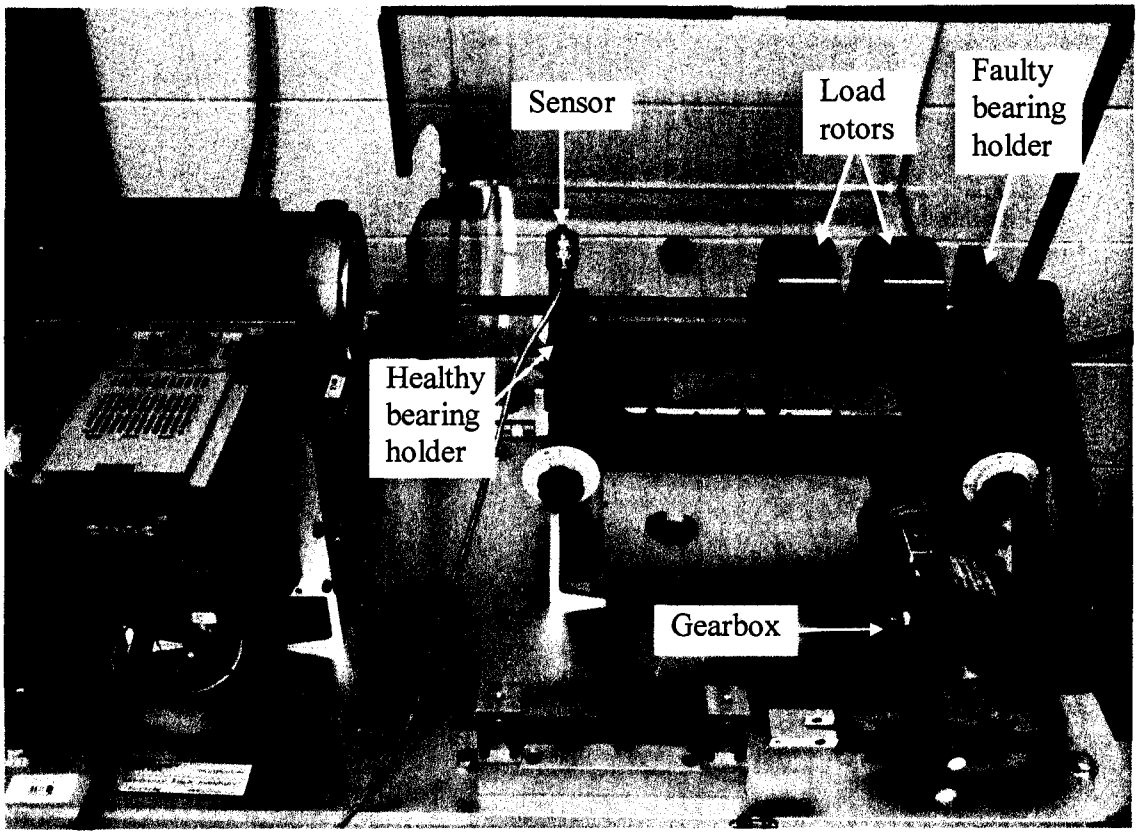

Figure 3-14. Setup of experiment 2

The drive shaft is operated at 707 rpm (11.8 Hz). Therefore, the calculated outer race fault characteristic frequency is 35.4 Hz (=3×11.8) while the calculated gear meshing frequency is roughly 81.7 Hz (=11.8×18/2.6). Obviously, the best location to mount the accelerometer to collect the primary input signal would be the top of the faulty

bearing holder. However, to mimic the situation where the sensor cannot be conveniently mounted on the optimal location, the accelerometer is installed on top of the normal bearing holder instead. The collected primary input signal and its frequency spectrum and envelope spectrum are plotted in Figure 3-15. In the time domain (Figure 3-15a), a little bit of impulse characteristic is suspected but cannot be confirmed without further analysis. The kurtosis value is 3.5. The third harmonic of the gear meshing frequency dominates the frequency spectrum (Figure 3-15b) at 244.8 Hz. The envelope spectrum (Figure 3-15c) reveals two distinct peaks. The peak at 35.6 Hz is associated with the outer race fault characteristic frequency while the peak at 81.6 Hz is the gear meshing frequency. Through the time and frequency fault identification, it is believed that the signal has shown enough faulty bearing characteristics, especially by the envelope spectrum analysis in Figure 3-15c. This is probably the result of extended fault on the bearing outer race that is provided by the manufacturer. Therefore, the following analysis will verify that the adaptive noise cancellation method can remove the interference gear signal and reveal a clearer faulty bearing signal.

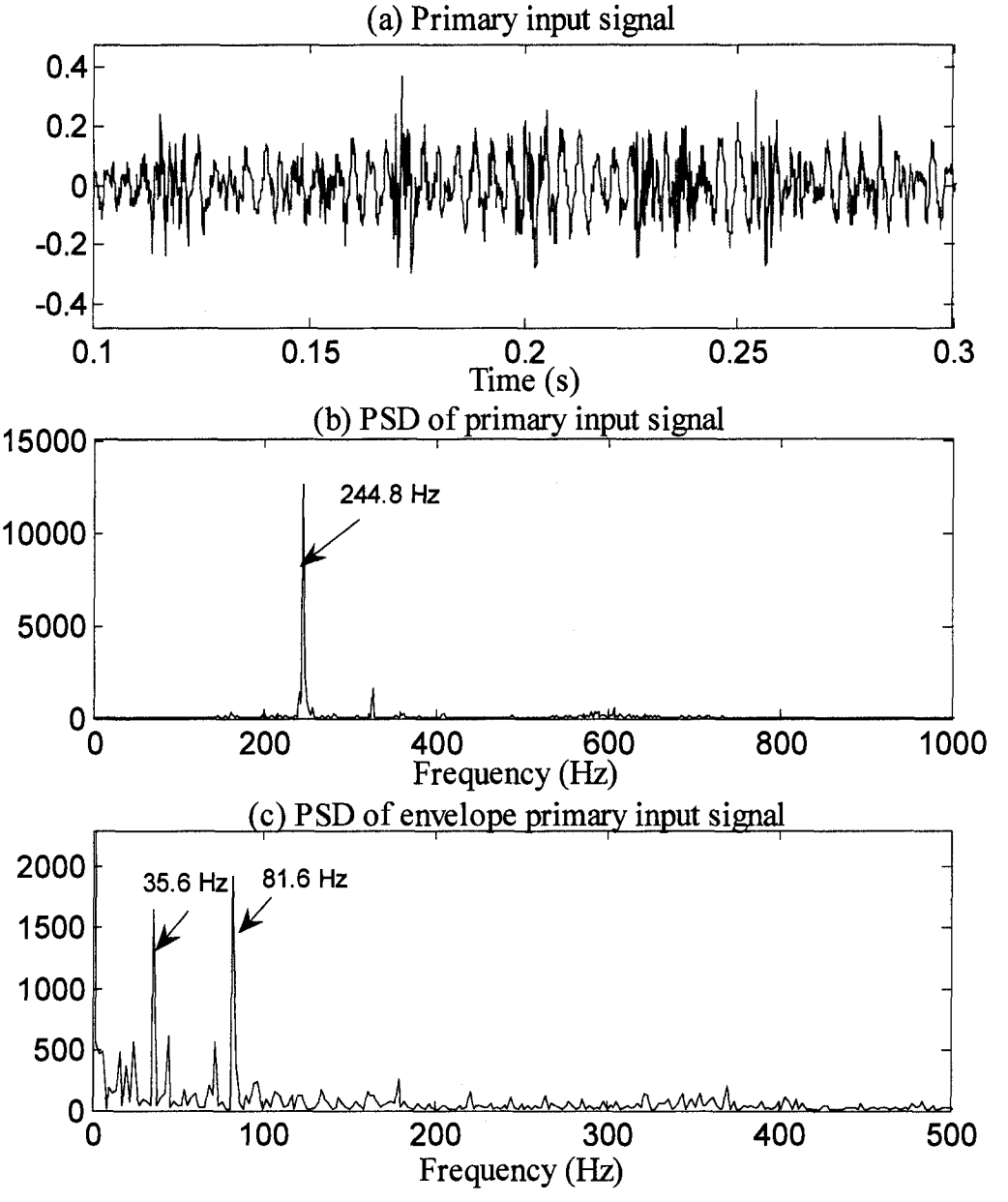

Figure 3-15. Primary input of experiment 2: (a) raw signal, (b) frequency domain representation of the primary input, and (c) envelope spectrum of the signal

The accelerometer is next mounted on the top of the gearbox where the gear signal or the interference would be the strongest while some faulty bearing signal would also exist. Figure 3-16 displays the reference input signal, its frequency spectrum, and envelope spectrum. Again, we can detect some impulses in the time domain signal (Figure 3-16a). The frequency spectrum (Figure 3-16b) reveals the third harmonic (244.8 Hz) and fourth harmonic (326.4 Hz) of the gear meshing frequencies. In the envelope spectrum (Figure 3-16c), gear meshing frequency (81.6 Hz) and its harmonics (163.2 Hz, 244.8 Hz, 326.4 Hz and 408 Hz) are clearly shown while a small peak (35.6 Hz) is also visible which implies that the reference input signal contains some content of the faulty bearing signal.

The calculated transversal filter length M is 128 and the step-size parameter μ is 0.0226 when the misadjustment value is equal to 0.025. The ANC output is shown in Figure 3-17. Comparing to the primary input time domain signal (Figure 3-15a), the ANC output time domain signal (Figure 3-17a) displays clearer impulsive characteristic. This is also reflected by the improved kurtosis value, 4.3, comparing to 3.5 in the primary input signal in Figure 3-15a. In the frequency spectrum (Figure 3-17b), the gear meshing harmonic frequencies is no longer detectable and the frequency spectrum shows the simulator resonance region (roughly between 200 and 300 Hz) of the faulty bearing signal. In the envelope spectrum (Figure 3-17c), the bearing outer race characteristic frequency 35.6 Hz can be easily identified while the gear meshing frequency 81.5 Hz has been eliminated and is no longer detected. From Figure 3-17, it is clear that the faulty bearing signal has been successfully extracted from the primary input signal and the resulting ANC output signal clearly indicates that outer race fault has developed on the bearing.

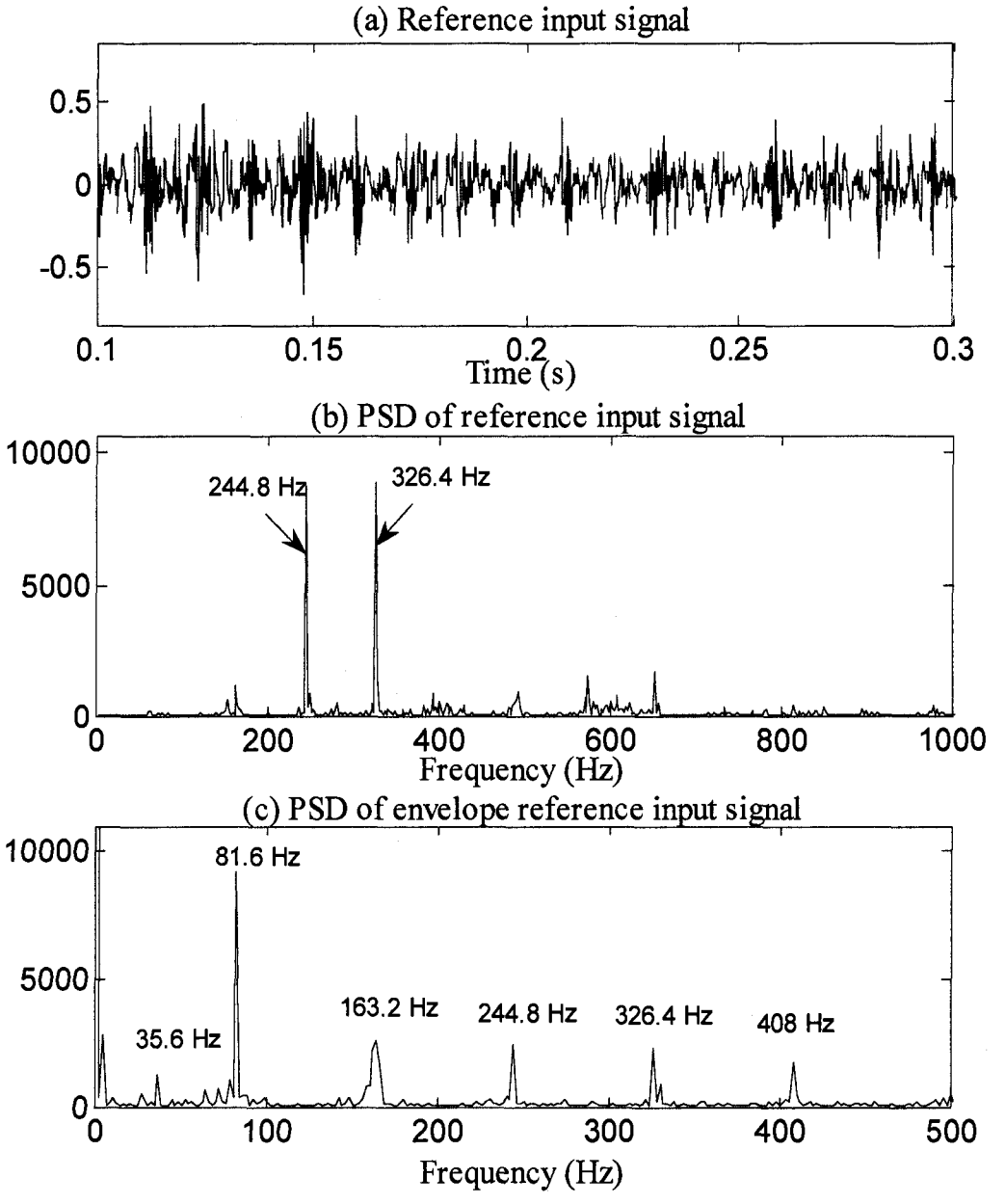

Figure 3-16. Reference input of experiment 2: (a) raw signal, (b) frequency domain representation of the reference input signal, and (c) envelope spectrum of the signal

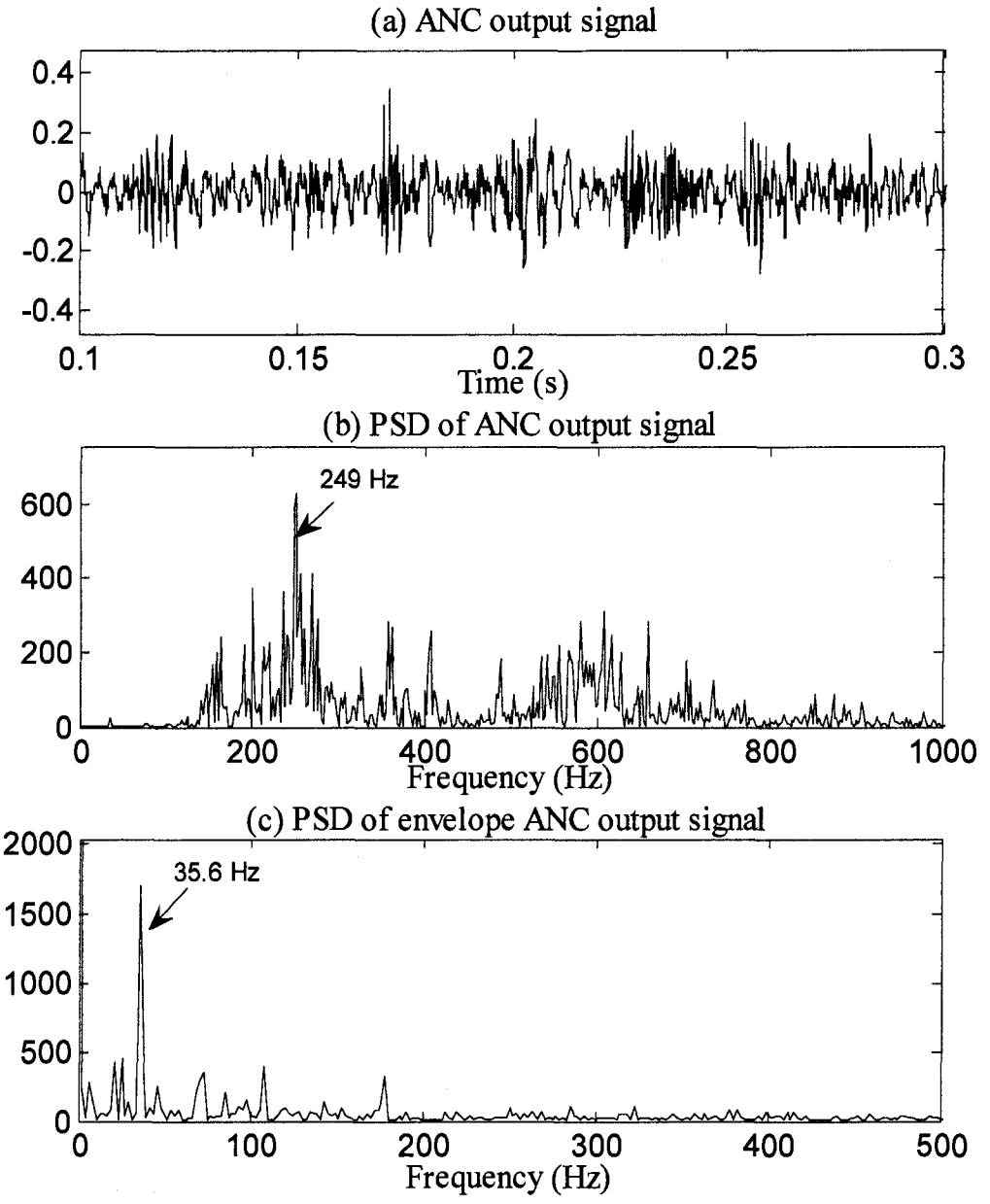

Figure 3-17. ANC result of experiment 2 (a) output signal, (b) frequency domain representation of the signal, and (c) envelope spectrum of the signal

3.4.3 Experiment 3

The setup of this experiment is shown in Figure 3-18. The locations of the faulty bearing and the normal bearing are switched from experiment 2 and the load rotors are relocated to examine the robustness of the adaptive noise cancellation method. The drive shaft rotating speed is also changed to 492 rpm (8.2 Hz). Accordingly, the outer race fault characteristic frequency is 24.6 Hz (three times of the shaft frequency). The associated gear meshing frequency is now roughly 56.8 Hz (=8.2×18/2.6). Again, to mimic an industrial setting where the sensor cannot be conveniently mounted on the optimal location (i.e., the top of the faulty bearing holder in this case) or even in its near vicinity, the sensor is mounted on the simulator base plate far from the faulty bearing to collect the primary input signal. The sampling rate is 8000 Hz and the sampled data length is 1 second.

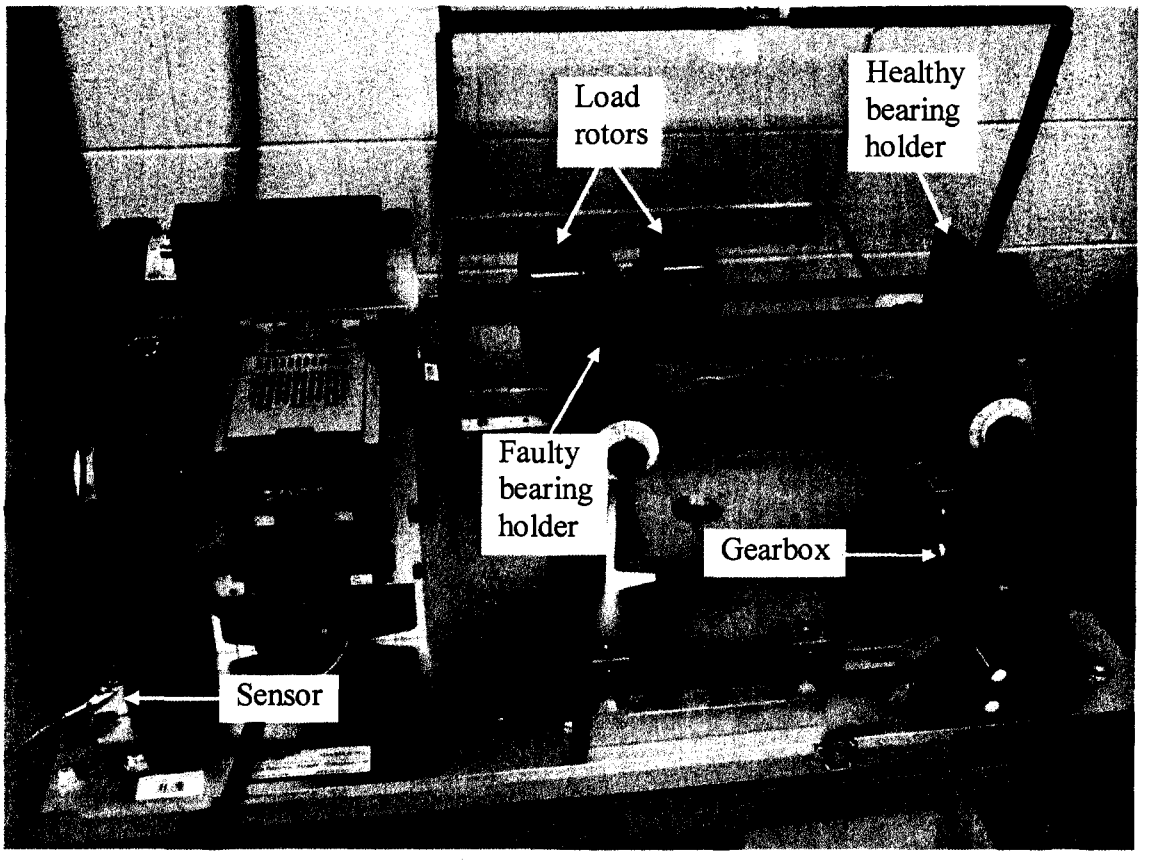

Figure 3-18. Setup of experiment 3

The primary input signal collected from the simulator base, its frequency spectrum and envelope spectrum are plotted in Figure 3-19. The time domain plot (Figure 3-19a) appears to display stronger impulse signatures comparing to that in experiment 2 (Figure 3-15a). The associate kurtosis value is also larger (4.2). The third and fourth harmonics (170 Hz and 227 Hz, respectively) of gear meshing frequency dominate the frequency spectrum (Figure 3-19b). In the envelope spectrum (Figure 3-19c), three dominating peaks are revealed. They are the outer race fault characteristic frequency (24.5 Hz), its second harmonic frequency (49 Hz) and the gear meshing frequency (56 Hz).

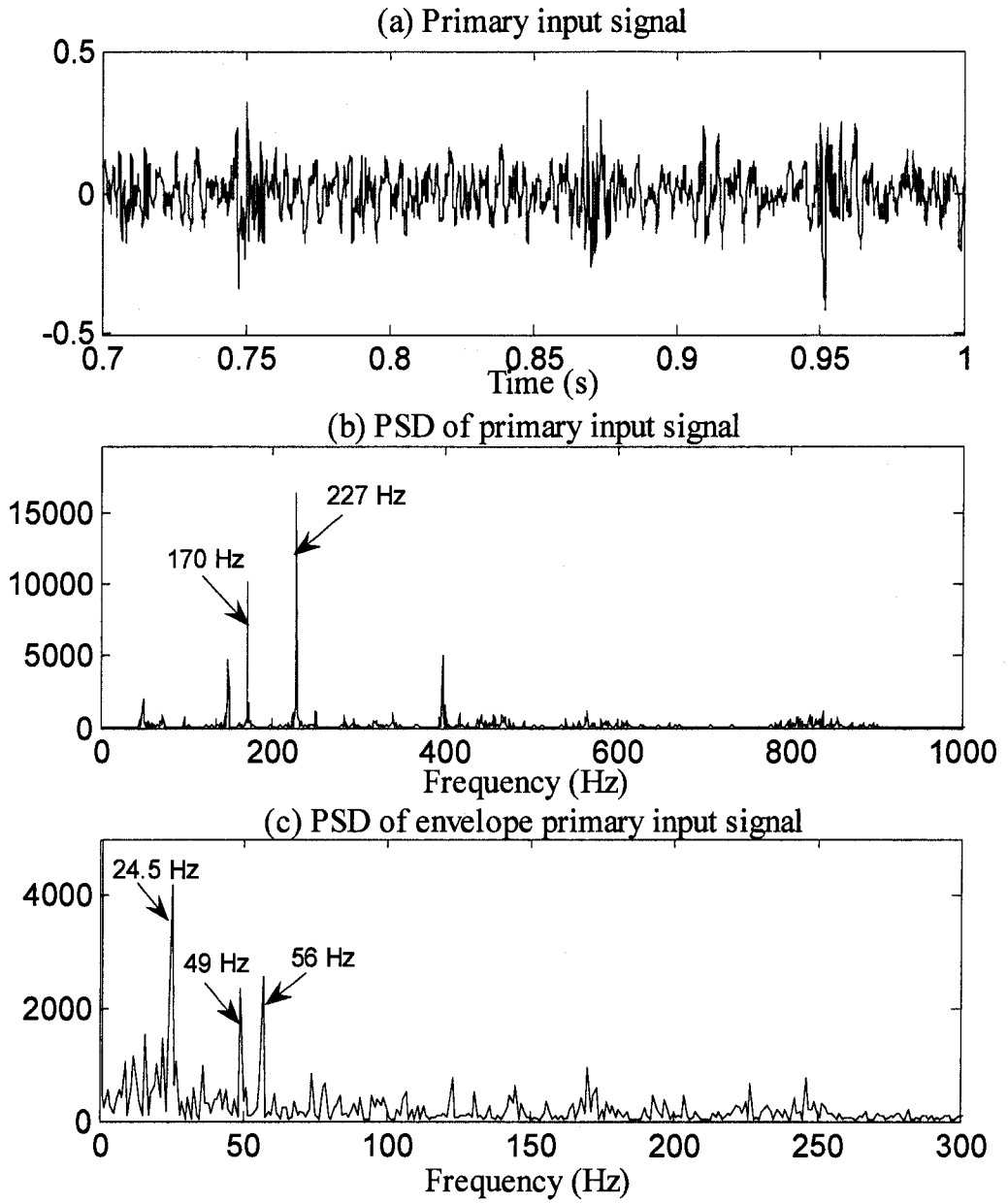

Figure 3-19. Primary input of experiment 3: (a) raw signal, (b) frequency domain representation of the primary input, and (c) envelope spectrum of the signal

To collect the reference input signal, the sensor is mounted on top of the gearbox. It is important to find a location where the reference input signal contains more interference signal and less monitored signal than in the primary input signal. In this case, the top of the gearbox satisfies this requirement because the interference signal is mostly generated by the gearbox and the faulty bearing is quite far away from this location. Figure 3-20 shows the reference input time domain signal, its frequency spectrum and envelope spectrum. In the frequency spectrum (Figure 3-20b) and the envelope spectrum (Figure 3-20c), multiple gear meshing harmonic frequencies are detected.

The ANC operating parameters obtained are: transversal filter length $M = 162$, step-size parameter $\mu = 0.072$. The transversal filter length is the model order obtained using Eq. 3-12 where the error power associated with the model order is calculated using the Levinson-Durbin recursion. The step-size parameter is calculated using Eq. 3-17 with the misadjustment value of 0.025. The ANC output signal is shown in Figure 3-21. In the time domain (Figure 3-21a), the kurtosis value of the ANC output signal increases to 4.7, comparing to 4.2 in the primary input signal. This increase of the kurtosis value indicates that the ANC output signal is more impulsive than the primary input signal. In the frequency spectrum (Figure 3-21b), peaks at 49 Hz and 147 Hz are detected which correspond to the harmonics of the bearing outer race characteristic frequency (24.5 Hz) while the gear meshing harmonic frequencies are greatly attenuated. This is precisely what the ANC is supposed to achieve. In the envelope spectrum (Figure 3-21c), only the outer race characteristic frequency (24.5 Hz) and its harmonic frequency (49 Hz) are detected while the interference gear meshing frequency shown in the primary input signal is removed.

In both experiments 2 and 3, the ANC is able to remove the interference gear vibration signal from the mixed gear and bearing signal. The experiment result verifies that the ANC can successfully extract impulsive faulty bearing signal from the gear and bearing signal mixture. Although there is only one interference gear vibration signal due to the simulator setup in the experiment, it is reasonable to expect that the ANC can also separate faulty bearing signal from multiple interference gear meshing vibration signals as shown in the simulation section.

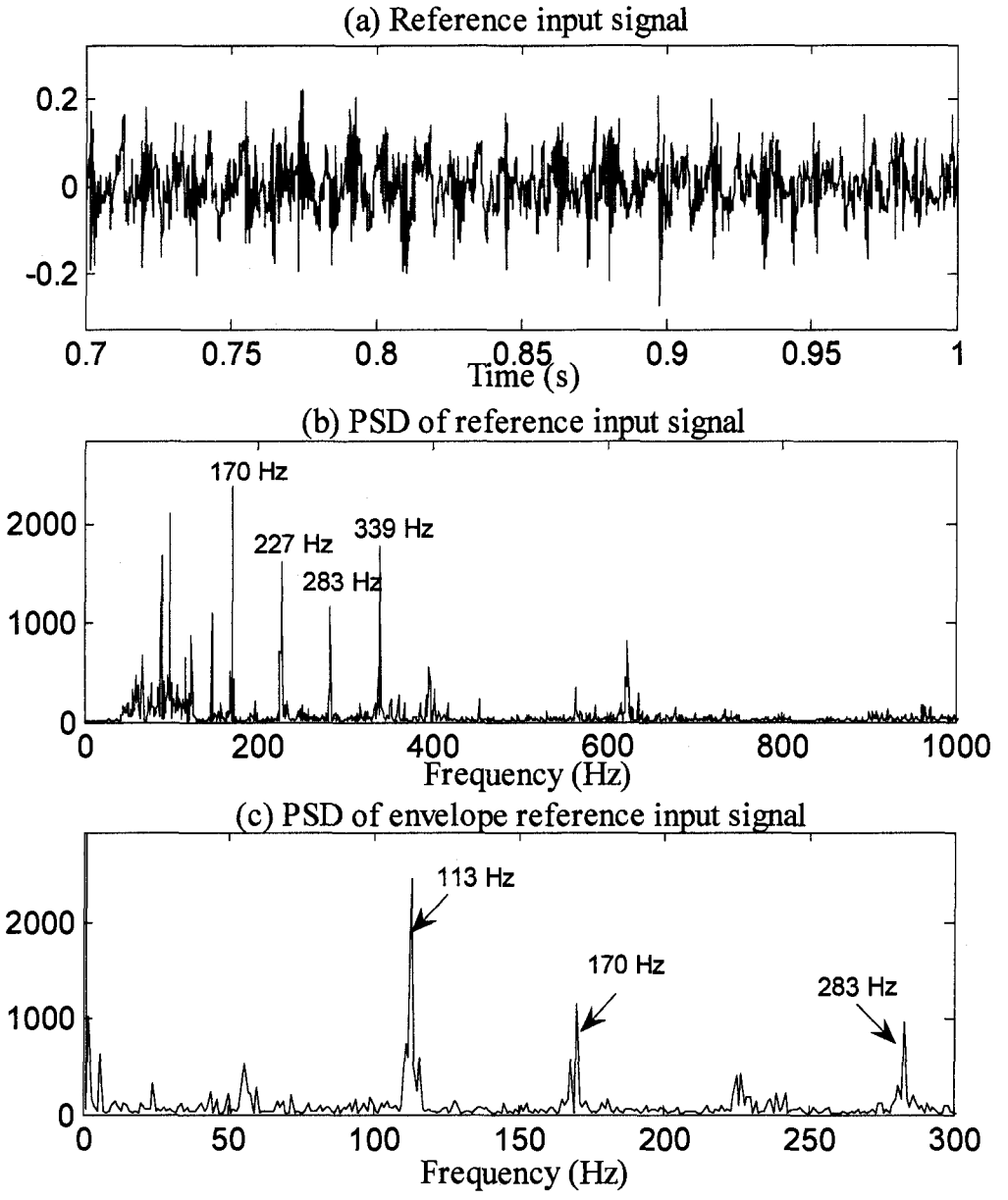

Figure 3-20. Reference input of experiment 3: (a) raw signal, (b) frequency domain representation of the reference input signal, and (c) envelope spectrum of the signal

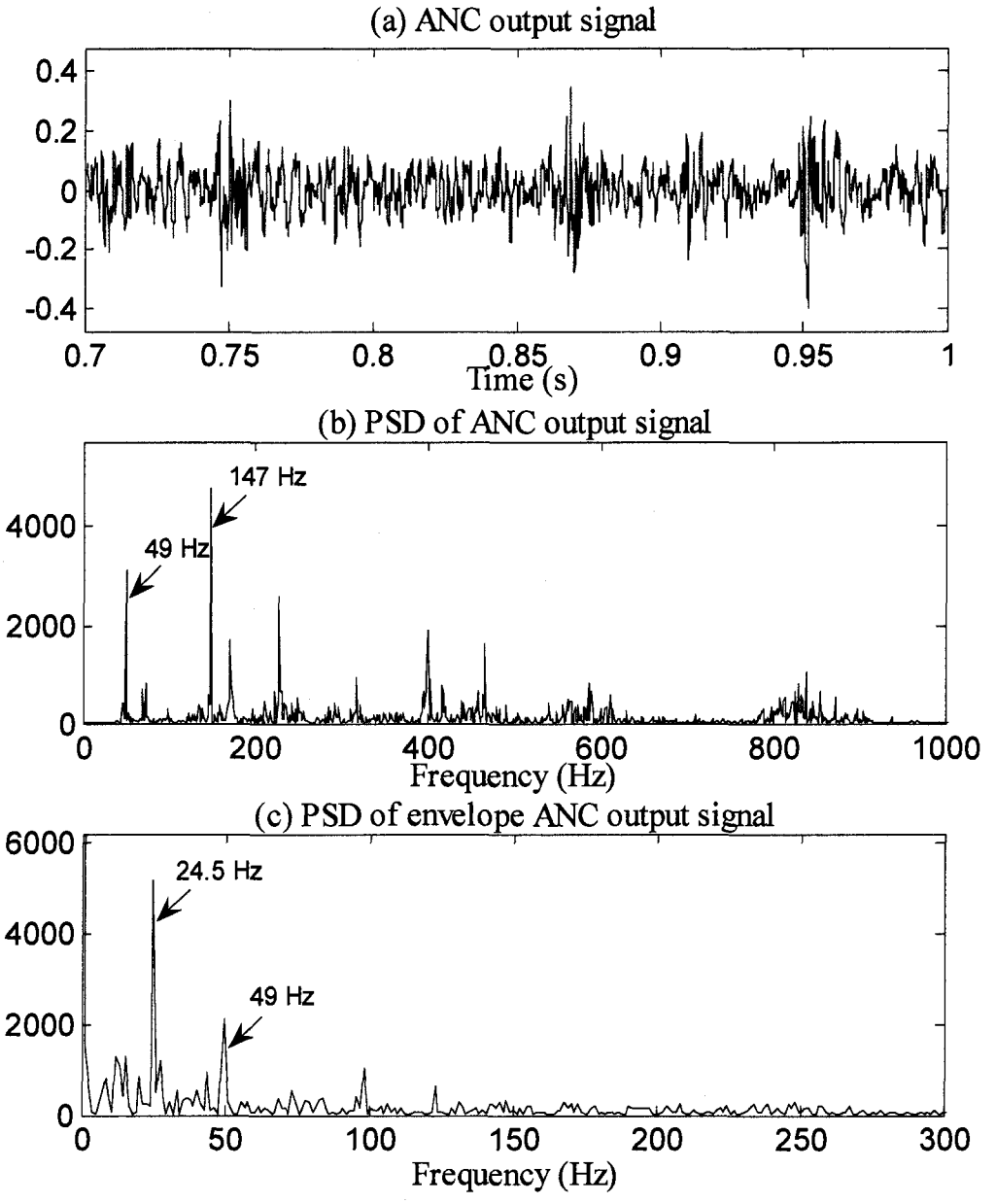

Figure 3-21. ANC result of experiment 3: (a) output signal, (b) frequency domain representation of the signal, and (c) envelope spectrum of the signal

3.5 Summary

The performance of the adaptive noise canceller is greatly affected by the operating parameters (e.g., the transversal filter length M and the step-size parameter μ). However, the lack of guidance in choosing the operating parameters has prevented many researchers from implementing ANC (Antoni and Randall 2004). In this chapter, criteria to determine the transversal filter length based on the AIC and the step-size parameter based on misadjustment value for bearing fault detection are adopted. The adopted criteria do not require any prior knowledge of the signal characteristics and are easy to apply. These criteria are robust and can be applied for different sampling rates and different sampled data lengths. In addition, a procedure is used to ensure that there is no settling time required to implement the ANC in a stationary environment. The results from both simulation and experiments confirm that the ANC is able to extract bearing signal from the mixed bearing and gear signals.

The ANC can be applied as a pre-process step before other bearing fault detection techniques are applied. The resulting ANC output signal removes other interference signal (e.g., gear signal) and can be used to detect incipient bearing fault. It is also important to point out that though the sensor mounting locations are important when acquiring primary input and reference input, the ANC can tolerate sensor locations that are less ideal due to various operational and technical restrictions.

4 Oil Debris Monitoring using Self Adaptive Noise Cancellation

Oil debris monitoring is a more direct approach commonly used in the industry for machine fault detection. An inductive ODM sensor detects the size and type of the metal particles produced by the faulty machine components in the lubricating oil line, providing useful information regarding the health condition of the machine components. The ODM sensor is subjected to vibration and other operating conditions of the machine. Interference such as the vibration signal experienced by the ODM sensor can corrupt the metal particle signatures in the collected signal. The metal particle signature detected by the ODM sensor is non-periodic in nature. It is the aim of this chapter to examine the effectiveness of the adaptive noise canceller to separate the non-periodic metal particle signature from the periodic interference signal. Simulations and experiments will be performed to verify the effectiveness of the ANC in removing the interfering vibration signal and revealing the hidden metal particle signature. The details are presented in the following sections.

4.1 Introduction

The inductive ODM sensor, with its cross section shown in Figure 4-1, is a device that is generally installed in the gearbox oil supply line and allows the lubricating oil flow through without obstruction. The sensor incorporates a magnetic coil assembly and functions by monitoring the disturbance to an alternating magnetic field caused by the passage of a metallic particle through the sensing coil assembly. The minimum detectable particle sizes are determined primarily by the inner diameter of the coil assembly and the operating environment (temperature, vibration, EMI etc.) of the sensor (Howe and Muir 1997).

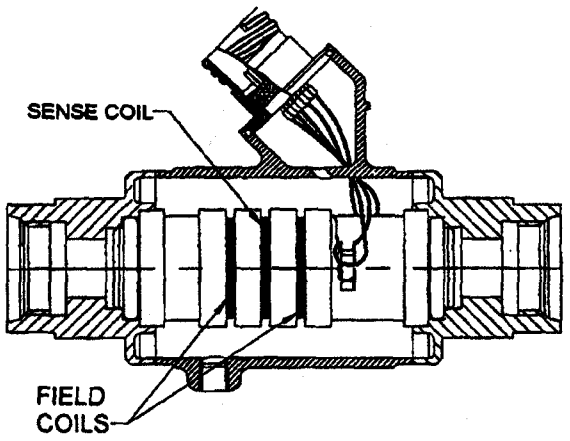

Figure 4-1. ODM sensor cross section (Miller and Kitaljevich 2000)

When a metallic particle passes through the magnetic field of the sensing region, it creates a characteristic output signature as shown in Figure 4-2. The amplitude and phase of the output signature are used to identify the size and nature of the particle. The amplitude of the signal is proportional to the mass of the ferromagnetic metal particles and to the surface area of the conductive non-ferromagnetic metal particles. The phase of the signal for non-ferromagnetic metals is opposite to that of ferromagnetic metals allowing a distinction to be made between the types of metal particles (Miller and Kitaljevich 2000).

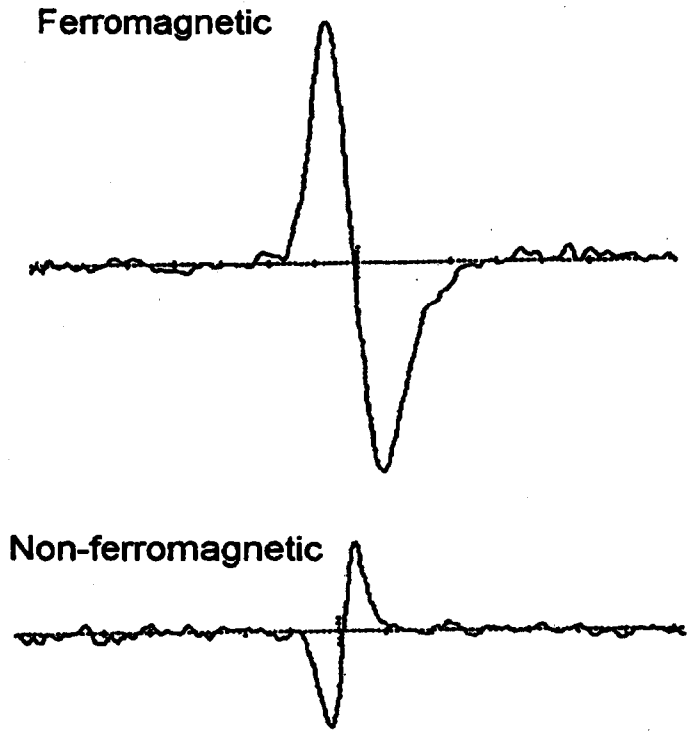

Figure 4-2. ODM sensor output signal (Miller and Kitaljevich 2000)

Harris (1984) indicated that if a rolling bearing in service is properly lubricated, properly aligned, kept free of abrasives, moisture, and corrosive reagents, and properly loaded, then all causes of damage can be eliminated except material fatigue. Rolling contact fatigue results in small particles breaking off from the surface of the raceways and rolling elements. The flaking eventually forms pits or spalls in the load-carrying surface and can lead to catastrophic failure of the bearing due to cracks. Townsend (1991) explained that pitting is a fatigue failure caused by exceeding the surface fatigue limit of the gear material. Pitting occurs when small pieces of material break off from the gear surface, producing pits on the contacting surfaces, and can eventually lead to cracks and catastrophic failure of the gear. By detecting the metal particle signatures and the magnitude of the signatures, we can monitor the number of the metal particles and their sizes over time and identify the increment of metal particle numbers and/or sizes in the oil line. Since the number and sizes of the metal particle have a direct relationship with

the condition of the bearings and gears, they are good indicators of the health condition of the bearings and gears in the rotating machinery.

4.2 Adaptive noise cancellation applied to oil debris monitoring

The operating environment of the ODM sensor affects the detection of the metal particles. The ODM sensor is not only sensitive to metal particles but also to the vibration experienced by the sensor. For example, when an ODM sensor is installed in an aircraft engine lubricating oil line, the sensor picks up the engine vibration signal as well. The vibration signal is a mixture of the periodic signals caused by various engine components and the vibration signal interferes with metal particle signal causing false metal particle detection and particle number count.

An adaptive noise canceller can be applied to remove the interference vibration signal and reveal the metal particle signal from the mixed signal, provided a reference input signal that contains only the vibration signal is available. A possible solution to obtain such a reference input signal is to mount another identical ODM sensor on the engine without connecting it to the engine oil line. Thus the sensor only collects the interference vibration signal without any metal particle signal. However, this is very costly and in many cases infeasible because of the already crowded environment.

For the above reason, this study proposes to implement ANC using a single ODM sensor. Unlike the faulty bearing signal, the metal particle signal is non-periodic and can be considered a broad-band signal. When ANC is used to remove periodic signals from a broad-band signal, a delayed primary input signal can be used as the reference input signal and no external reference source is required. Therefore, only one ODM sensor is required and additional hardware and software cost of installing another ODM sensor can be avoided.

The following sections will analyze this special form of the adaptive noise canceller that requires no external reference source (also refers to as self adaptive noise canceller and hence abbreviated as SANC hereafter). The same criteria used to determine the operating parameters from the bearing fault detection in the previous chapter will be

applied. In the end, procedures on how to apply the SANC to remove interference vibration signal in the oil debris monitoring application will be summarized.

4.2.1 Self adaptive noise cancellation

Self adaptive noise cancellation is a method that can be used to remove periodic interference signals from the mixed broadband and periodic signals. The block diagram of a SANC is illustrated in Figure 4-3. From the figure, we can see that SANC is different from the original ANC in that its reference input signal, instead of being obtained separately, consists of a delayed version of the primary input signal. The delay, denoted by Δ in the figure, is called the decorrelation delay, measured in units of the sampling period (Widorw et al 1975b). Because the broadband signal is non-periodic, the decorrelation delay, Δ, is able to make the broadband signal components in the reference input $u(n-\Delta)$ to become decorrelated from the broadband signal components in the primary input $u(n)$. The interference signal components, which are periodic, remain correlated in the primary input and the reference input.

The operation of SANC can be explained intuitively as follows. The delay causes decorrelation between the broadband components of the mixed signal in the primary input and the reference input while introducing a phase difference between the periodic components. The phase difference of the periodic components between the primary input and the reference input is readjusted so that they cancel each other at the summing junction. The adaptive filter that utilizes the LMS algorithm behaves like a notch filter with deep notches centered at frequencies of the periodic components. Thus the output signal produces a minimum error signal composed of the broadband component of the mixed signal alone.

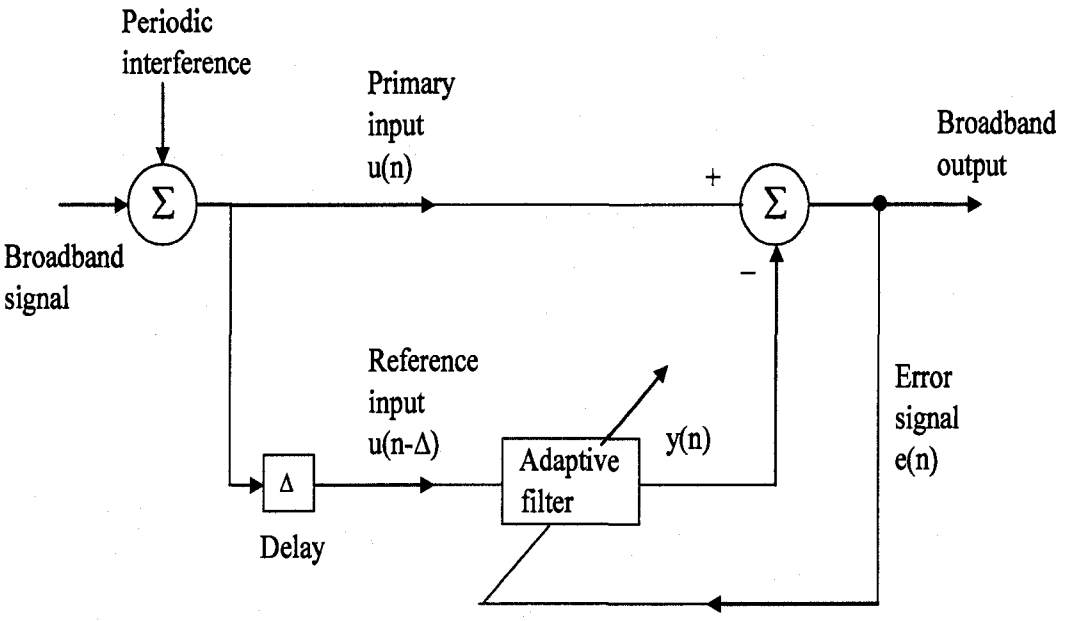

Figure 4-3. Block diagram of the self adaptive transversal filter

The signal-flow-graph representation of the LMS algorithm employed in the SANC is depicted in Figure 4-4. It is seen that the desired signal $d(n)$ that is obtained separately in the signal-flow-graph of the LMS algorithm used in the ANC (Figure 3-2) is replaced with the mixed signal $u(n)$. The delayed version of the mixed signal $u(n-\Delta)$ is fed to the LMS algorithm to update the transversal filter weights. The output of the transversal filter $y(n)$ consists the periodic interference components that are compensated for the phase difference created by the delay and is subtracted by the mixed signal $u(n)$. The SANC output signal is the error signal $e(n)$ which contains the broadband components in the primary input. SANC can be considered as a special form of the ANC and can be applied to separate broadband signal from periodic interference signals or vice versa.

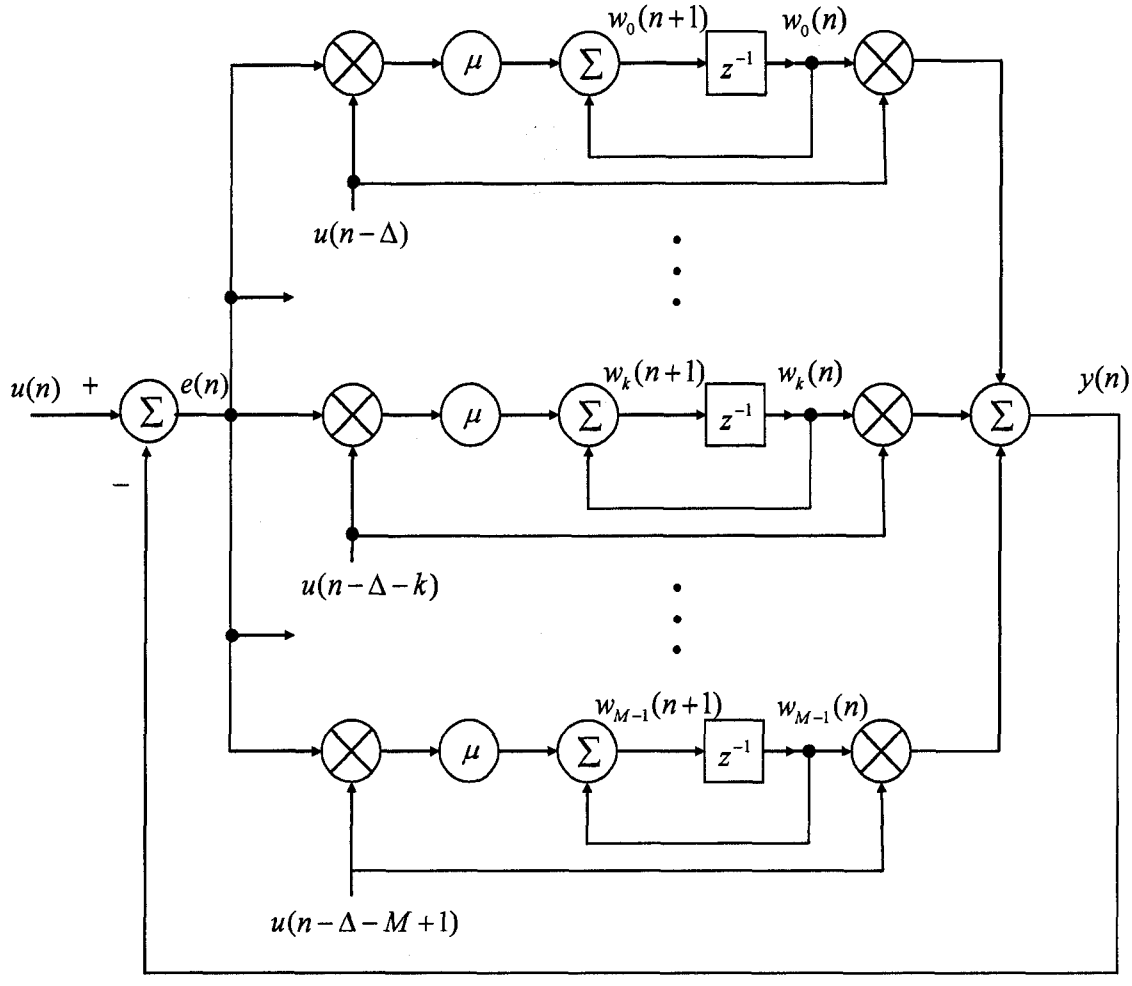

Figure 4-4. Signal-flow-graph representation of a self adaptive noise canceller

4.2.2 SANC operating parameters

The operating parameters determine the performance of the SANC in the same way as they do for the original ANC. Comparing to the original ANC, there is one more operating parameter in the SANC, i.e., the decorrelation delay, Δ. The following discussion is devoted to methods and criteria to select the proper SANC operating parameters for the ODM application.

4.2.2.1 The decorrelation delay Δ

The decorrelation delay, Δ, should be decided according to the broadband signal correlation. When the uncorrelated white noise is the broadband noise, a delay value of

one is sufficient to cause the decorrelation between the white noise in the primary input from the white noise in the reference input. When the broadband noise is the correlated color noise, the decorrelation delay should be assigned a value large enough to remove the correlation between the color noise in the primary input and the color noise in the reference input (Ziedler et al 1978).

In the ODM application, when a metal particle passes through the sensing region of the sensor, it creates a characteristic output signal. A delay value larger than the length of the characteristic output signal sampled time units is usually needed to achieve the decorrelation between the metal particle signal in the primary input and the metal particle signal in the reference input. When the delay value is smaller than the length of the characteristic output signal sampled time units, distortion of the characteristic output signal can occur, especially when there is more than one metal particle in the sampled data block.

The length (in terms of number of data samples) of the metal particle characteristic signal is related to the flow rate of the lubricating oil, the sampling rate and the size of the metal particles. When installing the ODM sensor in a particular application, knowledge of the lubricating oil flow rate is available and the sampling rate is pre-determined. Therefore, the minimum decorrelation delay value can be calculated when the estimated largest possible metal particle size is used. The reference input signal can therefore be derived by delaying the primary input signal with the delay, Δ, larger than the calculated minimum decorrelation delay value. A delay value larger than the minimum decorrelation delay value allows the metal particle characteristic signal in the primary input to become decorrelated from the metal particle characteristic signal in the reference input and minimizes the distortion.

4.2.2.2 The transversal filter length M

Since SANC employs the autoregressive model structure in the LMS algorithm, the AIC method can also be applied in the SANC. Eq. 3-12 and the Levinson-Durbin recursion are used to obtain the minimum model order which is used for the transversal filter length M. The simulation and experiments conducted in the later sections have

verified that the filter length obtained from Eq. 3-12 provides enough frequency selectivity for the ODM application.

4.2.2.3 The step-size parameter μ

The performance of the SANC also depends on adaptive filter weight fluctuations. A small misadjustment is positively correlated to small individual adaptive filter weight fluctuations and ensures the satisfactory performance of the SANC. The same misadjustment value (0.025) used in the bearing fault detection is used here to test the SANC performance. The result verifies that this value is suitable to deliver desirable SANC performance while achieves reasonable convergence rate for the ODM application in a stationary environment. For the ODM application in a non-stationary environment, a larger misadjustment value which ensures a faster convergence rate may be used. The associated step-size parameter μ is obtained by setting Eq. 3-17 equal to the appropriate misadjustment value.

4.2.2.4 Steady state self adaptive noise canceller

The initial values of the SANC filter weights affect the settling time to reach the steady state SANC. For on-line ODM applications in a stationary environment, zero settling time can be achieved. The first sampled data block can be used to reach the steady state SANC and the last updated filter weights of the first sampled data block is saved. The saved filter weights are used as the initial filter weights for the second sampled data block. The last updated filter weights of the second data block is again used as the initial filter weights for the next sampled data block. Utilizing this procedure, the initial filter weights are the steady state filter weights and there is zero settling time to reach the SANC output signal in a stationary environment.

4.2.3 SANC procedures for oil debris signature detection

The following steps summarize the SANC procedures applied to the detection of the metal particle signal contaminated by interfering vibration signals.

Step 1. Use the signal collected by the ODM sensor as the primary input signal.

Step 2. Set the delay Δ and derive the reference input signal. The delay should be larger than the length (in terms of number of data samples) of the estimated

largest metal particle characteristic signal. The reference input signal is derived by delaying the primary input signal by the obtained delay value Δ.

Step 3. Determine the transversal filter length M. Obtain the filter length by minimizing $AIC(l) = N\ln(\varepsilon_l) + 2l$ where l is the model order, N is the total data length, and ε_l is the error power associated with the model order l. The desired filter length is the model order which minimizes the AIC.

Step 4. Calculate the step-size parameter μ. Obtain the step-size parameter by setting the misadjustment $\beta = \frac{\mu}{2} E\left[\|u(n)\|^2\right] \approx 0.025$ where $E\left[\|\mathbf{u}(n)\|^2\right]$ is the average total reference input power. The misadjustment value can be tuned to achieve faster convergence rate without causing large fluctuation of filter weights in a non-stationary environment.

Step 5. The last adaptive filter weights are saved from each sampled data block and used as the initial filter weights of the following sampled data block. There is no settling time of the SANC in a stationary environment.

Step 6. Apply the SANC. The resulting steady state SANC output signal will remove the interference periodic vibration signal and reveal the metal particle signature.

4.3 Simulation

In the simulation study, one fine ferrous particle (175 microns in diameter) and one fine non-ferrous particle (508 microns in diameter) are used to generate the metal particle ODM signal. The metal particles are glued inside a thin plastic catheter and the catheter is pulled through the ODM sensor core. When the ferrous and non-ferrous particles pass through the sensing coil, two distinct signatures are generated with different phase orders.

Interference vibration signal is usually modelled as a combination of various periodic signals. Therefore, the simulated gear vibration signals that are modelled by Eq. 3-22 with a mixture of periodic signals are used to simulate the interference vibration signal. The simulated vibration signal contains two simulated gear vibration signals with meshing frequencies of 120 Hz and 170 Hz, each with five harmonics, respectively. The

white Gaussian noise with a signal to noise ratio of -3dB is added to the mixed metal particle and vibration signal. The sampling rate is set at 8000 Hz.

The simulated signal with the two metal particles and the added white Gaussian noise with a SNR of -3dB is displayed in Figure 4-5a. A close-up view of the two metal particles characteristic signatures are also shown in the figure. Figure 4-5b shows the primary input signal containing interference vibration and the two metal particle signals with added noise. The existing algorithm used in industry measures the particle signature amplitude and counts the number of passing particle based on the threshold values. It is obvious that if the signal as shown in Figure 4-5b is left untreated, the particle signatures cannot be distinguished from the vibration signal by the existing algorithm. The end result would be an overstated particle count and false alarms due to the large signal amplitude that could be way above the threshold values used in most applications.

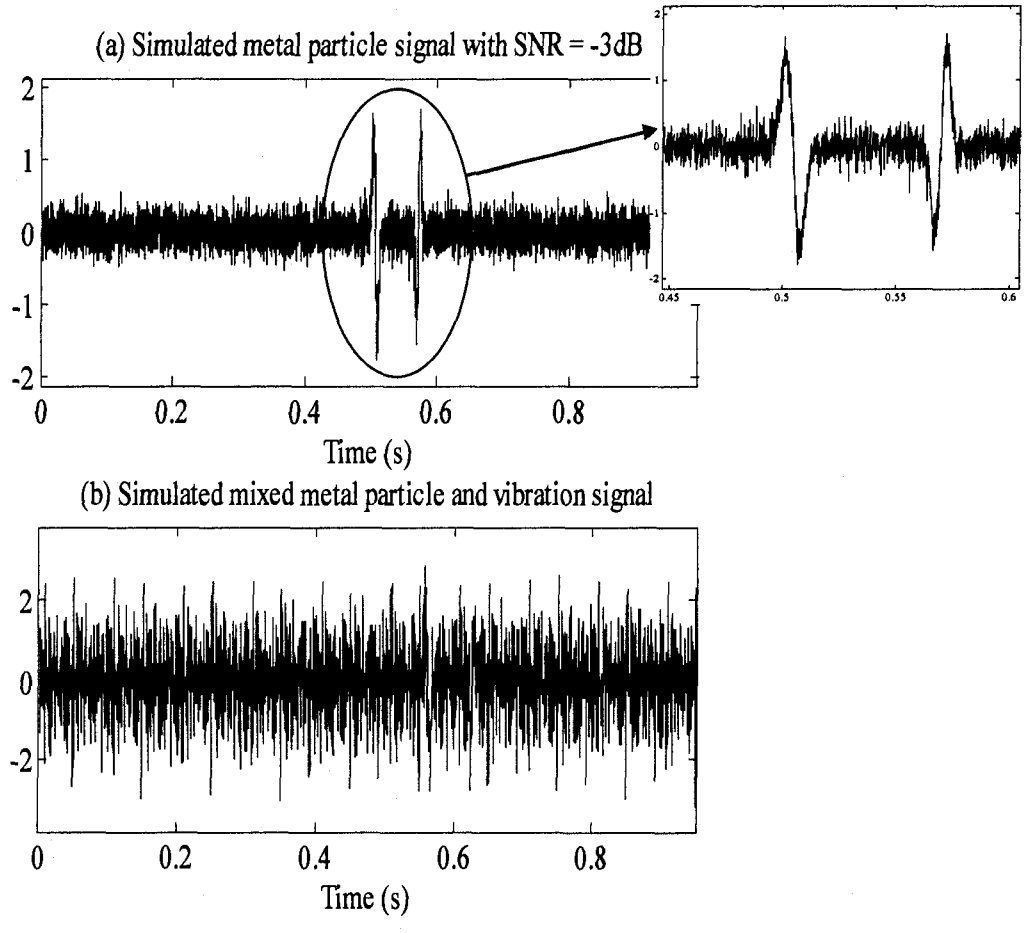

Figure 4-5. Simulated mixture of metal particle and vibration signals

In the context of this simulation study, the largest metal particle characteristic signal spans roughly 250 data samples. The reference signal is generated with a delay of 350 data samples from the primary input signal. The transversal filter length M equals 236 according to the AIC method using Eq. 3-12. The required error power associated with the model order in Eq. 3-12 can be calculated using the 'lpc' built-in function in MATLAB which calculates the error power using the Levinson-Durbin recursion. The step-size parameter μ is 0.000326 which is obtained using Eq. 3-17 with the misadjustment value of 0.025. The output signal of the SANC is shown in Figure 4-6 with a close-up view of the two metal particle characteristic signatures. Comparing to Figure 4-5b, we can see that the interference vibration signal has been removed. The two metal particle signals, one ferrous and one non-ferrous can be clearly identified along with the added white Gaussian noise. Comparing the close-up figures of Figure 4-5a and Figure 4-6, we can see they are very similar with very little distortion. With this SANC output, the particle detection algorithm will be able to correctly detect the two metal particles.

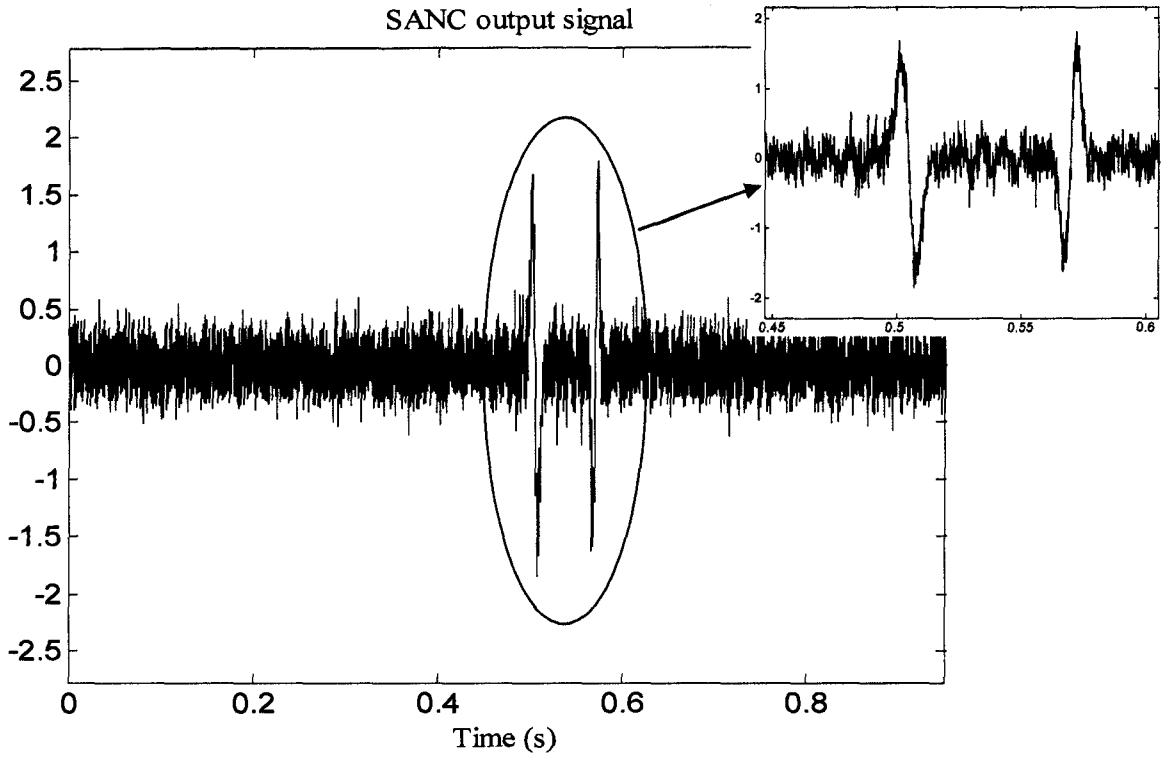

Figure 4-6. SANC output of separated metal particle signal

4.4 Experiments

To further examine the performance of the SANC, it is applied to experimental data. In the experiments, the oil debris sensor was mounted on a vibration shaker in a company to imitate the condition where the sensor is installed in the gearbox oil line experiencing engine vibration. The vibration signal is generated with the vibration shaker running at a controlled frequency. Again, the catheter with metal particles glued inside is pulled through the core of the sensor to create the metal particle signal with the shaker operating at a certain frequency and vibration amplitude.

Three tests are conducted. In the first test, the shaker is operated at 57 Hz and the catheter containing a non-ferrous particle (508 microns in diameter) is guided through the ODM sensor core. For the second test, the vibration frequency of the shaker is increased to 450 Hz and a ferromagnetic particle (175 micron in diameter) and a non-ferromagnetic particle (508 micron in diameter) pass through the sensor twice to generate the test signals. In the third test, a small paper ball is passed through the ODM sensor core while

the vibration frequency of the shaker is maintained at 450 Hz. The sampling frequencies for all the three tests are 8000 Hz.

4.4.1 Result of the first test

Figure 4-7 shows the primary input signal of the first test. The threshold based algorithm certainly cannot detect the non-ferrous metal particle signal from the plot. From the close-up view of the plot, the estimated length of the metal particle characteristic signature is about 40 data samples. Therefore, the decorrelation delay length is set to 40 data samples to obtain the reference input signal. Eq. 3-12 is used to obtain the transversal filter length where the error power is calculated using the Levinson-Durbin recursion. The obtained transversal filter length M is 57. The step-size parameter is calculated using Eq. 3-17 with the misadjustment value of 0.025. The obtained step-size parameter μ equals 0.038.

The SANC output signal is shown in Figure 4-8, which shows that the SANC has successfully removed the interference vibration signal and the metal particle signature can be easily detected. The non-ferrous metal particle characteristic (phase order) of the signal is clearly observed in the close-up window.

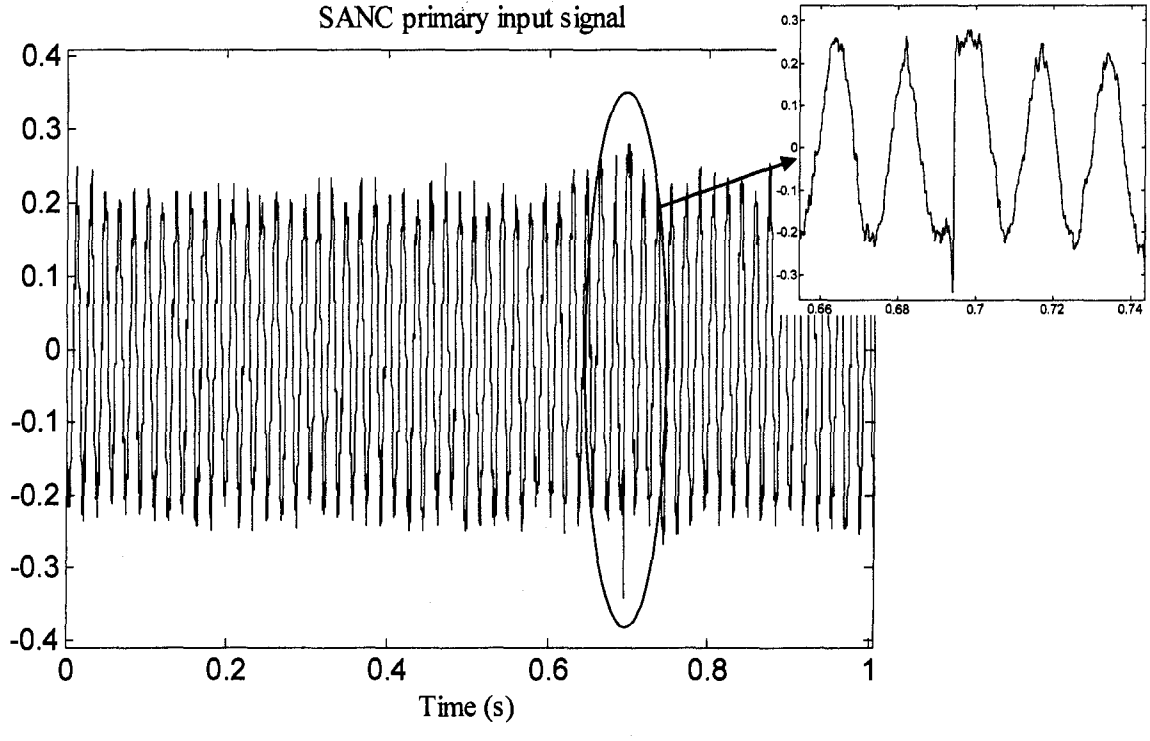

Figure 4-7. Primary input signal of the first test

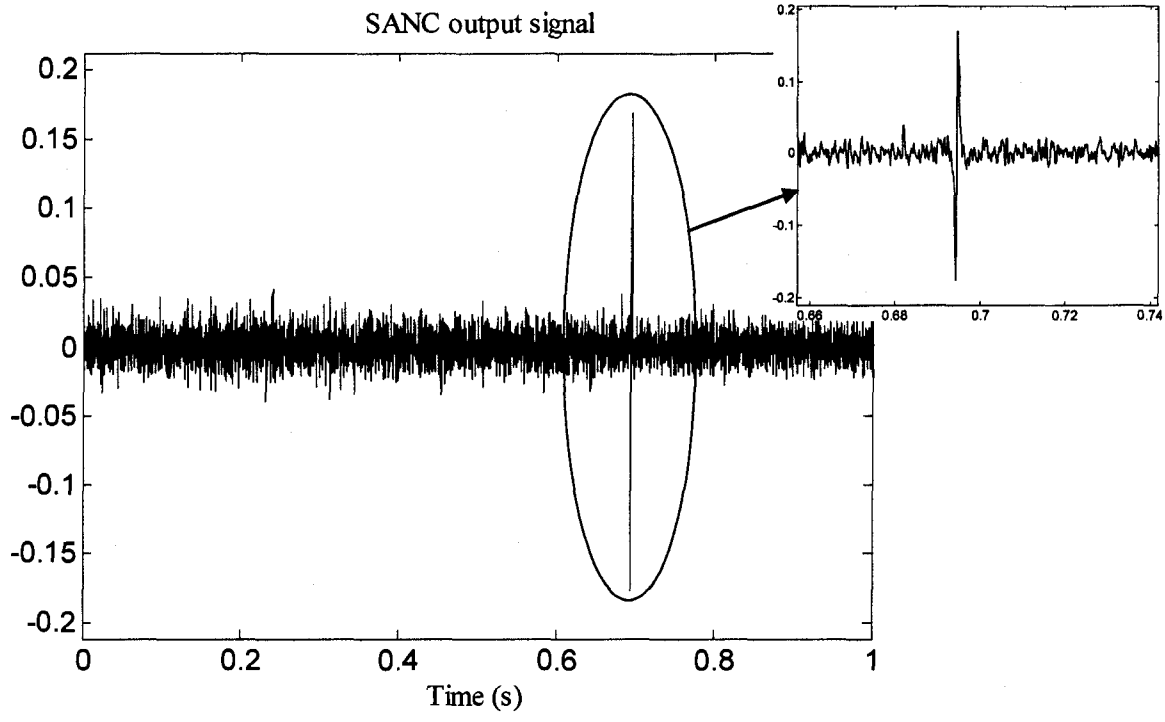

Figure 4-8. SANC output signal of the first test

4.4.2 Result of the second test

The primary input signal of this test is plotted in Figure 4-9. Although the four metal particles can be recognized from the primary input signal, the metal particle characteristic signatures are clouded with vibration signal. The SANC is applied to remove the heavy vibration signal. From Figure 4-9, the length of the largest metal particle is estimated to be 750 sample points, which is hence used as the decorrelation delay, Δ. The reference input signal with a delay of 750 samples from the primary input signal is derived. The transversal filter length, M, obtained using the AIC is 304. The step-size parameter, μ, is 0.00086 with 0.025 as the misadjustment value.

The SANC output signal of this test is displayed in Figure 4-10. The heavy vibration signal shown in Figure 4-9 has been mostly removed. The four metal particles (2 ferrous and 2 non-ferrous) can be clearly identified in the SANC output signal and little distortion can be observed.

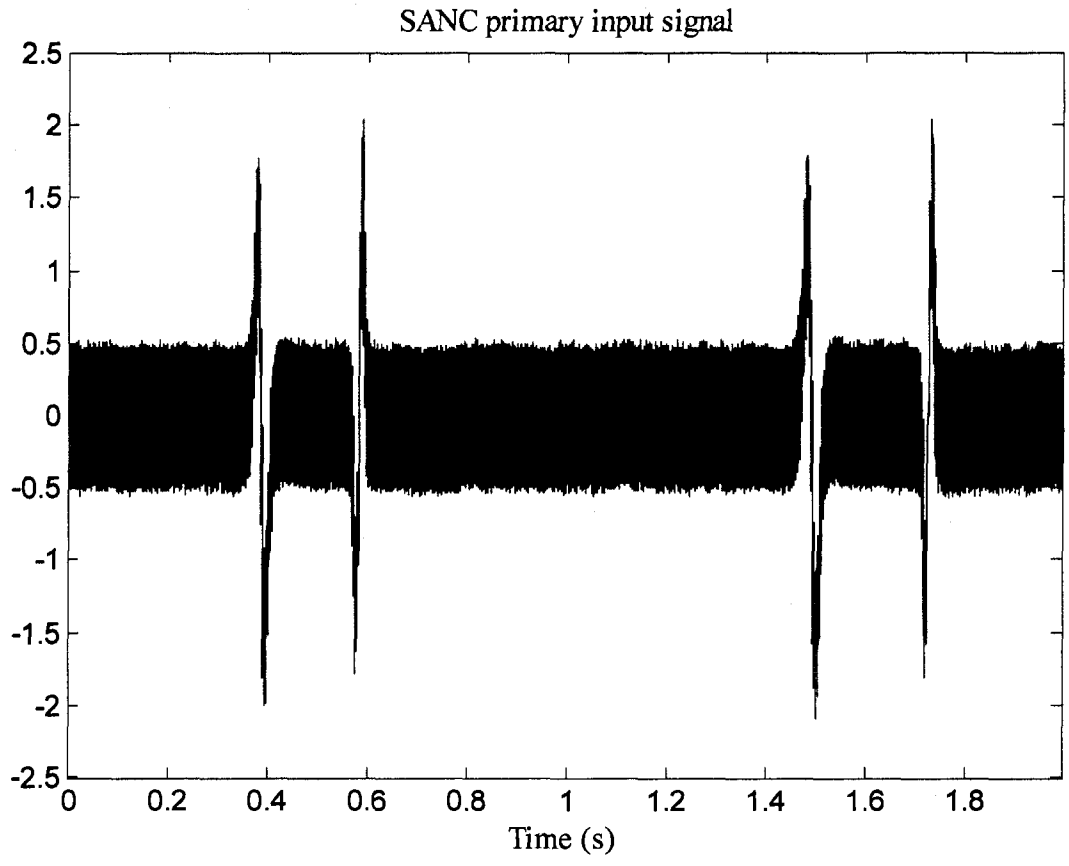

Figure 4-9. Primary input signal of the second test

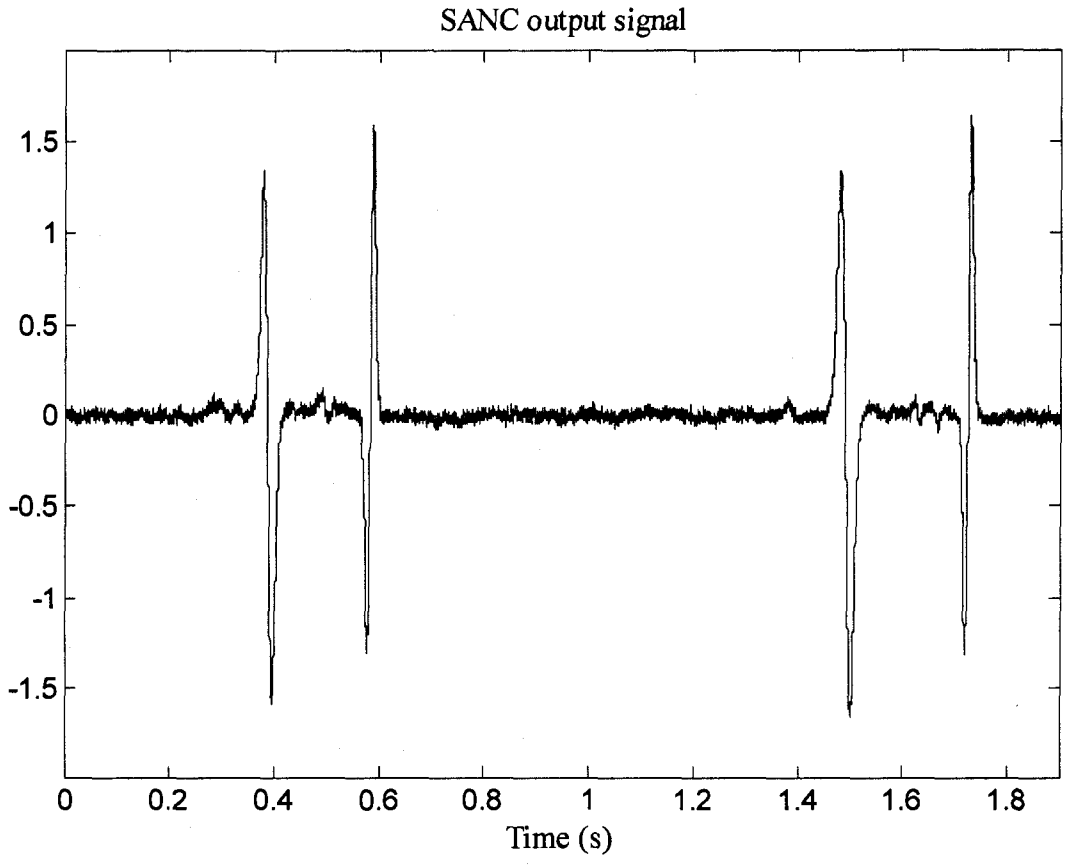

Figure 4-10. SANC output signal of the second test

4.4.3 Result of the third test

In test 3, a small paper ball is passed through the ODM sensor while the sensor is subject to heavy vibration generated by the shaker. Figure 4-11 shows the collected primary input signal containing a small paper ball corrupted by the interference vibration signal. The small paper ball signature detected by the ODM sensor is similar to one very small ferrous particle characteristic signature. Without proper signal processing, the existing algorithm adopted by industry cannot detect the small ferrous particle characteristic signature. For this reason, the SANC is applied to the collected signal. The estimated length of the metal particle characteristic signature is about 100 samples (according to Figure 4-11). The reference input signal is therefore obtained by delaying the primary input signal with the decorrelation value of 100. The obtained SANC

transversal filter length M is 54 and the step-size parameter μ is 0.0066 with the value of misadjustment equals 0.025.

As shown in Figure 4-12 and a more detailed view around 0.2 and 0.3 seconds, the SANC successfully separates the particle signal from the interference vibration signal. The ferrous particle signature can now be identified in the SANC output signal. This test indicates that the SANC can reveal very weak particle signal that has been almost completely submerged in the periodic signal.

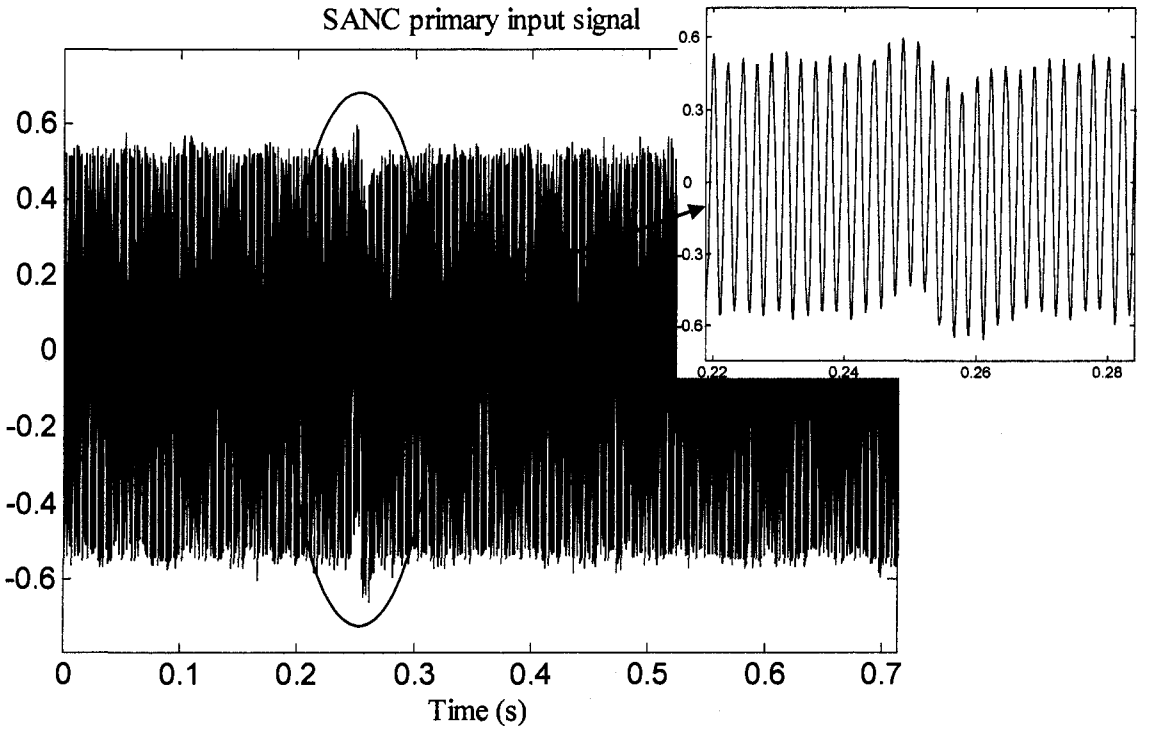

Figure 4-11. Primary input signal of the third test

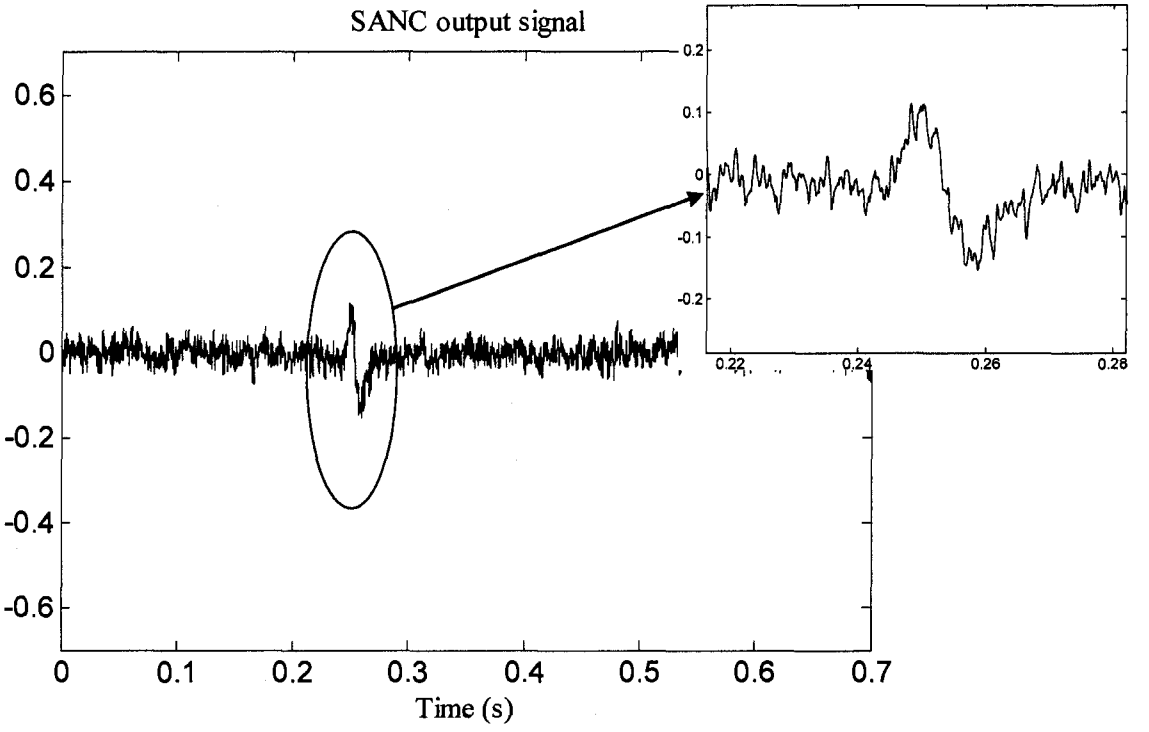

Figure 4-12. SANC output signal of the third test

4.5 Summary

In this chapter, it is shown that the self adaptive noise canceller, a special form of the adaptive noise canceller, can be applied to separate non-periodic signal from periodic interference signals. Unlike the original ANC, the reference input signal of the SANC does not require an external source. Because the signal to be recovered is a non-periodic broadband signal, the delayed primary input signal can be used as the reference input signal. The delay value should be large enough to cause de-correlation between the non-periodic broadband signals in the primary and the reference input. The same methods used in selecting the transversal filter length and the step-size parameter for the ANC in bearing fault detection can also be adopted in the SANC. The SANC is implemented to remove the interference vibration signal in the oil debris monitoring application in this chapter. The SANC output signal can reveal the metal particle signal that is partially or completely submerged in the primary input signal. The results from the simulation and

experiments have shown that the separated metal particle signal can be correctly detected and counted by the existing particle monitoring algorithm.

5 Conclusion and Future Research

5.1 Conclusion

In this thesis, the adaptive noise canceller based on the least mean square algorithm has been applied to bearing fault detection and oil debris monitoring. The criteria and guidelines for selecting the appropriate operating parameters for the LMS based ANC have been proposed. A procedure to achieve zero settling time of the steady state adaptive noise canceller is also illustrated for on-line adaptive noise cancellation application. In the bearing fault detection application, ANC is used to extract the bearing signal from corrupting periodic interfering signals originating from other sources. The simulation and experiment results have shown that ANC can successful remove interfering gear signals and reveal the bearing signal. In the oil debris monitoring application, the self adaptive noise canceller, a special form of the ANC, is applied to remove the vibration signal and reveal the hidden metal particle signal. Because of the non-periodic nature of the metal particle characteristic signal, no external source is required to obtain the reference input signal. In this case, the reference input signal is obtained as a delayed version of the primary input signal. The simulation and experiment results have demonstrated that SANC can remove the corrupting vibration signal and reveal the hidden metal particles characteristic signal.

The LMS based ANC is computationally efficient and is suitable for on-line application. The proposed ANC operating parameters selection criteria and the procedure to minimize the settling time have the following features:

1. The selection criterion of the ANC operating parameter can be applied to different sampling rates and different sampled data block lengths. The selection criteria are robust and easy to apply.
2. The signal processing procedure does not require any settling time to reach the steady state ANC output signal in a stationary environment. Therefore, it is not necessary to estimate the settling time when implementing the ANC for on-line applications.

5.2 Future research

Further studies may be carried out in the following directions:

1. When multiple interfering signals originating from different sources corrupt the monitored signal, multiple sensors mounted close to these different interfering sources may be used to collect multiple reference input signals. A multiple reference adaptive noise cancelling system may be implemented to eliminate these multiple interfering signals. Figure 5-1 shows the block diagram of a possible multiple reference adaptive noise cancelling system.

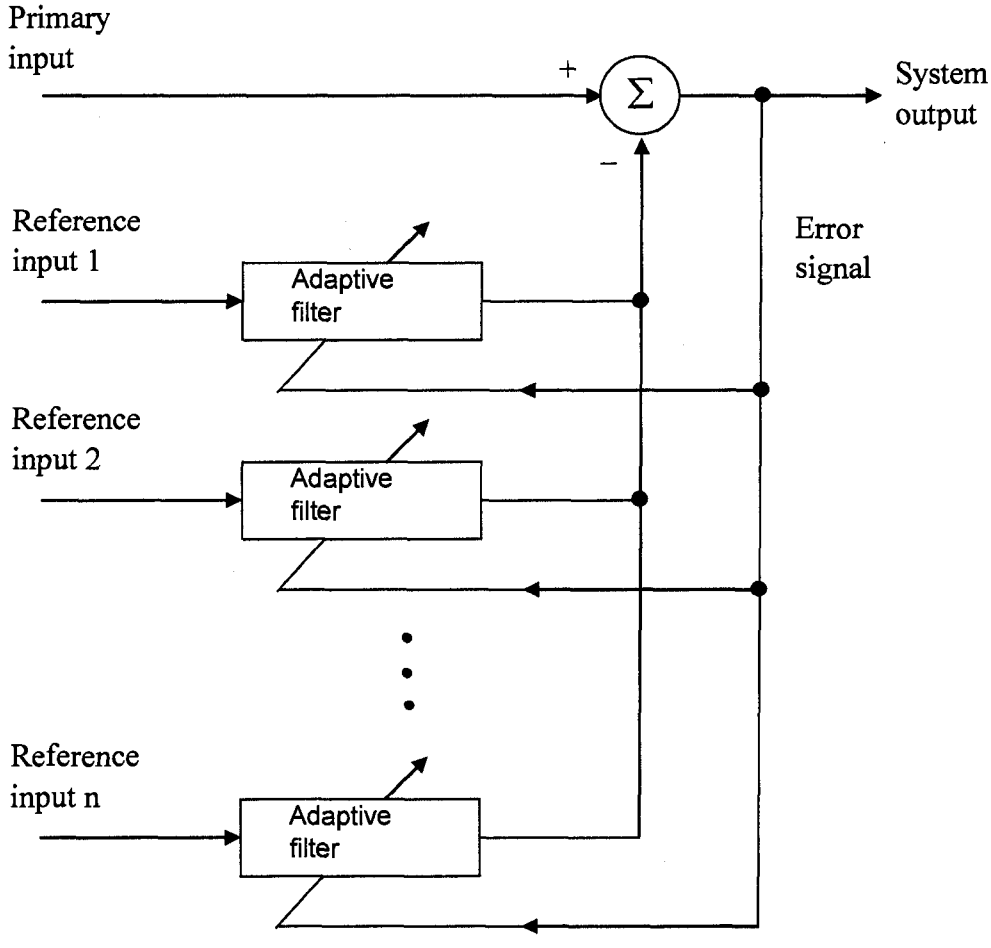

Figure 5-1. Block diagram of a multiple reference adaptive noise canceller

2. The performance of the proposed ANC/SANC in a non-stationary environment should be examined. Modification or improvement may be needed.

3. In a non-stationary environment, an adaptive step-size parameter $\mu(n)$ may improve the performance of ANC/SANC comparing to a constant step-size parameter μ. Different algorithm to update the adaptive step-size parameter needs to be investigated and evaluated.

References

Akaike, H., 1974, A new look at the statistical model identification. *IEEE Transactions on Automatic Control*, vol. 19(6), 716-723.

Akaike, H., 1973, Maximum likelihood identification of Gaussian autoregressive moving average models. *Biometrika*, vol. 60(2), 255-265.

Antoni, J., and Randall, R.B., 2004, Unsupervised noise cancellation for vibration signals: part I-evaluation of adaptive algorithms. *Mechanical Systems and Signal Processing,* vol. 18, 89-101.

Bennett, C., and Sharpley, R., 1988, *Interpolation of operators*, (Boston, MA: Academic Press).

Butterweck, H.J., 2001, A wave theory of long adaptive filters. *IEEE Transactions on Circuits and Systems – I: Fundamental Theory and Applications*, vol. 48(6), 739-747.

Butler, D.E., 1973, The shock pulse method for the detection of damaged rolling bearings, *NDT Int*, 92–95.

Carcaterra, A., and Sestieri, A., 1997, Complex envelope analysis: a quasi-static approach to vibrations. *Journal of Sound and Vibration,* vol. 201(2), 205-233.

Chaturvedi, G.K., and Thomas, D.W., 1981, Adaptive noise cancelling and condition monitoring. *Journal of Sound and Vibration*, vol. 76(3), 391-405.

Dempsey, P.J., 2000, A comparison of vibration and oil debris gear damage detection methods applied to pitting damage. *NASA Technical Memorandum*, 210371, 1-17.

Dempsey, P.J., 2001, Gear damage detection using oil debris analysis. *NASA Technical Memorandum*, 210936, 1-15.

Dempsey, P.J. and Afjeh, A.A., 2002, Integrating oil debris and vibration gear damage detection technologies using Fuzzy logic. *NASA Technical Memorandum*, 211126, 1-21.

Dempsey, P.J., Lewicki, D.G., and Decker, H.J., 2004, Investigation of gear and bearing fatigue damage using debris particle distributions. *NASA Technical Memorandum*, 212883, 1-18.

Dyer, D. and Stewart, R.M., 1978, Detection of rolling element bearing damage by statistical vibration analysis. *Trans ASME, Journal of Mechanical Design*, vol. 100(2), 229-235.

Fan, X., and Zuo, M.J., 2006, Gearbox fault detection using Hilbert and wavelet packet transform. *Mechanical Systems and Signal Processing,* vol. 20, 966-982.

Flanagan, I.M., Jordan, J.R. and Whittington, H.W., 1990, An inductive method for estimating the composition and size of metal particle. *Measurement Science Technology*, vol. 1, 381-384.

Flores, A. and Widrow, B., 2004, Assessment of the efficiency of the LMS algorithm based on spectral information. *Signals, Systems and Computers, Conference Record of the Thirty-Eighth Asilomar Conference*, vol. 1, 120 – 124.

Guo, L., Ljung, L. and Wang, G.J., 1997, Necessary and sufficient conditions for stability of LMS. *IEEE Trans. Signal Process*, vol. 37, 1072-1089.

Guo, Y., Tang, K, Cui, H., and Du, W., 2003, Convergence analysis of a deficient-length LMS filter and optimal-length sequence to model exponential decay impulse response. *IEEE Signal Processing Letters*, vol. 10(1), 4-7.

Hassibi, B. and Sayed, A.H., 1996, H^{∞} optimality of the LMS algorithm. *IEEE Transactions on the Signal Processing*, vol. 44(2), 267-280.

Hassibi, B., Sayed, A.H., and Kailath, T., 1993, LMS is H^{∞} optimal. *Proceeding of IEEE Conference on Decision and Control*, vol. 1, 74-79.

Harris, T.A., 1984, *Rolling bearing analysis*, Second ed., (New York, NY: John Wiley & Sons).

Harting, D.R., 1978, Demodulated resonance analysis – a powerful incipient failure detection technique. *ISA Transactions*, vol. 17(1), 35-40.

Haykin, S., 2002, *Adaptive Filter Theory*, 4th ed., (Upper Saddle River, NJ: Prentice-Hall).

Hochmann, D. and Bechhoefer, E., 2005, Envelope bearing analysis: theory and practice. *Proceeding of the IEEE Aerospace Conference*, 3658-3666.

Howe, B. and Muir, D.M., 1997, In-line oil debris monitor (ODM) for helicopter gearbox condition assessment. *Proceedings of the International Symposium on Air Breathing Engines*, Chattanooga, USA, 457-462.

Kay, S.M., 1988, *Modern Spectral Estimation: Theory and Application*, (Englewood Cliffs: Prentice-Hall).

Kay, S.M. and Marple, S.L., 1981, Spectrum analysis – a modern perspective. *Proceedings of the IEEE*, vol. 69(11), 1380-1419.

Lebold, M., McClintic, K., Campbell, R., Byington, C., and Maynard, K., 2000, Review of vibration analysis methods for gearbox diagnostics and prognostics. *Proceedings of the 54th Meeting of the Society for Machinery Failure Prevention Technology*, Virginia Beach, USA, 623-634.

Li, B., Chow, M.Y., Tipsuwan, Y., and Hung, J.C., 2000, Neural-network-based motor rolling bearing fault diagnosis. *IEEE Transactions on Industrial Electronics*, vol. 47(5), 1060-1069.

Lipovszky, G., Solyomvari, K. and Varga, G., 1990, *Vibration Testing of Machines and Their Maintenance*, (Amsterdam, The Netherlands: Elsevier).

Mader, A., Puder, H., and Schmidt, G.V., 2000, Step-size control for acoustic echo cancellation filters-an overview, *Signal Processing*, vol. 80, 1697-1719.

McFadden, P.D., 1986, Detecting fatigue cracks in gears by amplitude and phase demodulation of the meshing vibration, *ASME Transactions Journal of Vibration Acoustics Stress and Reliability in Design*, vol. 108, 165-170. (Reference from Antoni, J., and Randall, R.B., 2004, Unsupervised noise cancellation for vibration signals: part I-evaluation of adaptive algorithms. *Mechanical Systems and Signal Processing,* vol. 18, 89-101.)

McFadden, P.D., and Smith, J.D., 1984a, Model of the vibration produced by a single point defect in a rolling element bearing. *Journal of Sound and Vibration,* vol. 96(1), 69-82.

McFadden, P.D., and Smith, J.D., 1984b, Vibration monitoring of rolling element bearings by the high-resonance technique – a review. *Tribology International*, vol. 17(1), 3-10.

Miller, J.L. and Kitaljevich, D., 2000, In-line oil debris monitor for aircraft engine condition assessment. *Aerospace Conference Proceedings, 2000 IEEE*, Big Sky, USA, vol. 6, 49-56.

Monzingo, R.A. and Miller, T.W., 1980, *Introduction to Adaptive Arrays,* (New York: Wiley-Interscience).

Morando, L.E., 1988, Measuring shock pulses is ideal for bearing condition monitoring, *Pulp & Paper*, vol. 62(12), 96–98.

Ocak, H., and Loparo, K.A., 2001, A new bearing fault detection and diagnosis scheme based on hidden Markov modelling of vibration signals, *Proceeding of IEEE Conference on Acoustic, Speech, and Signal Processing*, vol. 5, 3141-3144.

Pachaud, C., Salvetat, R., and Fray, C., 1997, Crest factor and kurtosis contributions to identify defects inducing periodic impulsive forces. *Mechanical Systems and Signal Processing*, vol. 11(6), 903-916.

Randall, R. B. Ed., 2001, Special issue on gear and bearing diagnostics, *Mechanical Systems and Signal Processing*, vol. 15(5), 827–1029.

Raymond, J.and Guyer, A., 1996, *Rolling Bearings Handbook and Troubleshooting Guide*, (Radnor, PA: Chilton).

Roylance, R.J., 2005, Ferrography-then and now. *Tribology International*, vol. 38, 857-862.

Samanta, B., Al-Balushi, K.R., and Al-Araimi, S.A., 2004, Bearing Fault Detection Using Artificial Neural Networks and Genetic Algorithm, *EURASIP Journal on Applied Signal Processing*, vol. 3, 366–377.

Solo, V., 1997, The stability of LMS. *IEEE Trans. Signal Processing*, vol. 45, 3017-3026.

Simon, D.L., Gang, S., Hunter, G.W., Guo, T., and Semega, K.J., 2004, Sensor Needs for Control and Health Management of Intelligent Aircraft. *NASA Technical Memorandum*, 213202, 1-17.

Tandon, N. and Choudhury, A., 1999, A review of vibration and acoustic measurement methods for the detection of defects in rolling element bearings. *Tribology International*, vol. 32, 469-480.

Tandon, N. and Nakra, B.C., 1992, Vibration and acoustic monitoring techniques for the detection of defects in rolling element bearings – a review. *The Shock and Vibration Digest,* vol. 24(3), 3-11.

Townsend, D.P., 1991, *Dudley's Gear Handbook*, (New York, NY: McGraw Hill).

Tse, P.W., Peng, Y.H., and Yam, R., 2001, Wavelet analysis and envelope detection for rolling element bearing fault diagnosis – their effectiveness and flexibilities. *Journal of Vibration and Acoustics*, vol. 123(3), 303-310.

Wang, W., and Wong, A.K., 2002, Autoregressive model-based gear fault diagnosis. *Journal of Vibration and Acoustics*, vol. 124, 172-179.

Westcott, V.C. and Seifert, W.W., 1973, Investigation of the iron content of lubricating oil using a ferrographic and an emission spectrometer. *Wear*, vol. 23, 239-249.

Whittington, H.W., Flynn, B.W., and Mills, G.H., 1992, An online wear debris monitor. *Measurement Science and Technology*, vol. 3, 656-661.

Widrow, B., Glover, J.R., McCool, J.M., Kaunitz, J., Williams, C.S., Hearn, R.H., Zeidler, J.R., Dong, E., and Goodlin, R.C., 1975a, Adaptive noise cancelling: principle and applications. *Proceedings of the IEEE*, vol. 63(12), 1692-1716.

Widrow, B., McCool, J.M., and Ball, M., 1975b, The complex LMS algorithm, *Proceeding of the IEEE*, vol. 63, 719-720.

Widrow, B., McCool, J.M., Larimore, M.G., and Johnson, C.R., 1976, Stationary and nonstationary learning characteristics of the LMS adaptive filter. *Proceedings of the IEEE*, vol. 64(8), 1151-1162.

Widrow, B., and Stearns, S.D., 1985, *Adaptive Signal Processing*, (Englewood Cliffs, NJ: Prentice-Hall).

Yin, Yonghui, Wang, Weihua, Yan, Xinpin, Xiao, Hanliang, and Wang Chengtao, 2003, An integrated on-line oil analysis method for condition monitoring. *Measurement Science Technology*, vol. 14, 1973-1977.

Yu, D., Cheng, J., and Yang, Y., 2005, Application of EMD method and Hilbert spectrum to the fault diagnosis of roller bearings. *Mechanical System and Signal Processing*, vol. 19(2), 259-270.

Zeidler, J.R., 1990, Performance Analysis of LMS Adaptive Prediction Filters. *Proceedings of the IEEE*, vol. 78(12), 1783-1806.

Zeidler, J.R., Satorius, E.H., Chabries, D.M., and Wexler, H.T., 1978, Adaptive enhancement of multiple sinusoids in uncorrelated noise. *IEEE Transactions on Acoustics, Speech, and Signal Processing*, vol. 26(3), 240-254.

Appendices

A. Wiener filter theory

For stochastic stationary inputs, the steady state performance of the least mean square based adaptive filter closely approximates that of the Wiener filter. Thus the Wiener filter theory provides a convenient tool for analyzing statistical LMS based adaptive noise canceller mathematically (Widorw et al 1975b). Figure A-1 shows a single input and signal output Wiener filter. The input signal is $u(n)$, the output signal is $y(n)$ and $d(n)$ is the desired signal. The error signal is $e(n) = d(n) - y(n)$. When the input signal and desired signal are statistically stationary, the Wiener filter is a linear optimal filter in the minimum mean square error sense. The optimal impulse response of the Wiener filter may be described in the following manner. The autocorrelation function of the input signal $u(n)$ can be defined as

$$r_{uu}(k) = E[u(n)u^*(n-k)] \tag{A-1}$$

where the asterisk denotes complex conjugation. The cross correlation function between the input signal $u(n)$ and the desired response $d(n)$ is expressed as

$$r_{ud}(k) = E[u(n)d^*(n-k)] \tag{A-2}$$

The optimal impulse response $w^O(k)$ is then obtained from the discrete Wiener-Hopf equation in terms of the two correlation functions. The Wiener-Hopf equation is represented as (Widorw et al 1975a)

$$\sum_{l=-\infty}^{\infty} w^O(l) r_{uu}(k-l) = r_{ud}(k) \tag{A-3}$$

The transfer function of the Wiener filter can be derived as follows. The power spectrum of the input signal $u(n)$ is the Z transform of $r_{uu}(k)$:

$$S_{uu}(z) = \sum_{k=-\infty}^{\infty} r_{uu}(k) z^{-k} \tag{A-4}$$

The cross power spectrum between the input signal and the desired response is

$$S_{ud}(z) = \sum_{k=-\infty}^{\infty} r_{ud}(k) z^{-k} \tag{A-5}$$

The Z transform of the Wiener filter can be represented as

$$W^O(z) = \sum_{k=-\infty}^{\infty} w^O(k) z^{-k} \tag{A-6}$$

The optimal unconstrained Wiener transfer function is derived by Z transform of Eq. A-3. The convolution in Eq. A-3 becomes the multiplication after the Z transform and the Wiener transfer function is (Widorw et al 1975a):

$$W^O(z) = \frac{S_{ud}(z)}{S_{uu}(z)} \tag{A-7}$$

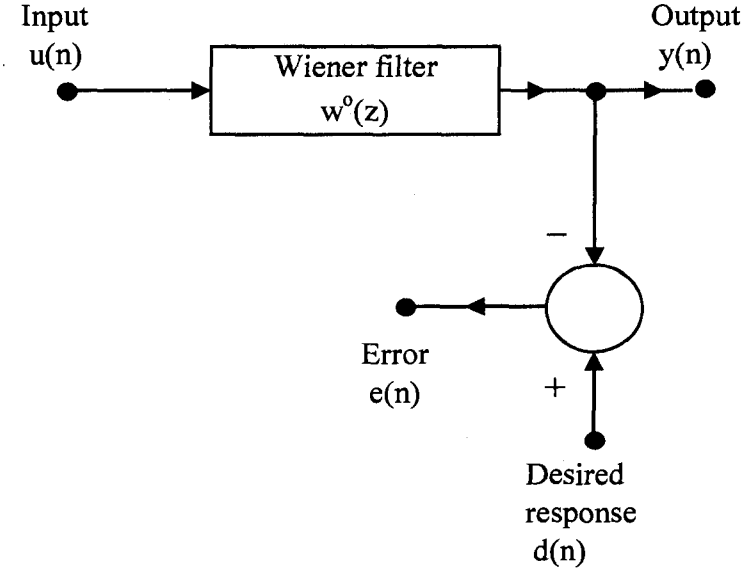

Figure A-1. Single channel Wiener filter

B. The Wiener solutions to statistical adaptive noise canceller in bearing health monitoring

When monitoring a critical component such as a bearing or a pair of gears in a complex machine which contains multiple bearings and gears, a sensor is placed in a location that is closest to the monitored component. In many cases, the sensor cannot be placed in the immediate vicinity of the monitored component due to the practical limitation and has to be mounted somewhere as close to the monitored component as possible. Therefore, the acquired signal contains the monitored signal as well as interferences from other gears and bearings in the machine. In machine fault detection,

the weaker faulty bearing signal can be corrupted by the stronger gears signals and hence the health condition of the monitored bearing can no longer be detected from the collected signal. When encountering situations like this, another sensor can be placed in a location near the interference gears source to collect the reference signal. This reference signal will likely contain mostly the interference signals from the stronger gears signals and much less monitored bearing signal component. In the following, statistical analysis using the Wiener filter theory will show that ANC can still be used to estimate the monitored bearing signal from the corrupted signal under such circumstances.

Figure B-1 shows an adaptive noise canceller applied to a simplified machine model. To simplify the analysis, the uncorrelated additive noise that varies due to the machine operation environment changes is not included and the interfering gear components in the machine are represented as one equivalent interference source $g(n)$. Depending on where the sensors are placed in the machine, the interference signal and bearing signal propagate though different channels to the primary input and reference input sensors location. The interference signal $g(n)$ is assumed to propagate to the reference input through the transfer function $H(z)$ and the transfer function from the bearing signal $b(n)$ to the reference input is $L(z)$. The primary input of the ANC in Figure B-1 consists of $b(n)$ and $g(n)$ while the reference input includes $g(n)*h(n)$ and $b(n)*l(n)$ where $h(n)$ and $l(n)$ are the impulse responses of the transfer functions $H(z)$ and $L(z)$ respectively.

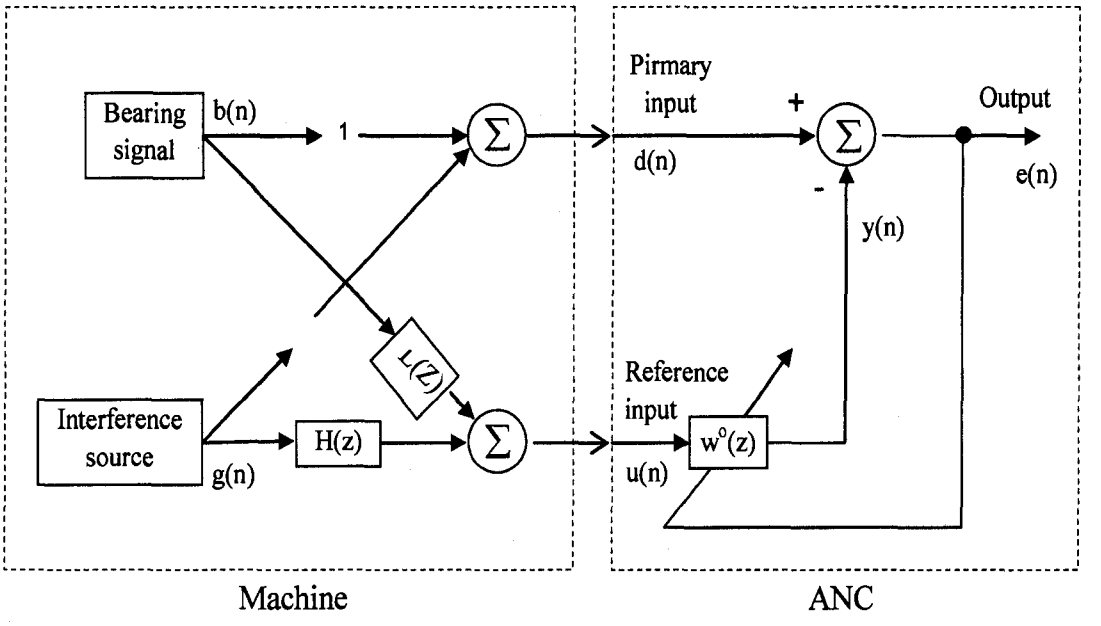

Figure B-1. Adaptive noise cancelling applied to a simplified machine model

Assuming the bearing signal $b(n)$ and interference signal $g(n)$ are uncorrelated. The power spectrum of the adaptive noise canceller's reference input signal $S_{uu}(z)$ can be represented as an addition of two mutually uncorrelated additive components. The power spectrum of the bearing signal arriving via transfer function $L(z)$ is $S_{bb}(z)|L(z)|^2$ where $S_{bb}(z)$ is the power spectrum of the bearing signal $b(n)$. The other component, $S_{gg}(z)|H(z)|^2$, is the power spectrum of the interference single arriving through transfer function $H(z)$ where $S_{gg}(z)$ represents the power spectrum of the interference signal $g(n)$. The adaptive noise canceller's reference input power spectrum is thus

$$S_{uu}(z) = S_{bb}(z)|L(z)|^2 + S_{gg}(z)|H(z)|^2 \qquad \text{(B-1)}$$

$S_{ud}(z)$ is the cross power spectrum between the adaptive filter's input $u(n)$ and the desired response which is the adaptive noise canceller's primary input $d(n)$ in Figure B-1. Since the cross power spectrum depends only on the mutually correlated primary and reference components, $S_{ud}(z)$ can be expressed as the addition of two components: the cross power spectrum of the bearing signal between the reference input and the

primary input, and the cross power spectrum of the interference source between the reference input and the primary input. Therefore, the cross power spectrum between the primary input and the reference input can be obtained as

$$S_{ud}(z) = S_{bb}(z)L(z^{-1}) + S_{gg}(z)H(z^{-1}) \tag{B-2}$$

Assuming: a) the adaptive process in Figure B-1 has converged and the adaptive filter has reached the minimum mean square solution, and b) the adaptive filter is equivalent to the optimal Wiener filter and the adaptive filter's transfer function is derived by the optimal unconstrained Wiener transfer function given in Eq. A-7, then the adaptive noise canceller's Wiener transfer function can be written as

$$W^O(z) = \frac{S_{bb}(z)L(z^{-1}) + S_{gg}(z)H(z^{-1})}{S_{bb}(z)\left|L(z)\right|^2 + S_{gg}(z)\left|H(z)\right|^2} \tag{B-3}$$

C. Effect of bearing signal present in the adaptive noise canceller reference input

$S_{bb,out}(z)$, the bearing signal power spectrum at the ANC output in Figure B-1, is obtained by subtracting the bearing signal component in the reference input from the bearing signal component in the primary input, i.e.

$$S_{bb,out}(z) = S_{bb}(z)\left|1 - L(z)W^O(z)\right|^2 \tag{C-1}$$

Similarly, the interference signal power spectrum $S_{gg,out}(z)$ at the ANC output can be obtained by subtracting the interference signal component in the reference input from the interference signal component in the primary input:

$$S_{gg,out}(z) = S_{gg}(z)\left|1 - H(z)W^O(z)\right|^2 \tag{C-2}$$

Therefore, the signal to interference ratio at the ANC output can be defined as

$$\rho_{out}(z) = \frac{S_{bb,out}(z)}{S_{gg,out}(z)} = \frac{S_{bb}(z)\left|1 - L(z)W^O(z)\right|^2}{S_{gg}(z)\left|1 - H(z)W^O(z)\right|^2} \tag{C-3}$$

Substituting Eq. B-3 into Eq. C-3 leads to

$$\rho_{out}(z) = \frac{S_{bb}(z)\left|S_{gg}(z)\left|H(z)\right|^2 - S_{gg}(z)L(z)H(z^{-1})\right|^2}{S_{gg}(z)\left|S_{bb}(z)\left|L(z)\right|^2 - S_{bb}(z)H(z)L(z^{-1})\right|^2}$$

$$= \frac{S_{bb}(z)\left|S_{gg}(z)H(z^{-1})[H(z)-L(z)]\right|^2}{S_{gg}(z)\left|S_{bb}(z)L(z^{-1})[L(z)-H(z)]\right|^2}$$

$$= \frac{S_{gg}(z)\left|H(z)\right|^2}{S_{bb}(z)\left|L(z)\right|^2} \tag{C-4}$$

Likewise, the signal to interference ratio at the ANC reference input can be represented as

$$\rho_{ref}(z) = \frac{S_{bb,ref}(z)}{S_{gg,ref}(z)} = \frac{S_{bb}(z)\left|L(z)\right|^2}{S_{gg}(z)\left|H(z)\right|^2} \tag{C-5}$$

where $S_{bb,ref}(z)$ and $S_{gg,ref}(z)$ are the bearing signal power spectrum and interference signal power spectrum at the ANC reference input respectively. Eq. C-4 and C-5 lead to the following relationship between $\rho_{out}(z)$ and $\rho_{ref}(z)$:

$$\rho_{out}(z) = \frac{1}{\rho_{ref}(z)} \tag{C-6}$$

This result shows that the signal to interference ratio at the ANC output and at the ANC reference input are reciprocal to each other at all frequencies provided that the adaptive solution has converged and is unconstrained. Therefore, a low signal to interference ratio which implies mainly interference signals with little bearing signal in the reference input of the ANC will result a high signal to interference ratio in the ANC output. This result also indicates that although the presence of bearing signal in the reference input is undesirable, the application of the ANC in machine fault detection can still achieve high signal to interference ratio provided a suitable reference input source is chosen.